1989

Phase transitions in CsCl-type intermetallic compounds

Bai-Hao Chen
Iowa State University

INFORMATION TO USERS

The most advanced technology has been used to photograph and reproduce this manuscript from the microfilm master. UMI films the text directly from the original or copy submitted. Thus, some thesis and dissertation copies are in typewriter face, while others may be from any type of computer printer.

The quality of this reproduction is dependent upon the quality of the copy submitted. Broken or indistinct print, colored or poor quality illustrations and photographs, print bleedthrough, substandard margins, and improper alignment can adversely affect reproduction.

In the unlikely event that the author did not send UMI a complete manuscript and there are missing pages, these will be noted. Also, if unauthorized copyright material had to be removed, a note will indicate the deletion.

Oversize materials (e.g., maps, drawings, charts) are reproduced by sectioning the original, beginning at the upper left-hand corner and continuing from left to right in equal sections with small overlaps. Each original is also photographed in one exposure and is included in reduced form at the back of the book. These are also available as one exposure on a standard 35mm slide or as a 17" x 23" black and white photographic print for an additional charge.

Photographs included in the original manuscript have been reproduced xerographically in this copy. Higher quality 6" x 9" black and white photographic prints are available for any photographs or illustrations appearing in this copy for an additional charge. Contact UMI directly to order.

U·M·I

University Microfilms International
A Bell & Howell Information Company
300 North Zeeb Road, Ann Arbor, MI 48106-1346 USA
313/761-4700 800/521-0600

Order Number 9014889

Phase transitions in CsCl-type intermetallic compounds

Chen, Bai-Hao, Ph.D.

Iowa State University, 1989

U·M·I
300 N. Zeeb Rd.
Ann Arbor, MI 48106

Phase transitions in CsCl-type intermetallic compounds

by

Bai-Hao Chen

A Dissertation Submitted to the
Graduate Faculty in Partial Fulfillment of the
Requirements for the Degree of
DOCTOR OF PHILOSOPHY

Department: Chemsitry
Major: Physical Chemistry

Approved:

Signature was redacted for privacy.

In Charge of Major Work

Signature was redacted for privacy.

For the Major Department

Signature was redacted for privacy.

For the Graduate College

Iowa State University
Ames, Iowa

1989

TABLE OF CONTENTS

GENERAL INTRODUCTION

The CsCl-structure (B2) with Pm3m symmetry is one of the most common compound types among binary intermetallic compounds. Review of the compilation, Binary Alloy Phase Diagram[1], published by American Society for Metals in 1986, shows that many kinds of phase transitions occur in the CsCl-type intermetallic compounds that have been reported previously.

The following gives some examples of high-temperature phase transitions in the CsCl-type binary intermetallic compounds.[1] All of these compounds have the CsCl-type structure at high-temperature and distorts to the other structures on cooling. The low-temperature form of the compounds AuCd, AuTi, PdTi, and PtTi (with homogeneity ranges) is the AuCd-type orthorhombic structure with Pmma symmetry; the low-temperature form of the stoichiometric AuDy, AuGd, AuHo, AuTb, and AuTm alloys is the BCr-type orthorhombic structure with Cmcm symmetry; the low-temperature form of stoichiometric AgYb and AuYb, as well as the nonstoichiometric DyPd, is the BFe-type orthorhombic structure with Pnma symmetry; the low-temperature form of the AlPd and AlPt alloys is the FeSi-type cubic structure with $P2_13$ symmetry; the low-temperature form of the NiTi alloy is the NiTi-type monoclinic structure with $P2_1/m$ symmetry; the low temperature form of the LiPb alloy in the

homogeneity range is the LiPb-type trigonal structure with R$\bar{3}$m symmetry. One of the most interesting examples is the phase transition observed in the stoichiometric AuNd and AuPr systems. The high-temperature CsCl-type AuNb and AuPr alloys distort to the BCr-type structure, and further transform to the BFe-type structure with decreasing temperature.

In the above examples, no two phase coexistence in the systems with the phase transitions between the CsCl-type - AuCd-type and the CsCl-type - BCr-type as well as the CsCl-type - BFe-type has been experimentally found. This means that these phase transitions could be second order. The nature of the phase behavior in the NiTi system is still not quite clear. The phase transition in AlPd and AlPt is first order. The CsCl-type LiPb has the lattice parameter a = 3.563 Å and the trigonal LiPb has the parameters a = 3.5642 Å and α = 89.5°. The phase transition is second order. The equilibrium phase relations in the Au-Nd system were not determined. However, there is no two phase coexistence in AuPr according to the Binary Alloy Phase Diagram.[1] This lack of coexistence implies that the two step phase transitions in both AuNd and AuPr may be second order. In order to understand the details of the phase behavior these and the other systems discussed above, further reinvestigations by a combination of the experimental observation and Landau theory[2] are necessary.

The best-known distortion of the CsCl-type is the phase transition to the AuCu-type tetragonal structure under a change in temperature and/or pressure. In this research, attention was focused on this transition. The phase transition has been previously studied in many binary intermetallic systems such as in the AuMn, CdPd, HgMn, IrMn, MnRh, NbRu, NiZn, RhTi, RuV, RuTa, SmTl systems, and so on. In addition, the phase transition in the rare-earth compounds RM (R = La, Ce, Pr, Nd; M = Ag, Cd, Tl) with the temperature effect and the pressure effect as well as the alloying effect ($RAg_{1-x}In_x$) was reported by Kadomatsu et al.[3] Since the properties of these compounds are associated with the phase transition, the study of phase behavior has led to the development of many new materials. For instance, the cubic phase alloys in Au-Mn are antiferromagnetic and have Néel points which correspond closely to the temperatures of a cubic-tetragonal ($c/a < 1$) transition.[4]

The subject of the phase transitions in CsCl-type intermetallic compounds is not only of interest to metallurgists but also to solid state scientists. The theoretical work carried out on this subject has been reviewed by Kadomatsu et al.[3] and Folkerts and Haas.[5] In the case of the CsCl-type rare-earth intermetallic compounds, this phase transition has been considered to arise from a band Jahn-Teller effect, by which d bands in the 5d6s bands of R are split so as to gain in band

energy.[3,6-8] The structural instability in compounds of this type is related to superconductivity and magnetic properties at low temperature, depending on the character of the 5d6s band electrons.[9-11] General considerations based on an expression for the free energy of these compounds support the idea of a band Jahn-Teller effect as the driving mechanism.[8]

The electronic structure of RhTi was studied recently by Folkerts and Haas.[5] From the band calculation, using the augmented spherical wave method, they found that the Ti 3d e_g band in the tetragonal phase is split to two bands and only contains one electron. This is a favorable situation for a Jahn-Teller instability. In addition, the energy of the compound is lowered by 0.04 eV per unit cell by the tetragonal distortion.

The details of the phase behavior in the systems with the CsCl-type structure are currently of theoretical interest to our research group because of the application of band theory methods to the consideration of symmetry breaking transitions. The transition, indicative of strong electron-phonon coupling, results in symmetry breaking from cubic to tetragonal to orthorhombic symmetry. Previous work in a number of systems has led to confused and contradictory structural interpretations. Thus it was the purpose of this research to study the phase behavior in Au-Mn, Ir-Ti, Nb-Ru, Rh-Ti, and RuTa by a variety of crystallographic techniques,

including high-temperature X-ray powder diffraction, and the Landau theory,[2,12,13] to provide new, consistent interpretations. A knowledge of the phenomenology of these transitions will add to our understanding of the relationship between electronic structure and crystal structure and will provide bases for further testing of modern theories of these relationships.

Although the V-Ir alloys do not have the CsCl-type structure and a phase diagram for the system has been reported,[14] the nature of the phase behavior was uncertain. As a result, an investigation of the phase transition in $V_{0.54}Ir_{0.46}$ by high temperature X-ray diffraction and Landau theory was included in this work.

EXPERIMENTAL

Sample Preparation

All binary intermetallic compounds were prepared by either the sealed quartz ampoule method or the arc-melting method. The powder samples were made as fine as possible (passed through a 325 mesh sieve (Humboldt Meg. Co., 0.045 mm)) before the X-ray diffraction measurement in order to minimize preferred orientation. The weight of each sample was about 4 grams. The purities and the sources of the elements used in this research were listed in Table 1.

Quartz ampoule method

The Au-Mn samples were prepared from gold powder and manganese chips. The manganese chips were cleaned by 10 % nitric acid (Mallinckrodt) and rinsed before use with distilled water followed by acetone (Fisher Scientific). The gold and manganese elements were weighed in the ratios Au/Mn = 0.88, 0.97, 1.01, and 1.05 and placed in cleaned quartz ampoules. The quartz ampoules were evacuated to about 10^{-6} torr residual pressure, then sealed, and finally placed in a furnace at 900°C. This temperature was sufficient to allow which was a gas (the manganese) - solid (the gold) reaction, which was sustained for one week. The sintered products were filed and the powder was annealed at 500°C in a sealed quartz ampoule.

Table 1 The purities and the sources of the elements

Elements	Purities	Sources
Gold powder	99.95	a
Iridium powder	99.95	a
Niobium foil	99.98	a
Manganese chips	unknown	b
Rhodium powder	99.95	a
Ruthenium powder	99.95	a
Tantalum foil	unknown	b
Titanium foil	99.95	a
Vanadium foil	unknown	b

a - from Alfa Products

b - from Ames Laboratory

Arc-melting method

The Ir-Ti, Ir-V, Nb-Ru, Rh-Ti, and Ru-Ta samples were prepared by arc melting the elements. In order to reduce mass loss during arc melting, the powdered elements were made into the pellets by arc melting and weighed before use. The ratios are uncertain to within less than 1 % because less than 1.2 % of the total mass was lost in each synthesis. The starting materials were melted on a water

cooled copper plate in an argon atmosphere. The sample pellets were turned over and melted several times to help insure homogeneities. The copper plate was cleaned by pipetting a few drops of 70.1 % nitric acid (Mallinckrodt) into the sample holes on the top of the plate for 1 minute, then washed by water to remove $CuNO_3$, and finally by acetone (Fisher Scientific). The quenched pellets were powdered in an impact mortar (and filed, if needed). The intermetallic ratios were taken to be the values calculated from the initial weighed quantities of the elements. The absence of significant phase impurities was determined by X-ray diffraction. The powdered samples were heat-treated in the high temperature diffractometer in order to anneal away stains and inhomogeneities.

X-ray Techniques

Guinier camera

X-ray powder diffraction using an Enraf-Nonius film camera with copper $k\alpha_1$ (λ = 1.540562 Å) radiation was employed at room temperature. The Guinier camera with a focusing monochromator provided high resolution patterns and short exposure time. Silicon powder (NBS Standard Reference Material 420 a) mixed with the samples was used as a standard to determine 2θ or d values. The Guinier patterns were read using an Enraf-Nonius Guinier film reader. The

reading from the Guinier patterns was converted to 2θ and d values by a least-squares computer program GUIN.[15]

High-temperature X-ray diffractometer

A Rigaku θ-θ diffractometer equipped with a Bühler sample chamber and temperature controller was used for studies at elevated temperatures shown in Figure 1. The X-ray tube with copper radiation (λ for $k\alpha_1$ = 1.5405 Å and λ for $k\alpha_2$ = 1.5443 Å) and the scintillation counter rotate in the opposite directions to each other at the speed ratio: 1:1, meeting the conditions for the focusing method. An exit monochromator (graphite single crystal) was used to suppress background radiation originating in the specimen and the nonmonochromatic nature of the Cu X-ray radiation.

The high temperature chamber consists of a cylindrical, double - walled, water-cooled pot made of stainless steel equipped with an irradiation window of beryllium and with a lid carrying two pairs of electrodes for heating specimens and the environment. The window allows the Bragg angle range of $0 \leqslant 2\theta \leqslant 180°$. A UHV turbomolecular pump is attached as close as possible to the chamber to maximize pumping efficiency. The residual pressure inside the chamber was in all cases below 10^{-6} torr. The water supply was used to cool the chamber and the electrodes as well as a high-voltage X-ray generator.

A temperature-program controlled heating of the samples (to 2400°C is possible) with a control system (RE 2400)

using WRe-thermocouples, Tungsten - W 3 % and W 25 % (Omega Engineering, Inc.). Molybdenum foil (Ames Laboratory, 0.2 mm thick) and tantalum foil (Ames Laboratory, 0.4 mm thick) were used as sample heater and environment heater (8.5 V - 100 A and 8.5 V - 250 A), respectively.

In this study, divergence slit, scatter slit, receiving slit, and monochromator receiving slit were 1°, 1°, 0.30 mm, and 0.45 mm, respectively. The samples in the chamber were heated or cooled slowly by programming the temperature controller at 1 degree per minute in order to reach phase equilibrium. All samples in this study were selected for careful scans at 16 minutes per θ-degree with 0.02 2θ-degree of the step size in order to obtain high statistic patterns.

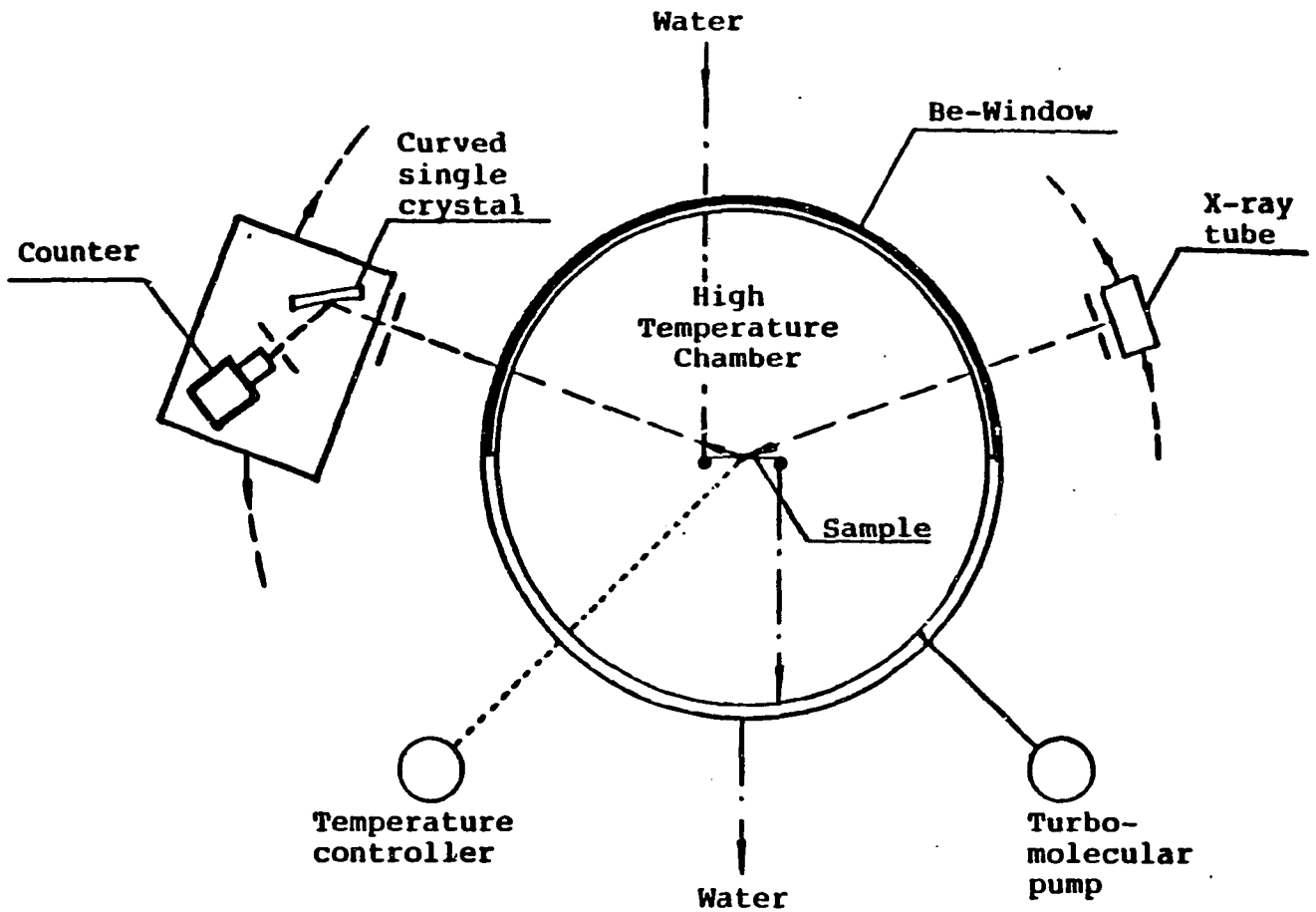

Figure 1 X-ray diffractometer equipped with a high-temperature sample chamber

RIETVELD REFINEMENT

Rietveld full-profile refinement computer program KDBW originally written by D. B. Wiles and R. A. Young[16] and then modified by Dr. Jacobson's group (Kim[17]) was used to aid in the interpretation of the X-ray diffraction data. The profile method for refining powder diffraction data, originally introduced by Rietveld,[18,19] has now become an important tool for the determination of crystal structures since many materials of great interest cannot be made in a form suitable for single-crystal techniques.

In the Rietveld method, structural (for two phases, if needed) parameters are adjusted via a least-squares refinement procedure until the best fit between the entire calculated and observed powder diffraction patterns is obtained. The parameters that can be refined simultaneously in this program include atom position, atom thermal vibrational, preferred orientation, atom site-occupancy, 2θ-zero correction, overall scale, overall isotropic thermal, profile breadth, profile asymmetry, background function(up to 6 parameters), and lattice parameters.

The Rietveld refinement program in use at ISU allows six reflection profile functions: Gaussian (G), Lorentzian (L), modified Lorentzian (ML), intermediate Lorentzian (IL), pseudo-Voigt (p-V), and Pearson VII (PVII). According to Young and Wiles, the Gaussian function was consistently the

worst performer, while the the pseudo-Voigt and Pearson VII were the best.[20] The PVII is given by

$$(1 + 4\,(2^{1/m} - 1)\,x^2)^{-m}$$

$$x = 2\Delta\theta_{jk}/H_k$$

where H_k is the full width at half maximum and m is a refinable profile parameter. Since the PVII goes from pure L with m = 1 to pure G with m = ∞, it has a characteristic between G and L. For this reason, the Pearson VII function was selected for this research.

The definition of the R-factors used in the Rietveld refinement program is

$$R_F = \frac{\Sigma \mid I_k\,(obs) - I_k\,(calc) \mid}{\Sigma\, I\ \ (obs)}$$

$$R_B = \frac{\Sigma \mid \sqrt{I_k\,(obs)} - \sqrt{I_k\,(calc)} \mid}{\Sigma \sqrt{I_k\,(obs)}}$$

$$R_P = \frac{\Sigma \mid Y_i\,(obs) - Y_i\,(calc) \mid}{\Sigma\, Y_i\,(obs)}$$

$$R_{wp} = \left[\frac{\Sigma\, w_i\,(Y_i\,(obs) - Y_i\,(calc))^2}{\Sigma\, w_i\,(Y_i\,(obs))^2} \right]^{1/2}$$

Here I_k is the intensity assigned to the kth Bragg reflection, Y_i is the intensity values at each of the i steps in the pattern, and W_i is the weight at the ith step. R_B (Bragg R-factor) is affected only slightly by background, second phase, and the fit of the observed reflection profiles. Thus it may be the best indicator of the fit of the crystal structure model to the average structure.[20,21] Therefore, the size of R_B has been used by our group as a principal criterion of fit in evaluation of the final results.

PROGRAMS FOR LATTICE PARAMETER REFINEMENT

LLR Program

Introduction

In powder diffraction, one is frequently faced with the need to obtain precise lattice parameters, often in the presence of diffraction lines from other materials. Studies might be carried out as a function of temperature, pressure or composition. Also in the analysis of diffraction patterns from uncharacterized materials, one often strives to ascertain the validity of some assumed structure, possibly using only a few diffraction lines. In order to better address such problems, a Fortran computer program,[22] LLR (see Appendix A), was written to carry out linear least-squares lattice parameter refinement in crystal systems with symmetry orthorhombic or higher in this work. In addition to lattice parameters, a 2θ-zero value can also be refined. The program has been used in this study for the past two years.

Details of the program

Input to the program consists of a file containing the observed 2θ values, and either the indices of a few of the diffraction lines, or approximate lattice parameters.

Based on these initial data, a set of calculated lines is generated and the best fit to observed lines within an

error window of E_1 (given by the user) is obtained. A 2θ-zero offset can be employed and can be refined, if desired.

In order to account for $k\alpha_1 - k\alpha_2$ splitting, the wavelength employed in the calculation is expressed as the following function of θ:[23]

$$\lambda(\theta) = \frac{2\,k\,\alpha_1 + k\,\alpha_2\,(1 - q)}{3 - q} \qquad (\theta < \theta_s)$$

$$q = \frac{\tan\theta}{\tan\theta_s}$$

where θ_s is supplied by the user. If θ is greater than θ_s, $\lambda = k\alpha_1$.

A linear least-squares method is used to refine the lattice parameters. The trigonometric quantity $\sin^2(\theta + \delta)$ was approximated to $\sin^2\theta + \delta/2 \sin 2\theta$. In the orthorhombic case, for example,

$$\sin^2\theta = U\,h^2 + V\,k^2 + W\,l^2 - \delta/2 \sin 2\theta$$

where $U = \frac{\lambda^2}{4\,a^2}$, $V = \frac{\lambda^2}{4\,b^2}$, and $W = \frac{\lambda^2}{4\,c^2}$. The program then proceeds to solve

$$U \Sigma h_i^4 + V \Sigma k_i^2 h_i^2 + W \Sigma l_i^2 h_i^2 - \delta \Sigma f_i h_i^2 = \Sigma g_i h_i^2$$

$$U \Sigma h_i^2 k_i^2 + V \Sigma k_i^4 + W \Sigma l_i^2 k_i^2 - \delta \Sigma f_i k_i^2 = \Sigma g_i k_i^2$$

$$U \Sigma h_i^2 l_i^2 + V \Sigma k_i^2 l_i^2 + W \Sigma l_i^4 - \delta \Sigma f_i l_i^2 = \Sigma g_i l_i^2$$

$$U \Sigma h_i^2 f_i + V \Sigma k_i^2 f_i + W \Sigma k_i^2 f_i - \delta \Sigma f_i^2 = \Sigma g_i f_i$$

where $f = 1/2 \sin 2\theta$ and $g = \sin^2\theta$, to obtain the parameters a, b, and c.

The refinement process can then be repeated through n cycles, where n in specified by the user, the maximum allowed error E_m is decreased on each cycle by setting

$$E_m = 0.9^{n-1} E_1$$

Results

The Tables 2 and 3 present selected input and output, respectively, in the application of this program to a AuMn two phase systems. The observed data were collected on a Rikagu X-ray diffractometer at room temperature.[24] Refinement of the tetragonal phase with c/a > 1 was carried out first and the 2θ-zero was also refined. Then the tetragonal phase with c/a < 1 was refined; here the 2θ-zero was now fixed at the value obtained from the refinement of the first phase.

For comparison, the same pattern was also refined via a Rietveld procedure which yielded a = 3.170(7) and c = 3.299(3) Å for the tetragonal phase with c/a > 1 phase. The 2θ-zero was found to be -0.494°. These results are in excellent agreement with those obtained by this program.

Table 2 Application of the refinement program to a AuMn two phase system; Run parameters

(i)	First phase:	tetragonal (c/a > 1)
	2θ-zero:	0.0
	2θ-zero refinement:	Yes
	Error limit:	0.4
	No. of cycles:	15
(ii)	Second phase:	tetragonal (c/a < 1)
	2θ-zero:	-0.462[a]
	2θ-zero refinement:	No
	Error limit:	0.2
	No. of cycles:	5

[a]From refinement of (i) above.

Table 3 The results of lattice parameter refinement for a two phase AuMn system

(i) First phase: tetragonal (c/a > 1)

Parameters (Å): a = 3.166(2) c = 3.298(6)

2θ-zero: -0.462

Standard deviation in 2θ: 0.0271

No.	h	k	l	obs-2θ	cal-2θ	|Δ2θ|	obs-$\sin^2\theta$	cal-$\sin^2\theta$
2	1	0	0	28.158	28.167	0.009	0.05918	0.05921
5	1	0	1	39.458	39.415	0.043	0.11395	0.11372
7	1	1	0	40.218	40.248	0.030	0.11820	0.11837
8	1	1	1	49.158	49.142	0.016	0.17301	0.17291
9	0	0	2	55.698	55.684	0.014	0.21822	0.21812
11	2	0	0	58.198	58.231	0.033	0.23651	0.23675
13	1	0	2	63.538	63.553	0.015	0.27720	0.27731
15	2	0	1	65.358	65.327	0.031	0.29153	0.29128
16	1	2	0	65.878	65.913	0.035	0.29566	0.29566
19	2	1	1	72.618	72.599	0.019	0.35063	0.35047
22	0	2	2	84.838	84.822	0.016	0.45501	0.45487
24	0	0	3	88.918	88.943	0.025	0.49056	0.49078

Table 3 (continued)

(ii) Second phase: Tetragonal (c/a < 1)

Parameters (Å): a = 3.271(5) c = 3.096(6)

2θ-zero: 0.000

Standard deviation in 2θ: 0.0297

No.	h	k	l	obs-2θ	cal-2θ	|Δ2θ|	obs-$\sin^2\theta$	cal-$\sin^2\theta$
1	1	0	0	27.238	27.244	0.006	0.05544	0.05547
3	0	0	1	28.798	28.813	0.015	0.06184	0.06190
6	1	0	1	39.998	40.060	0.062	0.11697	0.11731
8	1	1	1	49.148	49.119	0.039	0.17301	0.17275
10	2	0	0	56.178	56.187	0.009	0.22169	0.22176
12	0	0	2	59.638	59.669	0.031	0.24727	0.24750
13	2	1	0	63.538	63.538	0.000	0.27720	0.27720
14	2	0	1	64.378	64.359	0.019	0.28378	0.28363
17	1	0	2	66.798	66.789	0.009	0.30301	0.30294
18	2	1	1	71.178	71.225	0.047	0.33869	0.33907
20	1	1	2	73.538	73.546	0.008	0.35831	0.35838
21	2	2	0	83.538	83.513	0.025	0.44373	0.44351
23	0	2	2	86.498	86.475	0.023	0.46946	0.46926

MONO Program

In addition to the LLR program, another computer program, MONO (see Appendix B), written in Fortran also has been developed. It is used to refine the parameters for monoclinic symmetry by a Gridls least-squares method using a procedure similar to that of the LLR program.

THEORY OF PHASE TRANSITIONS

Phase transitions occur as responses to changes in state, e.g., temperature, pressure, or composition, and can be classified as first- and second-order by considering the behavior of thermodynamic quantities like entropy, volume, heat capacity, etc. Broadly speaking, phase transitions which occur without the coexistence of two phases, i.e., without the nucleation and growth of the new phase, are second order, otherwise the transition is first order.

Thermodynamics

In first-order transitions, the first derivatives of the Gibbs free energy with respect to temperature and pressure exhibit discontinuous changes. Therefore, since

$$\left(\frac{\partial G}{\partial T} \right)_P = -S$$

and

$$\left(\frac{\partial G}{\partial P} \right)_T = V$$

first-order phase transitions involve discontinuous changes in entropy and volume. At the transition temperature, T_t, $\Delta G = 0$, and then

$$\Delta S = \frac{\Delta H}{T}$$

In a second-order phase transition, the second derivatives of the free energy show discontinuous changes:

$$\left(\frac{\partial^2 G}{\partial P^2} \right)_T = - V \beta'$$

$$\left(\frac{\partial^2 G}{\partial P \, \partial T} \right) = V \alpha'$$

$$\left(\frac{\partial^2 G}{\partial T^2} \right)_P = \frac{- C_P}{T}$$

Here C_P, α', and β' are the heat capacity, volume thermal expansibility, and compressibility, respectively. Second-order transitions involve continuous changes in entropy and volume. The description of the thermodynamics at second-order transitions in systems with variable chemical content is the Gibbs-Konovalow (G-K) equation:[12]

$$\left(\frac{\partial T}{\partial X^{\alpha}} \right)_P = - \frac{\left[\left[\frac{\partial \mu_A^{\alpha}}{\partial X_A^{\alpha}} \right]_{T,P} + \left[\frac{\partial \mu_B^{\alpha}}{\partial X_B^{\alpha}} \right]_{T,P} \right] \Delta X}{\Delta \bar{S} + \left(\bar{S}_A^{\alpha} + \bar{S}_B^{\alpha} \right) \Delta X}$$

where α and β label two phases, each containing the same two components, A and B, μ is the chemical potential, ΔX is

the differences in the mole fraction of A in the two phases separated by a two-phase region enclosed by the boundary and $\Delta \bar{S}$ and $\bar{S}_A^{\alpha}$ are the difference in molar entropy of the phases and the partial molar entropy of A in α, respectively. Applying this equation to a second-order transition that occurs with changing X shows that $\Delta S = 0$ because $(\partial \mu / \partial X)_{T,P} \neq \infty$, $(\partial T / \partial X_A^{\alpha})_P \neq 0$, and $\Delta X = 0$. In addition, the continuity of the process also means that $\Delta V = 0$. An experimental distinction between first- and second-order phase transitions is provided by the observation of the presence or absence of a coexistence of two phases in equilibrium. Usually, a first-order phase transition is easy to detect. However, if the temperature range of the coexistence of two phase is quite narrow, and if a relatively long time is required to reach phase equilibrium, the distinction is very difficult. Strictly speaking, it is impossible to run an experiment with the temperature difference between two steps arbitrarily small in magnitude and to take arbitrarily long time to reach phase equilibrium. Fortunately, Landau theory of symmetry and phase transitions[2,12,13] provides a method to help distinguish between these two types of phase transitions. A discussion of Landau theory follows.

Landau Theory

A phase transition is associated with a change in symmetry at a certain thermodynamic state. Considering the thermodynamic quantities of a crystal for a given deviation from the symmetric state, Landau introduced the concept of an order-disorder parameter, η, and expressed the free energy, G, of the low-symmetry structure as a Taylor's series in η for second-order and some cases of first-order transitions, as follows:

$$G = G^{\circ} + \alpha \eta + A \eta^2 + B \eta^3 + C \eta^4 + \ldots$$

where α, A, B, C, ... are functions of P and T and G° is the free energy of the high-symmetry structure. Here, $\eta = 1$ in the completely ordered phase (at low temperature) and $\eta = 0$ in the completely disordered phase after the transition. Since $\alpha = (\partial G / \partial \eta)_{T_t}$ and G must be at a minimum at $\eta = 0$ if the state when $\eta = 0$ is stable at the transition point, it follows that α must be equal to zero. Thus the expansion of G becomes

$$G = G^{\circ} + A \eta^2 + B \eta^3 + C \eta^4 + \ldots$$

and if follows that $A > 0$ when $\eta^{eq} = 0$. Consider what happens when A goes to zero (e.g., with temperature). If B does not vanish, $\partial(G-G^\circ)/\partial\eta = 0$ has two solutions indicating that there are two minima. If different G values correspond to an absolute minimum at $\eta = 0$ (stable) and a relative minimum at $\eta \neq 0$ (metastable) then $\eta^{eq} = 0$. As A decreases the G values at the two minima approach equality and when they are equal the two phases at $\eta = 0$ and $\eta \neq 0$ are in equilibrium. This is the case of a first-order phase transition. Therefore, B must vanish for symmetry reasons if a second-order transition occurs. Hence, we have

$$G = G^\circ + A\,\eta^2 + C\,\eta^4 + \ldots$$

for second-order transition. Here $A > 0$ for the high-symmetry phase and $A < 0$ for the low-symmetry phase; $C > 0$ for both. A vanishes at the transition point.

Landau theory[12,13] provides four conditions that a phase transition must meet in order that it be possible for the transition to occur continuously:

1. the space group of two structures related by such a transition must be in a group-subgroup relationship;
2. the difference in the particle density functions of the two structures must be a basis function, or a combination of basis functions, of an irreducible

representation (irr. rep.) of the higher symmetry space group;

3. it must not be possible to form a totally symmetric third-order combination of such basis functions;
4. the space lattice of a low-symmetry structure must be locked in by symmetry (otherwise the low-symmetry structure is incommensurate).

The fourth condition (Lifschitz condition) must be tested by determining directly whether the antisymmetric square of the representation, times the vector representation of G°, V(g), contains the totally symmetric representation:[13]

$$\Sigma\ [\chi^2(g) - \chi(g^2)]\ V(g) = 0$$

where g are the elements of G, and $\chi(g)$ are the characters of the representation.

The approach described here is to assume on the basis of temperature dependent X-ray diffraction patterns that the distorted and/or ordered structure is formed from the high-symmetry structure via a second-order transition. This assumption limits the lattice, space groups and structures that must be considered. If a solution to the structure is found it follows that the transition could have occurred by a second-order transition.

One of the starting points of Landau theory is the consideration of a particle density function which gives the probability distribution of the atoms in the crystal. The density function, ρ, of the low-symmetry structure can be expressed in terms of that of the high-symmetry structure, ρ°, and the distortion functions, ϕ_1, ϕ_2, ..., ϕ_m, which are basis functions for an m-dimensional irr. rep. of the high-symmetry space group:

$$\rho = \rho^\circ + \Sigma\, C_i\, \phi_i = \rho^\circ + \Sigma\, (\, \gamma_i\, \phi_i\,)\, \eta.$$

Here $\eta^2 = \Sigma\, C_i{}^2$, $C_i = \eta\gamma_i$, and $\Sigma\, \gamma_i{}^2 = 1$. Since $\rho \to \rho^\circ$ as C_i's $\to 0$, the Gibbs free energy of a general distortion is expanded to the fourth-order in the coefficients of the ϕ_i's:

$$G = G^\circ + A\, \eta^2 + \Sigma\, C_j\, f_j{}^4(\gamma_i)\, \eta^4$$

The function $f_j{}^4(\gamma_i)$ is an invariant of the 4th order constructed from the γ_i's since G must be invariant under symmetry operations and the sums with respect to j contain as many terms as there are independent invariants of the fourth-order. To determine the stable state solutions it is necessary to minimize G with respect to the γ_i's subject to the restraint $\Sigma\, \gamma_i{}^2 = 1$. Since the invariance under consideration includes invariance with respect to the space-

group operations that do not include pure translational operations as a factor (called the essential symmetry operations) as well as with respect to translational symmetry operations, it is necessary to consider the behavior of the basis functions under the essential symmetry operations. The essential symmetry operations can be divided into two sets - those the rotational parts of which carry a wave vector in the star into another wave vector in the star, and those the rotational parts of which carry the wave vector into itself modulo a reciprocal lattice vector. The latter set is called the group of the wave vector, even though it is not a group in every case. The rotational parts of the group of the wave vector together form a point group called point group of the wave vector.

There are published tables[25] of matrices that are called "small representations" that show how the basis functions behave under the essential symmetry operations in the group of the wave vector. As with irr. reps. of point groups, with which the small reps. are sometimes isomorphous, the matrices may be one-dimensional or have a higher dimensionality. The total dimension of an irr. rep. is the product of the dimension of the small rep. and the number of vectors in the star.

A superlattice is determined by the specification of a wave vector, or set of wave vectors, in the following way: all translational symmetry operations the vectors of which

when dotted with the wave vector(s) yield an integer remain, all others are lost. For example, if the wave vector is $k = b^*/2$ and $T = ma + nb + pc$, then $k \cdot T = n/2$ and only those translations with n even remain. The functions $\cos(2\pi k \cdot r)$ or $\exp(2\pi i k \cdot r)$ are bases for irreducible representations of the translational subgroup, e.g., with $k = b^*/2$, $\cos\pi y$ which is symmetric for even n and antisymmetric for odd n translations, results. The fourth condition of Landau theory restricts possible wave vectors to which a second-order transition can correspond to the high-symmetry points of the first Brillouin zone. It is necessary to consider all possible combinations of vectors forming a star corresponding to a particular high-symmetry point.

For example, if the high-symmetry structure is CsCl-type then the high-symmetry points shown in Figure 2 are $\Gamma(k = 0)$, $X(k = \pm a^*/2, \pm b^*/2, \pm c^*/2)$, $M[k = \pm(a^* + b^*)/2, \pm(a^* + c^*)/2, \pm(b^* + c^*)/2]$, and $R[k = (a^* + b^* + c^*)/2, (-a^* + b^* + c^*)/2, (a^* - b^* + c^*)/2, (a^* + b^* - c^*)/2]$. If the transition corresponds to Γ then the only possible lattices are those that can continuously transform into the simple cubic lattice of the CsCl-type structure (simple cubic lattice with $a = a^\circ$) without change in the number of lattice points. The symmetry change of any transition corresponding to Γ does not include translational symmetry and no superstructure results. On the other hand, if $k \neq 0$ superlattice can result. Examples of a transition at the Γ

point corresponding to the 3-dimensional small reps., and at the M point corresponding to the 2-dimensional small reps. in Pm3m will discuss below.

Space-lattices that can result from a second-order phase transition can be determined as follows:[23]

1. determine the high-symmetry points in reciprocal space;
2. determine the wave vectors in the star at each point;
3. determine whether third-order combinations of basis functions can be translationally invariant;
4. if there are translationally invariant third-order combinations then determine whether these combinations are also invariant to essential symmetry operations;
5. if there are third-order invariants the point need not be considered further;
6. if there are none examine the fourth-order invariants subject to $\Sigma\ \gamma_i^2 = 1$ and identify the combinations associated with minima;
7. from the solutions to the minimization of the fourth-order term the combinations of wave vectors to which possible superlattices correspond are found, these in turn yield the superlattice vectors by retaining those vectors which when dotted with the wave vector(s) yield an integral multiple of 2π.

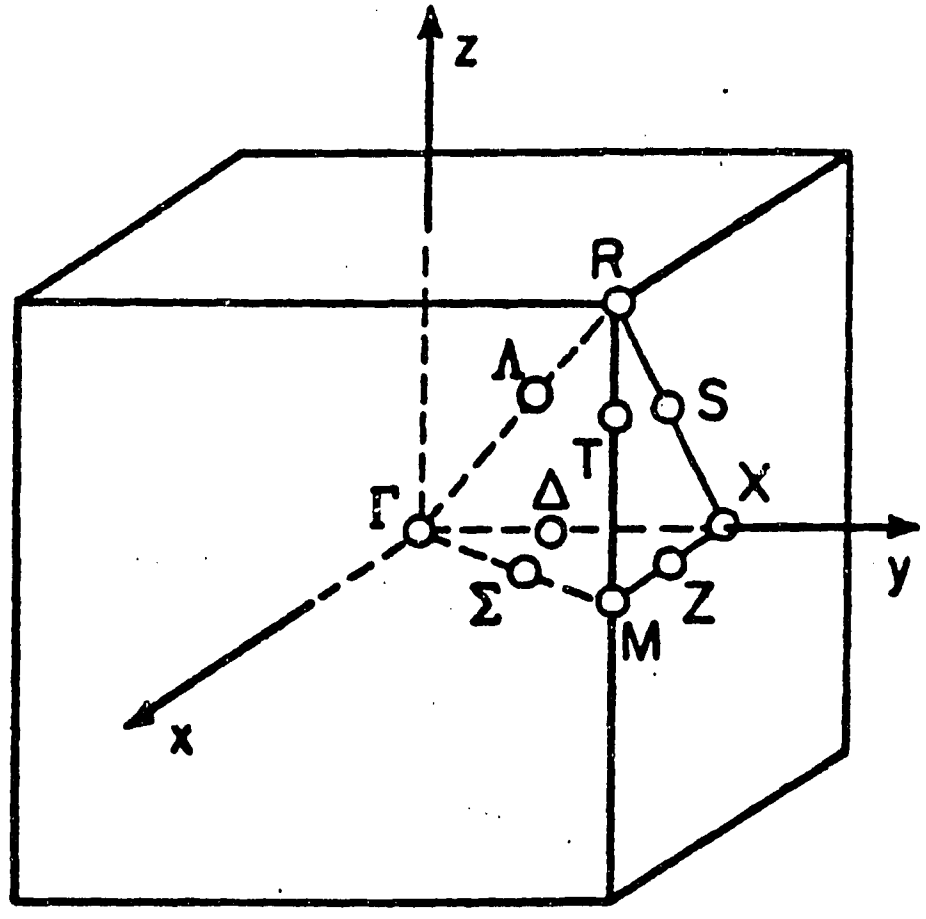

Figure 2 Symmetrical unit cell for the simple cubic lattice

An example of a transition at Γ point

As examples of space-group determination consider the case of the 3-dimensional small representations at Γ (k = 0) point in the Pm3m point group. There are four 3-dimensional small representations isomorphous with T_{1g}, T_{2g}, T_{1u}, and T_{2u} of the point group O_h. The products of the antisymmetric squares of the 3-D irr. reps. at the Γ and the vector representation do not contain the totally symmetric representation. Therefore, the four irr. reps. meet the fourth condition. Furthermore, three of the four irr. reps. (not T_{1g}) change the sign of an odd number of the three basis functions under some symmetry operations and thus no third-order invariant exists in these cases.

Next, irr. reps. allowed by the fourth-order term should be determined. Recalling that $\Sigma\ \gamma_i^2 = 1$, it follows that $(\Sigma\ \gamma_i^2)^2 = \Sigma\ \gamma_i^4 + 2\Sigma_{i<j}\ \gamma_i^2\gamma_j^2 = 1$. If, as is frequently the case, and is true for the case under consideration, no symmetry operation takes $\phi_i^2\phi_j^2$ into ϕ_k^4, then the two terms $\Sigma\ \gamma_i^4$ and $\Sigma_{i<j}\ \gamma_i^2\gamma_j^2$ are independent fourth-order invariants and, using $(\Sigma\ \gamma_i^2)^2 = 1$, the two fourth-order invariants can be taken to be a constant plus $\Sigma\ \gamma_i^2\gamma_j^2$ or a constant plus $\Sigma\ \gamma_i^4$. Thus, to terms of fourth order (in the absence of a third-order term):

$$G = G^\circ + A\eta^2 + [C_1 + C_2(\gamma_1^2\gamma_2^2 + \gamma_2^2\gamma_3^2 + \gamma_1^2\gamma_3^2)]\eta^4$$

and the possible space lattices are found by minimizing G with respect to the γ_i subject to the constraint $\Sigma\ \gamma_i^2 = 1$. On one hand, if $C_2 > 0$, then G is minimized if $\Sigma_{i<j}\ \gamma_i^2\gamma_j^2 = 0$, which is the case $\gamma_1 = 1$ and $\gamma_2 = \gamma_3 = 0$. Thus, a stable structure is given by

$$\rho = \rho^\circ + \eta\phi_1.$$

On the other hand, if $C_2 < 0$, then the fourth order term is minimized by maximizing $\Sigma\ \gamma_i^2\gamma_j^2$ subject to the constraint $\Sigma\ \gamma_i^2 = 1$. This maximum is found by the method of undetermined multipliers to be given by $\gamma_1 = \gamma_2 = \gamma_3 = 1/\sqrt{3}$, and the particle density is:

$$\rho = \rho^\circ + (\phi_1 + \phi_2 + \phi_3)\eta/\sqrt{3}.$$

In the T_{1g} case, a single basis function, for example ϕ_1, transforms into itself under the symmetry operations E, C_{2x}, $C_{2(z-y)}$, $C_{2(z+y)}$, i, σ_x, σ_{z-y}, and σ_{z+y} to yield the space group Pmmm. The basis function $\phi_1 + \phi_2 + \phi_3$ transforms into itself under the symmetry operations E, $2C_{3(x+y+z)}$, $C_{2(y-x)}$, $C_{2(z-y)}$, $C_{2(z-x)}$, i, $2S_{6(x+y+z)}$, σ_{y-x}, σ_{z-y}, and σ_{z-x} to yield space group $R\bar{3}m$. However, as discussed above, in this case there exists a third-order invariant. For example, the functions (ϕ_1, ϕ_2, ϕ_3) transform into $(\phi_1, -\phi_2, -\phi_3)$ under the symmetry operation

C_{2x} and thus the third-order combination $\phi_1\phi_2\phi_3$ transforms into itself. Therefore, the space group $R\bar{3}m$ is eliminated.

In the T_{2g} case, the basis function ϕ_1 transforms into itself under the symmetry operations E, C_{2x}, $2C_{4x}$, i, σ_x, and $2S_{4x}$ to yield the space group P4/m. The basis function $\phi_1 + \phi_2 + \phi_3$ transforms into itself under the symmetry operations E, $2C_{3(x+y+z)}$, i, and $2S_{6(x+y+z)}$ to yield space group $R\bar{3}$.

In the T_{1u} case, the basis functions ϕ_1 transforms into itself under the symmetry operations E, C_{2x}, $C_{2(z-y)}$, $C_{2(z+y)}$, σ_y, σ_z, and $2S_{4x}$ to yield the space group $I\bar{4}m2$. The basis function $\phi_1 + \phi_2 + \phi_3$ transforms into itself under the symmetry operations E, $2C_{3(x+y+z)}$, $C_{2(y-x)}$, $C_{2(z-y)}$, and $C_{2(z-x)}$ to yield the space group R32.

In the T_{2u} case, the basis ϕ_1 transforms into itself under the symmetry operations E, C_{2x}, $2C_{4x}$, σ_y, σ_z, σ_{z-y}, and σ_{z+y} to yield the space group P4mm. The basis function $\phi_1 + \phi_2 + \phi_3$ transforms into itself under the symmetry operations E, $2C_{3(x+y+z)}$, σ_{y-x}, σ_{z-y}, and σ_{z-x} to yield the space group R3m.

A previous paper[26] reported that the alloy LiPb has a rhombohedral lattice with space-group symmetry $R\bar{3}m$ and the lattice parameters $a = 3.542$ Å and $\alpha = 89°30'$ at room temperature, and that it transforms continuously to the CsCl-type structure with increasing temperature. However, application of Landau theory to the transition at the Γ

point, as discussed above, shows that the space-group symmetry of the low-temperature form of LiPb must be R3m with two atomic positions at x, x, x (~0, ~0, ~0, and ~1/2, ~1/2, ~1/2) and $a \simeq a^{\circ}$ if the phase transition is to be second order. The two space groups $R\bar{3}$ and R32 are consistent with distortion of the CsCl-type structure only with atoms in 0, 0, 0 and 1/2, 1/2, 1/2, i.e., in the positions of $R\bar{3}m$ symmetry which was shown to imply a third-order in invariant.

An example of a transition at M point

There are two 2-dimensional small representations at the M-point in Pm3m, E_g and E_u. One for E_g is shown in Table 4, and another for E_u is equal to Eg x A_{1u}.

Table 4 Two-dimensional small representation at the M-point

E	C_{4z}	C_{2z}	C_{4z}^3	C_{2x}	$C_{2(y-x)}$	C_{2y}	$C_{2(x+y)}$
$\begin{pmatrix} 1 & 0 \\ 0 & 1 \end{pmatrix}$	$\begin{pmatrix} 0 & -1 \\ 1 & 0 \end{pmatrix}$	$\begin{pmatrix} -1 & 0 \\ 0 & -1 \end{pmatrix}$	$\begin{pmatrix} 0 & 1 \\ -1 & 0 \end{pmatrix}$	$\begin{pmatrix} -1 & 0 \\ 0 & 1 \end{pmatrix}$	$\begin{pmatrix} 0 & 1 \\ 1 & 0 \end{pmatrix}$	$\begin{pmatrix} 1 & 0 \\ 0 & -1 \end{pmatrix}$	$\begin{pmatrix} 0 & -1 \\ -1 & 0 \end{pmatrix}$
i	S_{4z}^3	σ_z	S_{4z}	σ_x	σ_{y-x}	σ_y	σ_{x+y}
$\begin{pmatrix} 1 & 0 \\ 0 & 1 \end{pmatrix}$	$\begin{pmatrix} 0 & -1 \\ 1 & 0 \end{pmatrix}$	$\begin{pmatrix} -1 & 0 \\ 0 & -1 \end{pmatrix}$	$\begin{pmatrix} 0 & 1 \\ -1 & 0 \end{pmatrix}$	$\begin{pmatrix} -1 & 0 \\ 0 & 1 \end{pmatrix}$	$\begin{pmatrix} 0 & 1 \\ 1 & 0 \end{pmatrix}$	$\begin{pmatrix} 1 & 0 \\ 0 & -1 \end{pmatrix}$	$\begin{pmatrix} 0 & -1 \\ -1 & 0 \end{pmatrix}$

For these 2-dimensional irr. reps., the fourth condition of Landau theory must be tested first. This consideration is carried out for the 2-D small rep. at the M-point in Table 5. The conclusion from Table 5 is that the vector rep. and antisymmetric square of the small rep. are orthogonal for the E_g and E_u reps. ($\Sigma\ V(g)\cdot\{\chi^2(g)-\chi(g^2)\} = 0$) and therefore the product does not contain the vector representation, and hence the fourth condition is met by the 2-D small rep. at the M-point.

Table 5 Fourth condition of Landau theory at the M-point

g	E	$2C_4$	C_2	$2C_2'$	$2C_2''$	i	$2S_4$	σ_h	$2\sigma_v$	$2\sigma_d$
g^2	E	$2C_2$	E	2E	2E	E	$2C_2$	E	2E	2E
$\chi(g)$	2	0	-2	0	0	2	0	-2	0	0
$\chi(g^2)$	2	-2	2	2	2	2	-2	2	2	2
$\chi^2(g)$	4	0	4	0	0	4	0	4	0	0
$\chi^2(g)-\chi(g^2)$	2	2	2	-2	-2	2	2	2	-2	-2
$V(g)$	3	1	-1	-1	-1	-3	-1	1	1	1
$V(g)\cdot\{\chi^2(g)-\chi(g^2)\}$	6	2	-2	2	2	-6	-2	2	-2	-2

$\Sigma\ V(g)\cdot\{\chi^2(g)-\chi(g^2)\} = 0$

If a transition corresponds to the wave vector $k = (a^* + b^*)/2$, the basis functions are antisymmetric with respect to

the translational symmetry operations, a° and b°, and symmetric with respect to $a^\circ + b^\circ$ and c°.

In the E_g case, the allowed symmetries of the low-symmetry structure can be determined by examining basis functions that transform as the irr. rep.:

$$\phi_1 = \sin \pi x \cos \pi y \sin 2\pi z \, \phi_t$$

$$\phi_2 = \sin \pi y \cos \pi x \sin 2\pi z \, \phi_t$$

and

$$\phi_t = (\cos 2\pi x - \cos 2\pi y)(\cos 2\pi y - \cos 2\pi z)(\cos 2\pi z - \cos 2\pi x)$$

There are no third-order invariant combinations of these functions. For example, the basis function $\phi_1 \rightarrow -\phi_2$ and $\phi_2 \rightarrow \phi_1$ under the operation of C_{4z}, and thus $\phi_1^3 + \phi_2^3 \rightarrow \phi_2^3 - \phi_1^3$ and $\phi_1\phi_2^2 + \phi_1^2\phi_2 \rightarrow \phi_1\phi_2^2 - \phi_1^2\phi_2$. As a result, the third condition of Landau theory is met.

There are two independent fourth-order invariants, namely $\phi_1^4 + \phi_2^4$ and $\phi_1^2\phi_2^2$, and thus two fourth-order terms in the expansion of the Gibbs free-energy. Thus, making use of $\gamma_1^2 + \gamma_2^2 = 1$, G to terms of fourth-order is:

$$G = G^\circ + A\eta^2 + [C_1 + C_2(\gamma_1^4 + \gamma_2^4)]\eta^4$$

There are two possible minima for this G, namely $\gamma_1 = 1$ and $\gamma_2 = 0$ (or vice versa) and $\gamma_1 = \gamma_2 = 1/\sqrt{2}$. For the first solution, the single basis function ϕ_1 transforms into

itself under the operations E, C_{2y}, i and σ_y and also under the operations C_{2z}, C_{2x}, σ_z and σ_x when those operations are combined with a lost translation, a° or b°. The resultant space group is Cmma with the lattice parameters a ≃ b ≃ 2a° and c ≃ a°. For second solution, the basis function $\phi_1 + \phi_2$ transforms into itself under the operations E, $C_{2(y-x)}$, i, and σ_{y-x} and also under the operations C_{2z}, $C_{2(x+y)}$, σ_z, and σ_{x+y} when those operations are combined with a lost translation, a° or b°. The resultant space-group symmetry is Pmna with the lattice parameters b ≃ a° and a ≃ c ≃ $\sqrt{2}$a°. Since neither of these results correponds to a known structure the analysis of the E_g case is terminated here.

In the E_u case, a complete analysis is given. Two basis functions corresponding to the E_u irr. rep. at k = (a* + b*)/2 are:

$$\phi_1 = \sin \pi x \cos \pi y$$
$$\phi_2 = \sin \pi y \cos \pi x$$

and the other four basis functions corresponding to the rest wave vectors in the star, (a* + c*)/2 and (b* + c*)/2 are:

$$\phi_4 = \sin \pi z \cos \pi x$$
$$\phi_3 = \sin \pi x \cos \pi z$$

and

$$\phi_5 = \sin \pi y \cos \pi z$$

$\phi_6 = \sin \pi z \cos \pi y$

respectively.

Next it is necessary to consider the third-order invariants. Since the basis functions $\phi_i \rightarrow -\phi_i$ under the operation of inversion through the origin, no third-order invariant exists.

The following independent fourth-order invariants are found:

1. $\phi_1^4 + \phi_2^4 + \phi_3^4 + \phi_4^4 + \phi_5^4 + \phi_6^4$
2. $\phi_1^2\phi_2^2 + \phi_3^2\phi_4^2 + \phi_5^2\phi_6^2$
3. $\phi_1^2\phi_3^2 + \phi_3^2\phi_5^2 + \phi_1^2\phi_5^2 + \phi_2^2\phi_4^2 + \phi_4^2\phi_6^2 + \phi_2^2\phi_6^2$
4. $\phi_1^2\phi_4^2 + \phi_3^2\phi_6^2 + \phi_2^2\phi_5^2$
5. $\phi_1^2\phi_6^2 + \phi_2^2\phi_3^2 + \phi_4^2\phi_5^2$

Since $(\Sigma\ \gamma_i^2)^2 = \Sigma\ \gamma_i^4 + 2 \underset{i<j}{\Sigma}\ \gamma_i^2\gamma_j^2 = 1$, the $\Sigma\ \gamma_i^4$ term can be eliminated. Thus the expansion of the Gibbs free-energy, G, to terms of fourth order, is expressed by

$$\begin{aligned} G = G^\circ + A\eta^2 + [&C_1 + (\gamma_1^2\gamma_2^2+\gamma_3^2\gamma_4^2+\gamma_5^2\gamma_6^2)C_2 \\ &+ (\gamma_1^2\gamma_3^2+\gamma_3^2\gamma_5^2+\gamma_1^2\gamma_5^2+\gamma_2^2\gamma_4^2+\gamma_4^2\gamma_6^2+\gamma_2^2\gamma_6^2)C_3 \\ &+ (\gamma_1^2\gamma_4^2+\gamma_3^2\gamma_6^2+\gamma_2^2\gamma_5^2)C_4 \\ &+ (\gamma_1^2\gamma_6^2+\gamma_2^2\gamma_3^2+\gamma_4^2\gamma_5^2)C_5]\eta^4, \end{aligned}$$

and the possible stable space groups are found by minimizing G with respected to the γ_i under the constraint $\Sigma\ \gamma_i^2 = 1$. This can be accomplished using Lagrange's method of undetermined multipliers. The following equations are obtained

$$\lambda\gamma_1 + C_2\gamma_1\gamma_2^2 + C_3\gamma_1(\gamma_3^2 + \gamma_5^2) + C_4\gamma_1\gamma_4^2 + C_5\gamma_1\gamma_6^2 = 0$$
$$\lambda\gamma_2 + C_2\gamma_2\gamma_1^2 + C_3\gamma_2(\gamma_4^2 + \gamma_6^2) + C_4\gamma_2\gamma_5^2 + C_5\gamma_2\gamma_3^2 = 0$$
$$\lambda\gamma_3 + C_2\gamma_3\gamma_4^2 + C_3\gamma_3(\gamma_1^2 + \gamma_5^2) + C_4\gamma_3\gamma_6^2 + C_5\gamma_3\gamma_2^2 = 0$$
$$\lambda\gamma_4 + C_2\gamma_4\gamma_3^2 + C_3\gamma_4(\gamma_2^2 + \gamma_6^2) + C_4\gamma_4\gamma_1^2 + C_5\gamma_4\gamma_5^2 = 0$$
$$\lambda\gamma_5 + C_2\gamma_5\gamma_6^2 + C_3\gamma_5(\gamma_1^2 + \gamma_3^2) + C_4\gamma_5\gamma_2^2 + C_5\gamma_5\gamma_4^2 = 0$$
$$\lambda\gamma_6 + C_2\gamma_6\gamma_5^2 + C_3\gamma_6(\gamma_2^2 + \gamma_4^2) + C_4\gamma_6\gamma_3^2 + C_5\gamma_6\gamma_1^2 = 0$$
$$\gamma_1^2 + \gamma_2^2 + \gamma_3^2 + \gamma_4^2 + \gamma_5^2 + \gamma_6^2 = 1$$

where λ is the undetermined multiplier. These equations can be solved step by step to setting different sets of γ_i's to zero. These are two types of solutions, "discrete" and "continuous". All nonzero γ_i in the case of discrete solutions are equal, but they are not equal in the case of continuous solutions. The discrete solutions are listed below:

1. $\gamma_1 = 1,\ \gamma_{i\neq1} = 0;\ C_i > 0$
2. $\gamma_1 = \gamma_2 = 1/\sqrt{2},\ \gamma_{i>2} = 0;\ C_2 < 0,\ C_{i\neq2} > 0$
3. $\gamma_1 = \gamma_4 = 1/\sqrt{2},\ \gamma_2 = \gamma_3 = \gamma_5 = \gamma_6 = 0;\ C_4 < 0,\ C_{i\neq4} > 0$

4. $\gamma_1 = \gamma_6 = 1/\sqrt{2}$, $\gamma_2 = \gamma_3 = \gamma_4 = \gamma_5 = 0$; $C_5 < 0$, $C_{i\neq 5} > 0$

5. $\gamma_1 = \gamma_3 = \gamma_5 = 1/\sqrt{3}$, $\gamma_2 = \gamma_4 = \gamma_6 = 0$; $C_3 < 0$, $C_{i\neq 3} > 0$

6. $\gamma_i = 1/\sqrt{6}$; $(C_2 + 2C_3 + C_4 + C_5)/3 < C_2$, C_4, C_5, and $4C_3/3$.

The symmetry of the first solution (for the transition corresponding to a single wave vector $k = (a^* + b^*)/2$) can determined by examining the single basis function ϕ_1. The basis function ϕ_1 transforms into itself under the operations E, C_{2x}, σ_y and σ_z and also under the operations C_{2y}, C_{2z}, i and σ_x when those operations are combined with a lost translation such as a° or b°. The resultant space group is Cmmm with the lattice parameters $a \simeq b \simeq 2a°$ and $c \simeq a°$.

The second solution can be determined by examining the combination of basis functions $\phi_1 + \phi_2$. The basis function $\phi_1 + \phi_2$ translation into itself under the operations E, $C_{2(x+y)}$, σ_z and σ_{y-x} and also under the operations C_{2z}, $C_{2(y-x)}$, i and σ_{x+y} when those operations are combined with a lost translation such as a° or b°. The resultant space group is Pmma with lattice parameters $a \simeq c \simeq \sqrt{2}a°$ and $b \simeq a°$. The known example for this case is AuCd which has a high-temperature form with the CsCl-type structure and a low-temperature form with Pmma symmetry. The parameters for the low-temperature are a = 4.7644 Å, b = 3.1540 Å, and c =

4.8643 Å with atomic positions at 1/4, 1/2, 0.812 and 1/4, 1/2, and 0.313.[27]

The remainder of the solutions can be determined by the procedure described above. The low-symmetry structures for these solutions have space-groups I4/mmm, I4/mmm, I23, and R3m, respectively, with $a \simeq b \simeq c \simeq 2a°$.

The continuous solutions are found to be combinations of two discrete solutions. For example, the combination of the $\gamma_1 = \gamma_2 = 1/\sqrt{2}$ and the $\gamma_1 = \gamma_4 = 1/\sqrt{2}$ is $\gamma_1 \neq \gamma_2 \neq \gamma_4 \neq 0$ and $\gamma_3 = \gamma_5 = \gamma_6 = 0$. The possible space groups are found by minimizing G with respected to γ_i under the constraint $\Sigma \gamma_i^2 = 1$, just as in the discrete cases. For example, the following equations are obtained for the case γ_1, γ_2, and $\gamma_4 \neq 0$ and all other $\gamma_i = 0$:

$$\lambda + C_2\gamma_2^2 + C_4\gamma_4^2 = 0$$
$$\lambda + C_2\gamma_1^2 + C_3\gamma_4^2 = 0$$
$$\lambda + C_3\gamma_2^2 + C_4\gamma_1^2 = 0$$

Thus the continuous solution for the case are:

$$\gamma_1^2 = (C_2C_3 + C_3C_4 - C_3^2)/(2(C_2C_3 + C_3C_4 + C_2C_4) - C_2^2 - C_3^2 - C_4^2)$$

$$\gamma_2^2 = (C_2C_4 + C_3C_4 - C_4^2)/(2(C_2C_3 + C_3C_4 + C_2C_4) - C_2^2 - C_3^2 - C_4^2)$$

$$\gamma_4^2 = (C_2C_3 + C_2C_4 + C_2^2)/(2(C_2C_3 + C_3C_4 + C_2C_4) - C_2^2 - C_3^2 - C_4^2)$$

where the γ_i' s are functions of state because the C_i's are. For some choice of the C_i's these γ_i's yield a G lower than for any discrete solution, insuring that the continuous solutions correspond to minima as well, perhaps, as saddle points. For the case of negative C_2, C_3, C_4 and positive C_5, if C_2 is sufficiently negative then the stable solution is the discrete solution $\gamma_1 = \gamma_2 = 1/\sqrt{2}$ with Pmma symmetry, if C_4 sufficiently negative then the stable solution is the discrete solution $\gamma_1 = \gamma_4$ with I/4mmm symmetry, and if $C_3 < 3C_2/4$ and $3C_4/4$ then the stable solution is the discrete solution $\gamma_1 = \gamma_2 = \gamma_3 = 1/\sqrt{3}$ with I23. The low-symmetry structure for the continuous solution with γ_1, γ_2, and γ_4 nonzero is P2/m with $a \simeq b \simeq c \simeq 2a°$ and this symmetry with $G = G° + A\eta^2 + (C_1 + C')\eta^4$ is stable when $C' < C_2/4$, $C_4/4$, and $C_3/3$. Similarly, the continuous solutions for the combination of nonzero γ_1, γ_2 and γ_6 and γ_1, γ_4, and γ_6 can be obtained. The low-symmetry forms for these two case are P2/m and Pmm2, respectively, with $a \simeq b \simeq c \simeq 2a°$.

REFERENCES

1. Massalski, T. B.; Murray, J. L.; Benett, L. H.; Baker, H. "Binary Alloy Phase Diagrams"; American Society for Metals: Metals Park, OH, 1986.

2. Landau, L.; Lifshitz E. "Statistical Physics"; Pergamon Press: London, 1958.

3. Kadomatsu, H.; Kurisu, M.; Fujiwara, H. J. Phys. F. 1987, 17, L305.

4. Morris, D. P.; Morris, J. G. Acta Met. 1978, 26, 547.

5. Folkerts, W.; Haas, C. J. Less-Common Met. 1989, 147, 181.

6. Kadomatsu, H.; Kurisu, M.; Fujiwara, H. Phys. Lett. A 1983, 94, 178.

7. Ihrig, H.; Vigren, D. T.; Kubler, J.; Methfessel, S. Phys. Rev. B 1973, 8, 4525.

8. Ghatak, S. K.; Ray, D. K.; Tannous, C. Phys. Rev. B 1978, 18, 5379.

9. Schilling, J. S.; Methfessel, S.; Shelton, R. N. Solid State Commun. 1977, 24, 659.

10. Kurisu, M.; Kadomatsu, H.; Fujiwara, H. J. Phys. Soc. Jpn. 1983, 52, 4349.

11. Kadomatsu, H.; Kurisu, M.; Fujiwara, H. J. Phys. Soc. Jpn. 1984, 53, 1819.

12. Franzen, H. F. "Physical Chemistry of Inorganic Crystalline Solids"; Springer-Verlag: Heidelberg, 1986.

13. Tolédano, J. -C.; Tolédano, P. "The Laudau Theory of Phase Transition"; World Scientific Lecture Notes in Physics, Vol. 3, World Scientific Publishing: Singapore, 1987.

14. Giessen, B. C.; Dangel, P. N.; Grant, N. J. J. Less-Commom Met. 1967, 13, 62.

15. Imoto, H. Ames Laboratory, Iowa State University, Ames, IA, Unpublished research, 1978.

16. Wiles, D. B.; Young, R. A. J. Appl. Crystallogr. Chem. 1981, 14, 149.

17. Kim, S.-S. Ph.D. Dissertation, Iowa Sate University, Ames, IA, 1986.

18. Rietveld, H. M. Acta Crystallogr. 1967, 22, 151.

19. Rietveld, H. M. J. Appl. Crystallogr. 1969, 2, 65.

20. Young, R. A.; Wiles, D. B. J. Appl. Crystallogr. 1982, 15, 430.

21. Young, R. A.; Wiles, D. B. Adv. X-ray Anal. 1981, 24, 1.

22. Chen, B. H.; Jacobson, R. A., to be published, Department of Chemistry, Iowa State University.

23. Franzen, H. F., private communication, Department of Chemistry, Iowa State University.

24. Chen, B. H.; Franzen, H. F. J. Less-Common Met. 1988, 143, 331.

25. Kovalev, O. V. "Irreducible Representations of the Space Groups"; Translated by A. Murray Gross, Gordon and Breach: New York, 1965.

26. Zalkin, A; Ramsey, W. J. J. Phys. Chem. 1957, 61, 1413.

27. Chang, L. C.; Read, T. A. J. Metals 1951,33, 47.

SECTION I PHASE TRANSITIONS IN THE $Mn_{1\pm x}Au_{1\pm y}$ HOMOGENEITY RANGE

INTRODUCTION

The crystal structures and the phase diagrams of gold-manganese alloys in the equiatomic region have been largely determined by the measurement of X-ray diffraction, neutron diffraction, microscopy, magnetic susceptibility, electrical resistivity, and thermodynamic properties. Most of the previous papers showed that the AuMn alloy has the CsCl-type structure at high temperature and it distorts to antiferromagnetic tetragonal material, t_1, with $c/a < 1$, and also t_2, with $c/a > 1$ on cooling. In addition, below 240°C, an orthorhombic AuMn was reported by Stolz and Schubert.[1]

The constitution in the region 45-55 atomic % Au is rather complex. Although many phase diagrams[2-10] with a CsCl-type phase Au-Mn have been reported, a satisfactory construction based on the available data has not been obtained. The construction of the phase boundaries in the phase diagrams mentioned above is unusual. Analysis of the boundaries using the Gibbs-Konovalow equation[11] and the Landau theory[12,13] of symmetry and phase transitions indicates some unresolved problems.

The previously accepted phase diagram[7,8] showed the CsCl-type phase to distort to t_1 by a second-order transition. On further cooling, alloys containing less than 50 atomic % Au underwent a first-order transition to t_2. The diagram shows that the $t_1 \rightarrow t_2$ phase transition under a

change in temperature is first order but in composition second order.

The currently accepted phase diagram[1] (Figure I-1) for the Au-Mn system shows the formation of two tetragonal forms, t_1 with Au/Mn > 1 and t_2 with Au/Mn < 1, at low temperatures and a CsCl-type cubic form, c, at high temperature in the region 0.9 < Au/Mn < 1.1 and T < 200°C. According to the phase diagram, there is no two phase region separating t_1 and t_2, and, therefore, the phase transition between t_1 and t_2 should be second order. Since both t_1 and t_2 have AuCu-type structure with P4/mmm symmetry, during a continuous transition from t_1 to t_2 the phase must pass through a cubic system with Pm3m symmetry. However, no cubic phase is shown in the phase diagram between the two tetragonal phases. A transition from Pm3m to P4/mmm without loss of translation symmetry involves a decrease by a factor of 3 in the number of symmetry elements, a factor which requires a third-order invariant in the order parameter, which in turn requires a first-order transition. In addition, the slope, $(\partial T / \partial X_A^{\alpha})_P$, of the T-X phase diagram is infinity. In contrast, applying the Gibbs-Konovalow equation to this case indicates the slope should not be infinity because $\Delta X = 0$ and $\Delta S = 0$ if the transition is second-order. Therefore, a study of the Au-Mn system in the region 0.88 < Au/Mn < 1.05 was undertaken

using high-temperature powder X-ray diffraction to study the phase equilibria.[14]

RESULTS

As mentioned above, the X-ray analysis for the Au-Mn system in this study was complex because c, t_1, and t_2 have diffraction peaks at nearly the same Bragg angles and because two phase fields, c-t_1 and t_1-t_2, are quite narrow in some regions. The difficulties of the X-ray analysis have resulted in many mistakes in previous investigations of the Au-Mn system. In this study, the intensities of the diffraction lines were carefully analyzed between room temperature and 150°C with 3°C per step in order to identify the one- and two-phase regions. For example, the intensity of the {101} diffraction line is twice as large as that of the line {110} for a single tetragonal phase.

By careful investigation, it was found that the CsCl-type AuMn distorts to a tetragonal structure with $c/a < 1$ and further distorts to another tetragonal structure with $c/a > 1$ on cooling as shown in Figure I-2. Some calculated and observed X-ray diffraction patterns in the Au-Mn system are shown in Figures I-3, I-4, and I-5. The diffraction patterns for Au/Mn = 1.01 at 600°C in Figure I-3 are an example of the CsCl-type cubic with a = 3.2423 Å. The diffraction patterns for Au/Mn = 1.05 at room temperature in Figure I-4 are an example of the AuCu-type tetragonal, t_1, with a = 3.2627 Å and b = 3.1375 Å. The diffraction patterns for Au/Mn = 1.01 at room temperature in Figure I-5

are mixture of t_1 and t_2 with a = 3.2735 Å and b = 3.1012 Å for t_1 and a = 3.1707 Å and b = 3.2993 Å for t_2. The ΔV = 0.063 $Å^3$ for these two phases indicating that the phase transition is first order. Also, it is interesting to note that both t_1 and t_2 have the same {111} diffraction line because the bond lengths are the same for both phases in equilibrium. The phase diagram based on the X-ray diffraction data with full lines for the investigated region was shown in Figure I-6. The regions enclosed by broken lines are schematic and were constructed so as to agree with Landau theory and the Gibbs-Konovalow equation.

The Landau theory can be applied to the $c \rightarrow t_1 \rightarrow t_2$ transitions because these transitions meet the following conditions: (1) P4/mmm is a subgroup of Pm3m; (2) the transition corresponds to the E_g irreducible representation of the cubic group at the zone center; (3) the product of the antisymmetrized square with the vector representation does not contain the identity representation, meeting the Lifschitz condition as shown in Table I-1. Furthermore, a third-order invariant exists requiring that there should be a third-order term in the expansion of the Gibbs free energy in the order parameter, and thus that the transition should occur as a first-order transition.

Table I-1 The application of Lifschitz condition for E_g

	E	$8C_3$	$6C_2$	$6C_4$	$3C_2$	i	$6S_4$	$8S_6$	$3\sigma_h$	$6\sigma_d$
g^2	E	$8C_3$	6E	$6C_2$	3E	E	$6C_2$	$8C_3$	3E	6E
$\chi(g)$	2	-1	0	0	2	2	0	-1	2	0
$\chi(g^2)$	2	-1	2	0	2	2	0	-1	2	2
$\chi^2(g)$	4	1	0	0	4	4	0	1	4	0
$\chi^2(g)-\chi(g^2)$	2	2	-2	0	2	2	0	2	2	-2
$V(g)$	3	3	-1	1	-1	-3	-1	0	1	1
$V(g)\{\chi^2(g)-\chi(g^2)\}$	6	0	2	0	-2	-6	0	0	2	-2

$\Sigma\, V(g)\{\chi^2(g) - \chi(g^2)\} = 0.$

It has been shown[13] that the sign of the third-order term determines whether $c/a > 1$ or $c/a < 1$, and thus the observation that both t_1 and t_2 are stable phases requires that the coefficient of the third-order term should vanish at some of the states under consideration. This conclusion in turn leads to the following as the appropriate Landau expansion of G in the order parameter η (corresponding to the E_g irreducible representation of Pm3m at the zone center)

$$G = G^\circ + A\,\eta^2 + B\,\eta^3 + C\,\eta^4 + D\,\eta^6$$

where G° is the Gibbs free energy of the cubic phase and the coefficients are functions of T and X (= n_{Au} / n_{Mn}) at constant pressure. A > 0 (otherwise the value $\eta = 0$ would correspond to a maximum of G), B > 0 when t_1 is stable and B < 0 when t_2 is stable[13], C < 0, and D > 0 (otherwise G goes toward minus infinity for large values of η and G would decrease without bound). A variety of circumstances is then possible for a given t-X point: (1) c stable (Figure I-7(d)); (2) c and t_1 stable (Figure I-7(b)); (3) t_1 stable (Figure I-7(c)); (4) t_1 and t_2 coexist (Figure I-7(d)); (5) t_2 stable (Figure I-7(e)); (6) c, t_1, and t_2 coexist (Figure I-7(f)). Figures I-7(b), I-7(d), and I-7(f) represent hypothetical equilibria because for each diagram the coexisting phases would have the same value of X. What must be considered, in addition to the phase change, is the redistribution of components allowing the compositions to change.

For example, consider a stable system at 110°C with Mn/Au = 1.00. When the sample is cooled to some temperature in the c + t_1 two-phase region Figure I-7(b) is appropriate for the hypothetical equicomposition equilibrium of c and t_1, and redistribution of gold and manganese results in coexistence of c and t with different compositions. Further cooling to temperatures below the c + t_1 two-phase region results in the situation of Figure I-7(c).

Somewhere in the $t_1 + t_2$ two-phase region, B = 0 and Figure I-7(d) is appropriate for the hypothetical equicomposition equilibrium and redistribution of gold and manganese results in the two-phase $t_1 + t_2$ equilibrium. Similarly further cooling would eventually result in the situation of Figure I-7(e), and t_2 would then be stable with respect to phase change.

The points defined by B = 0 in t_1 and t_2 two-phase region define a T-X line. If the states along this line (t_1 and t_2 coexist)) are considered with increasing temperature, then because A increases with T (relative to the magnitudes of B and C) eventually the circumstance of Figure II-7(f), i.e., hypothetical coexistence of c, t_1 and t_2 all with the same X, would be reached. After redistribution a $c + t_1 + t_2$ three-phase equilibrium would result. This line of reasoning is the basis for the broken line extensions shown in Figure I-6.

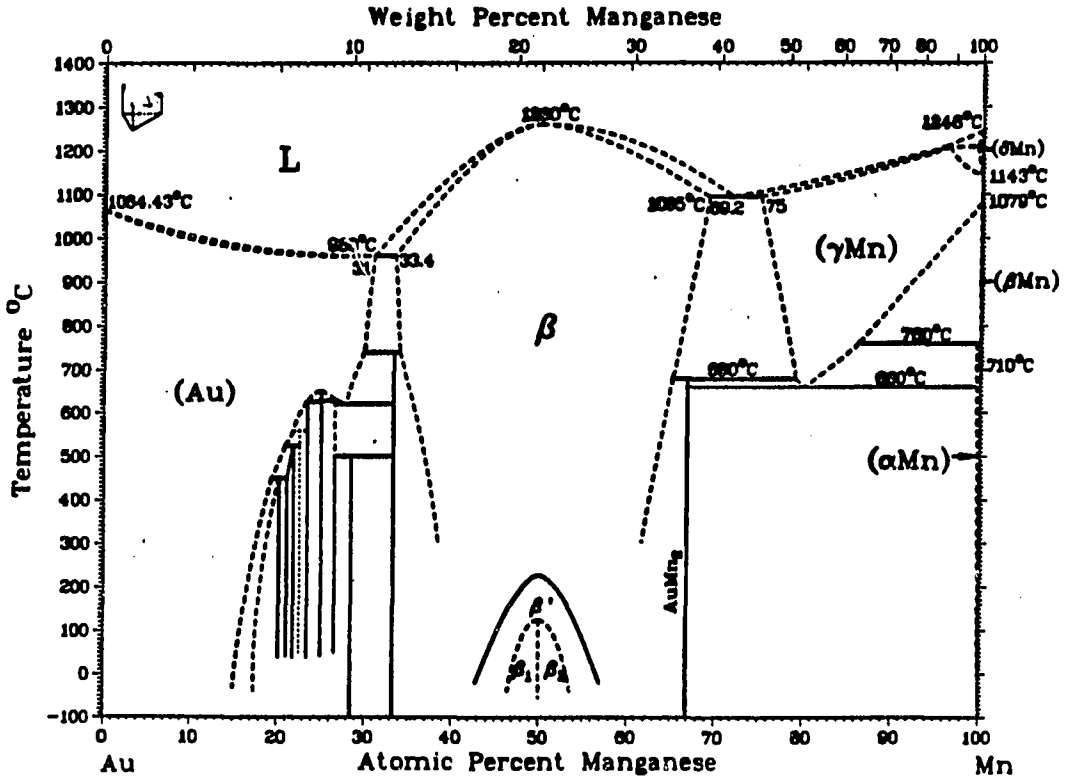

Figure I-1 The currently accepted phase diagram for the Au-Mn system.[1] The β′ phase has the CsCl-type structure and the β_1 with c/a < 1 and β_2 with c/a > 1 phase have the AuCu-type structure

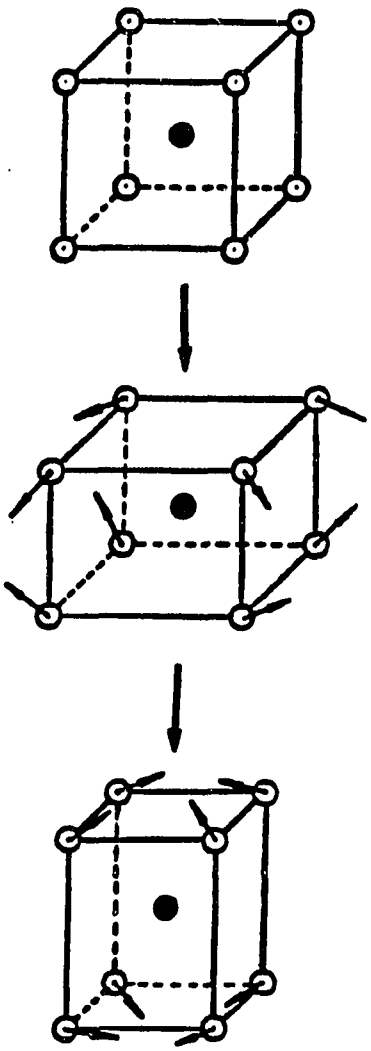

Cubic (c)

CsCl-type

Pm3m

Tetragonal (t_1)

AuCu-type, c/a < 1

P4/mmm

Tetragonal (t_2)

AuCu-type, c/a > 1

P4/mmm

● Au Atoms ○ Mn Atoms

Figure I-2 The phase transitions c → t_1 → t_2 on cooling

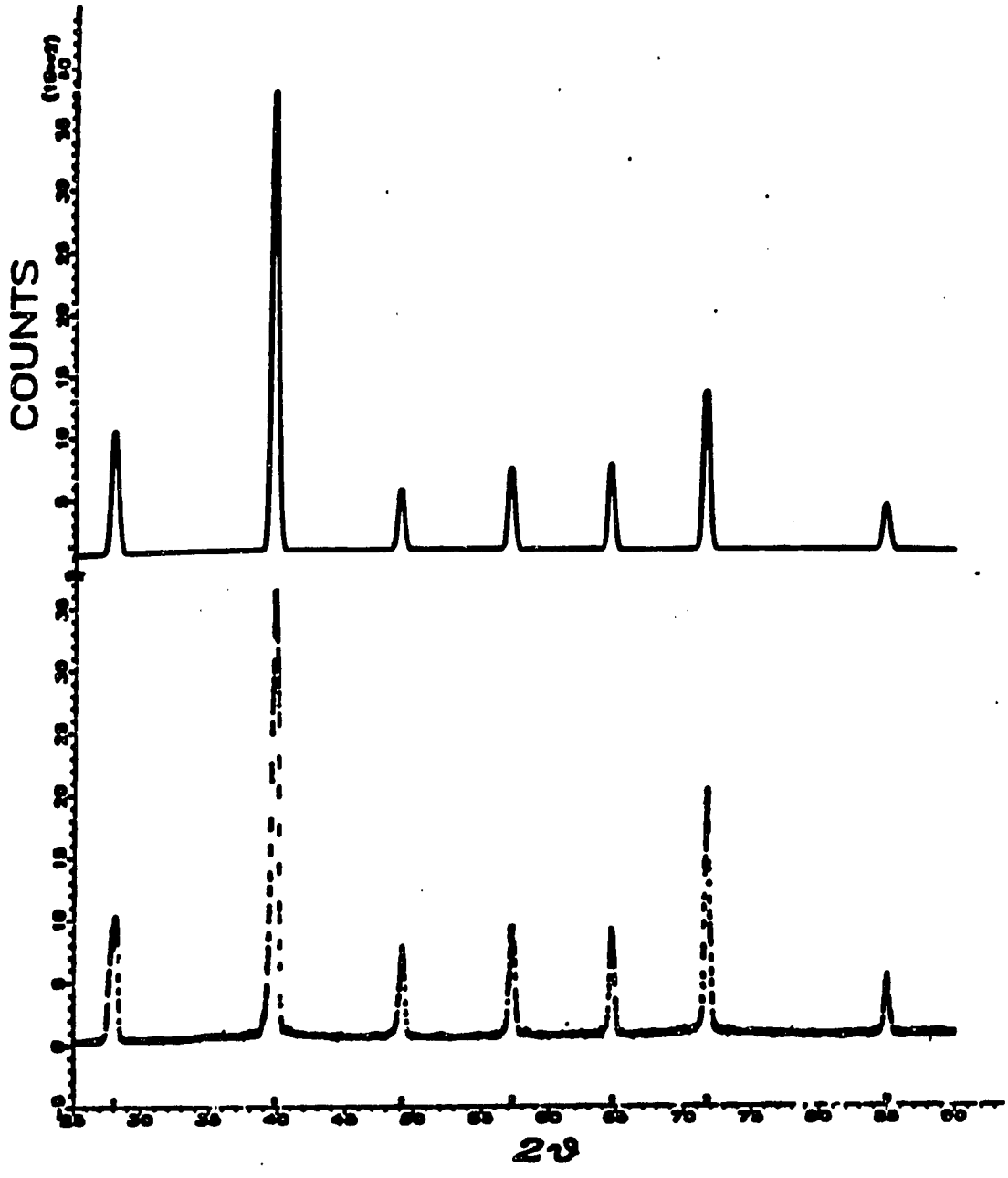

Figure I-3 Comparison of calculated and observed diffraction patterns for Au/Mn = 1.01 at 600°C

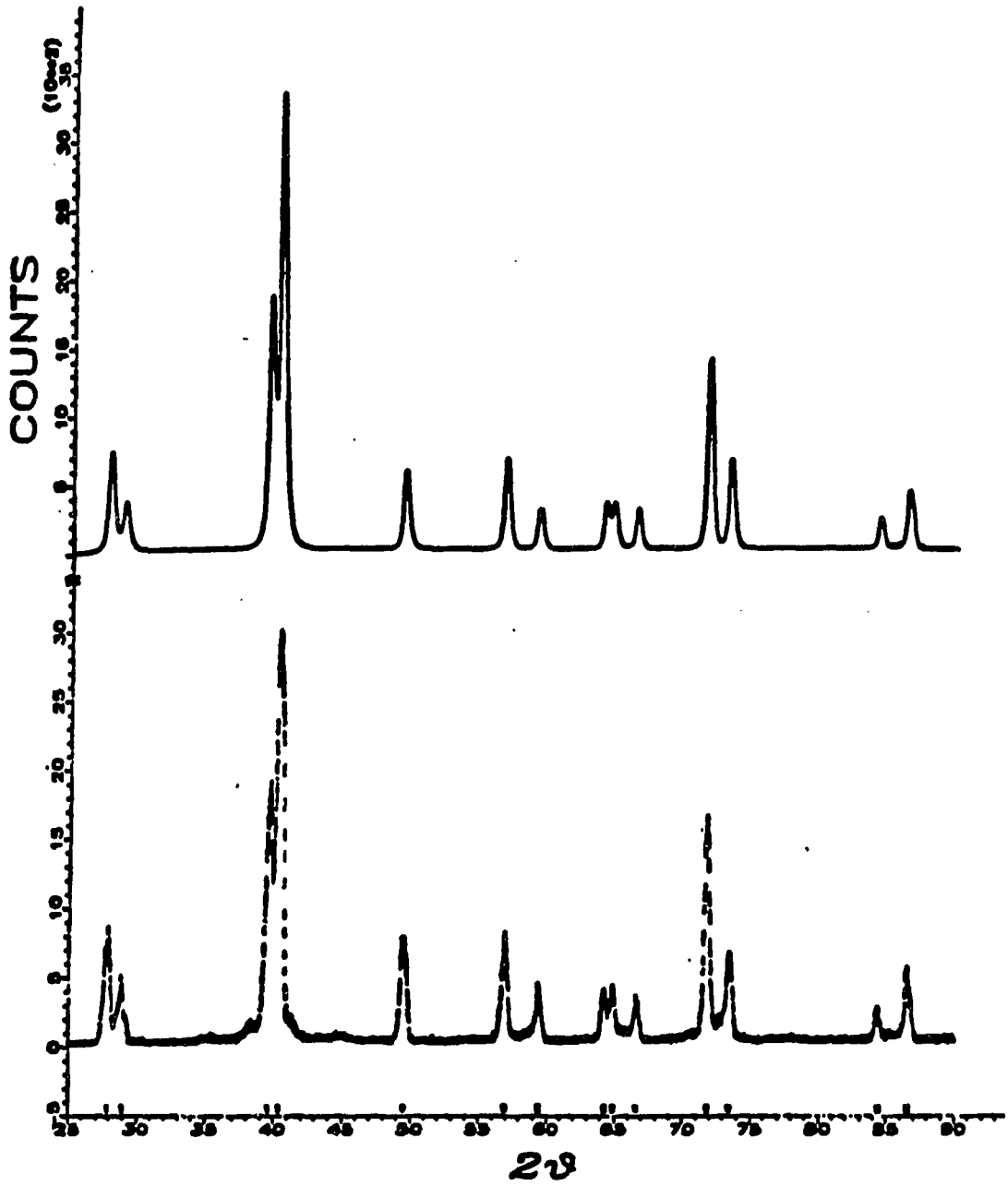

Figure I-4 Comparison of calculated and observed diffraction patterns for Au/Mn = 1.05 at room temperature

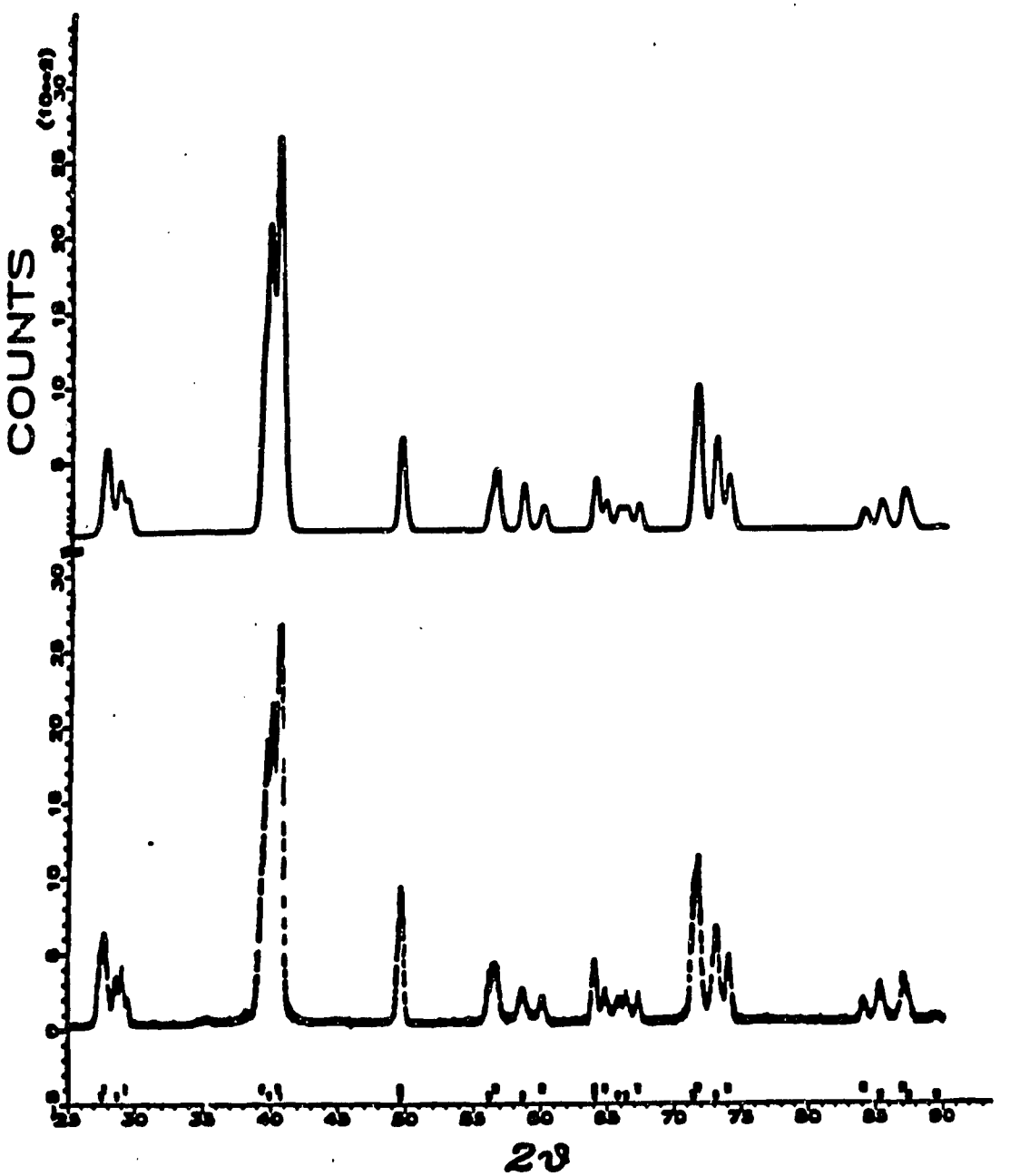

Figure I-5 Comparison of calculated and observed diffraction patterns for Au/Mn = 1.01 at room temperature

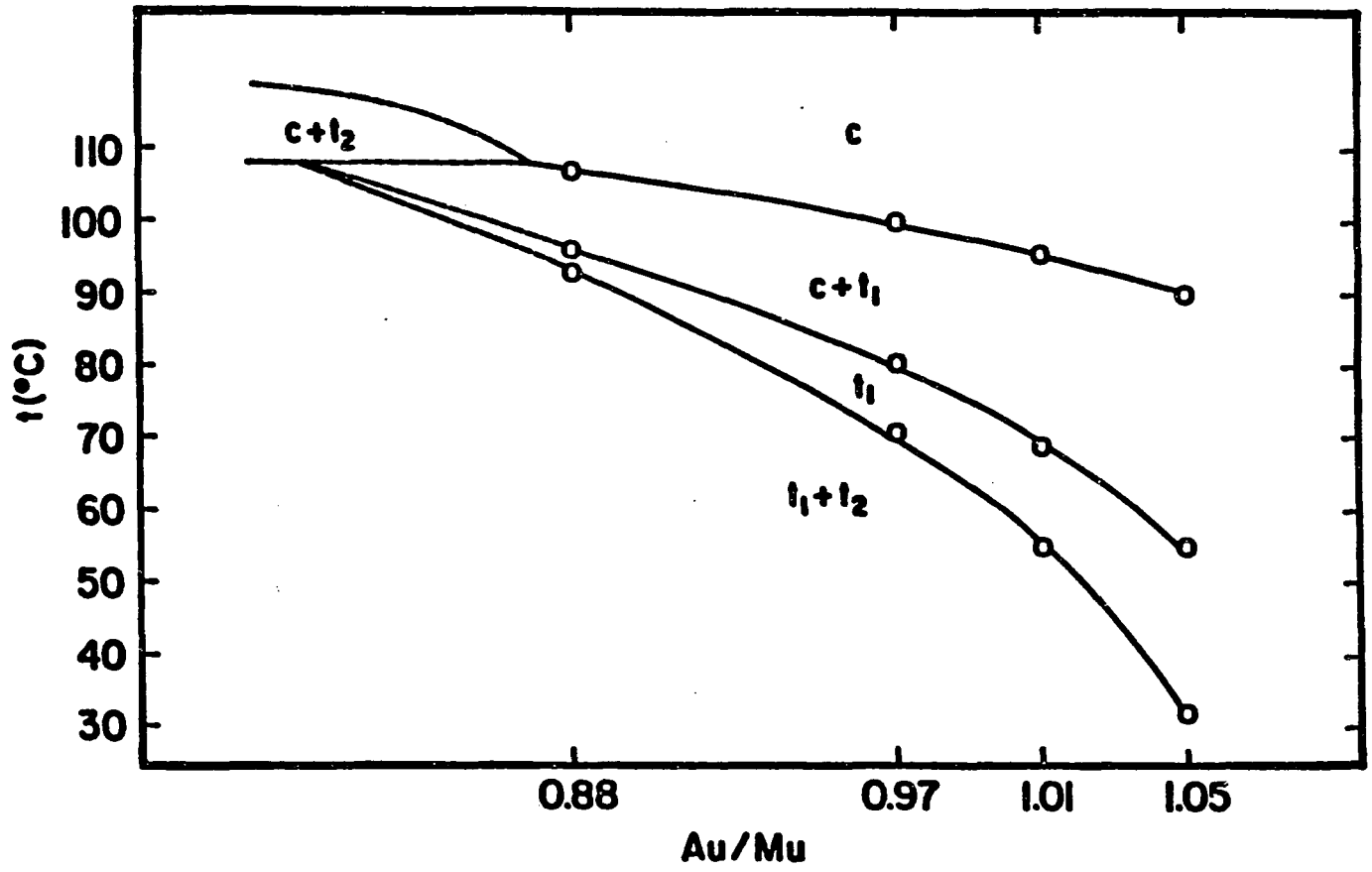

Figure I-6 Phase diagram for the Au-Mn system in the region $0.88 < AuMn < 1.05$ and $25°C < T < 110°C$ with suggested extension to the $c \rightarrow t_1 \rightarrow t_2$ equilibrium

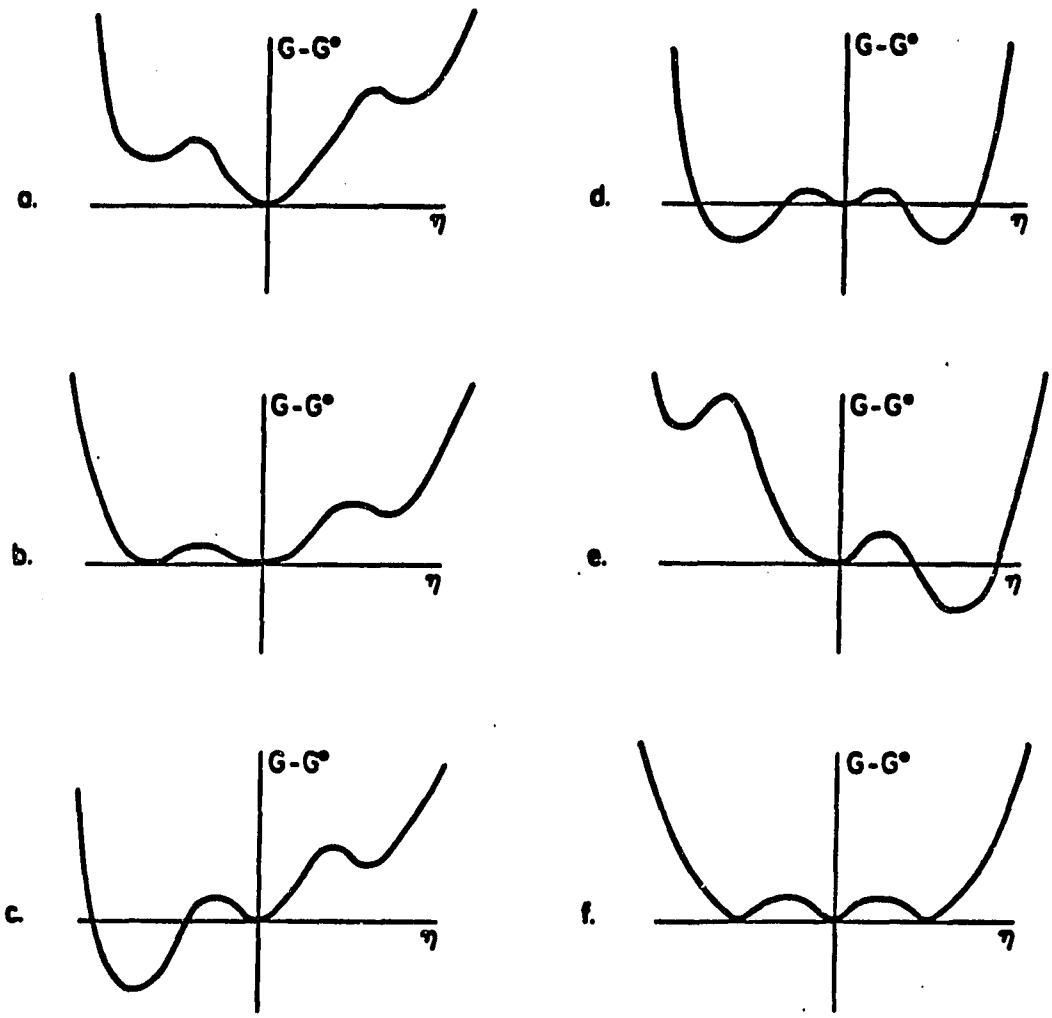

Figure I-7 G vs. η curves for different relative values of the expansion coefficients (a) c stable; (b) c + t_1 coexist; (c) t_1 stable; (d) t_1 + t_2 coexist; (e) t_2 stable; (f) c + t_1 + t_2 coexist

CONCLUSIONS

Observations in the AuMn homogeneity using powder X-ray diffraction at temperatures between 25 and 150°C demonstrate that the transitions $c \rightarrow t_1 \rightarrow t_2$ occur consecutively as first-order phase transitions with decreasing temperature. An allowed continuation of the T-X phase diagram is suggested via broken lines in Figure I-6.

REFERENCES

1. Stolz, E.; Schubert, K. Z. Metallk. 1962, 53, 433.
2. Massalski, T. B.; Murray, J. L.; Benett, L. H.; Baker, H. "Binary Alloy Phase Diagrams"; American Society for Metals: Metals Park, OH, 1986.
3. Raub, E.; Zwicker, U.; Raub, H. Z. Metallkd. 1953, 44(7), 312.
4. Kussmann, A.; Raub, E. Z. Metallkd. 1956, 47(1), 9.
5. Hansen, M.; Anderko, K.; "Constitution of Binary Alloys"; McGraw-Hill: New York, 1958, 214.
6. Bacon, G. E.; Street, R. Proc. Phys. Soc. London, 1958, 72, 470.
7. Smith, J. H.; Gaunt, P. Acta Met. 1961, 9, 819.
8. Elliott, R. P. "Constitution of Binary Alloys"; First Supplement, McGraw-Hill: New York, 1965.
9. Shunk, F. A. "Constitution of Binary Alloys"; Second Supplement, McGraw-Hill: New York, 1969.
10. Finbow, G. E.; Gaunt, Acta Met. 1969, 17, 41.
11. Franzen, H. F. "Physical Chemistry of Inorganic Crystalline Solids"; Springer-Verlag: Heidelberg, 1986.
12. Landau, L.; Lifshitz E. "Statistical Physics"; Pergamon Press: London, 1958.
13. Tolédano, J. -C.; Tolédano, P. "The Laudau Theory of Phase Transition"; World Scientific Lecture Notes in Physics, Vol. 3, World Scientific Publishing: Singapore, 1987.
14. Chen, B. H.; Franzen, H. F. J. Less-Common Met. 1988, 143, 331.

SECTION II PHASE TRANSITIONS IN RhTi

INTRODUCTION

Several structures for phases in the homogeneity range of RhTi were listed in the Atomic Energy Review in 1983 on basis of X-ray diffraction data.[1] Some of the structures are as follows: the stoichiometric RhTi alloy at 700°C is tetragonal, AuCu-type, with a = 4.173 Å and C = 3.354 Å and δ-RhTi at low temperature is monoclinic with a = 2.96 Å, b = 2.81 Å, c = 3.41 Å, and β = 90°37′; $Rh_{55}Ti_{45}$ is orthorhombic, NbRu-type, with a = 4.15 Å, b =4.11 Å, and c = 3.40 Å; $Rh_{35}Ti_{65}$ at high temperature is cubic, CsCl-type, with a = 3.11 Å. The accepted phase diagram[2] (see Figure II-1) shows that RhTi has a CsCl-type structure at high-temperature and it distorts to a AuCu-type phase with decreasing temperature as a second-order phase transition. No orthorhombic phase is in this diagram.

There are several reasons why the subject of the phase transitions in RhTi is interesting. First, the structures and the phase behavior were not clearly understood. Second, the high-temperature structures of RhTi may not be obtained by quenching and their study necessitates the use of high-temperature X-ray diffraction. Finally, the phase transitions in RhTi provide an excellent example for tests of the application of Landau theory[3-5] and band theory to[6] the understanding of the relationship between structure and bonding in solids. As a result, the phase transitions in

RhTi were studied between room temperature and 1000°C in this work by a variety of crystallographic techniques, including high-temperature X-ray powder diffraction.[7,8]

RESULTS

The regions of transition temperature within ±100°C of a transition were studied with was particular care. The samples were held on a molybdenum holder which was maintained at constant temperature (±1°C) during X-ray scans between 2θ slightly less than 20° and 2θ as high as 90°. Long heating at high temperature resulted in observable surface oxidation (oxide diffraction peaks in the vicinity of 2θ = 37.5°). In order to avoid complications arising from oxidation the length of time the sample was at high temperature was minimized by collecting data for the lines in the 110 family that split initially into a pair and finally into a triplet. The measurement of the 2θ values for these lines allowed calculation of γ for the monoclinic case which is equivalent to the orthorhombic case because the a and b lattice parameters of the monoclinic structure are the same. The high-temperature cubic structure was found to be tetragonal and to further distort to orthorhombic with decreasing temperature as shown in Figure II-2. The structure data for RhTi are listed in Table II-1. The principal results are as follows.

(1) For T > 900°C a simple-seven line powder pattern was observed. The positions, but not always the intensities, were those of the CsCl-type (Pm3m). The line positions dictate the structure type. The mismatch between calculated

and observed intensities varied depending upon thermal treatment and was not improved by allowing for substitutional disorder. A pattern which provided a relatively good fit is shown in Figure II-3. It is concluded that there is preferred orientation in the as-grown cubic RhTi (from tetragonal RhTi, see below).

(2) For 900°C $\geq$ T $\geq$ 700°C a powder pattern with splitting of the cubic 110 family of diffraction lines into triples of lines was observed. The intensity of center line decreases and the intensities of the other two lines increase simultaneously with decreasing temperature. It is clear that two phases coexist in the region. The center line originates from the cubic 110 family, and the other two lines originate from the tetragonal 101 and 110 families, respectively. The coexistence of cubic and tetragonal RhTi indicates that the phase transition is first-order.

(3) For 700°C > T > 83°C the cubic 110 family of diffraction lines disappears completely. The powder diffraction pattern was fitted well with a tetragonal model (see Figure II-4) with c/a varying from 1 at 900°C to 1.093 at 200°C, and 1.121 at 83°C (calculated from the data shown in Figure II-5 by Rietveld refinement).

Table II-1 RhTi phases

1000°C	Cubic, CsCl-type		
	Pm3m		
	a = 3.126 Å		
83°C	Tetragonal, AuCu-type		
	P4/mmm		
	a = 2.988 Å		
	c = 3.350 Å		
25°C	Orthorhombic, NbRu-type	or	Monoclinic
	a = 4.144 Å		a = 2.960 Å
	b = 4.229 Å		b = 2.960 Å
	c = 3.366 Å		c = 3.366 Å
			γ = 90.17°

The principal structure change in this temperature range is the large decease in the Rh-Rh and Ti-Ti distances in the planes perpendicular to the unique tetragonal axis. This change occurs with an essentially constant Rh-Ti distances (2.70 Å) and amounts to a 0.13 Å decrease in the in-plane like atom distances and a 0.23 Å increase along the unique axis.

(4) For 83°C > T > 25°C the structure further distorts yielding orthorhombic symmetry (see Figure II-5). The major experimental effect is the splitting of the two lines at 2θ

= 43° to 44° (by about 0.7° = Δ (2θ) at 25°C). The principal structure change in this temperature is that the ratio a/b is equal to one, while the γ angle (see Figure II-2) distorts continuously from 90° to 91.17° with decreasing temperature (see Figure II-6) in the region. In fact, the monoclinic cell containing one Rh and one Ti is equivalent to an end-centered orthorhombic cell with two Rh and two Ti (Figure II-2). Therefore, the two lines obtained from a splitting of the tetragonal 110 family of diffraction lines belong to the orthorhombic 200 family and 020 family, respectively. The phase transition between the tetragonal and the orthorhombic which occurs without the coexistence of two phases indicates that the transition could be second-order.

(5) Subsequent attempts to fit the single, weak diffraction at 2θ ≃ 20° thought to be a superstructure reflection have not be successful,[8] principally because Since the best estimate for the 2θ location of the low-angle line is not in good agreement with a superstructure of the lattice determined by the substructure diffraction peaks. Therefore, the low-angle diffraction line originates from impurity phase. It possibly is the low-temperature form of $RhTi_2$ with $MoSi_2$-type structure.[1]

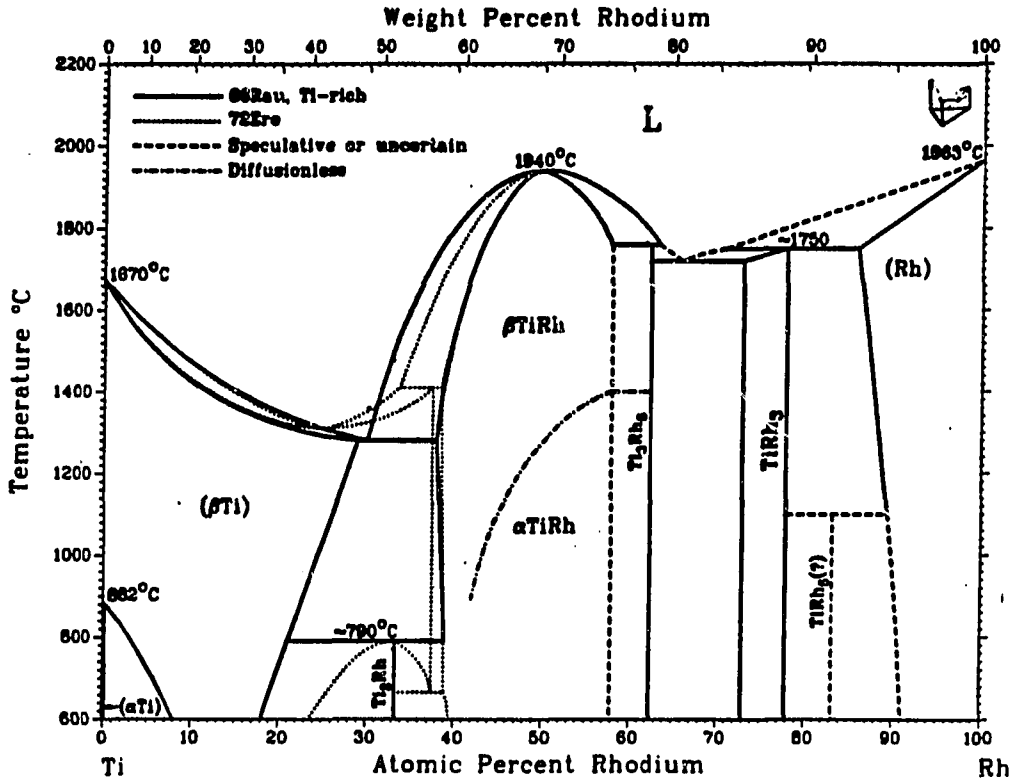

Figure II-1 The currently accepted phase diagram for the Rh-Ti system.[2] The high-temperature form, β TiRh, has the CsCl-type structure and transforms on cooling to α TiRh, which has the tetragonal AuCu structure

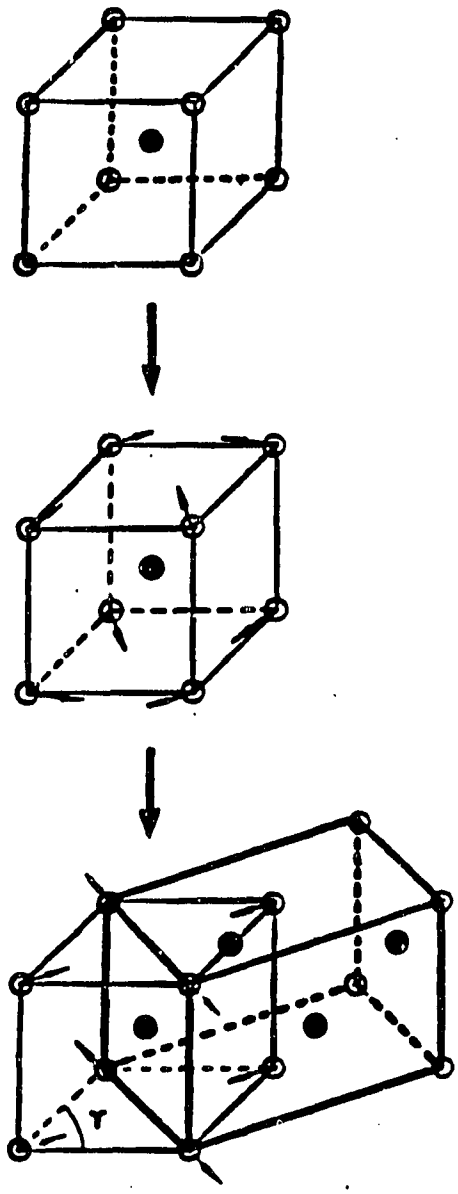

(a) Cubic

CsCl-type

Pm3m

(b) Tetragonal

AuCu-type

P4/mmm

(c) Orthorhombic

NbRu-type

Cmmm

$a_o \approx \sqrt{2}a_t$

$b_o \approx \sqrt{2}a_t$

$c_o \approx c_t$

$\gamma \neq 90°$

Figure II-2 The phase transitions c → t → o in RhTi with decreasing temperature

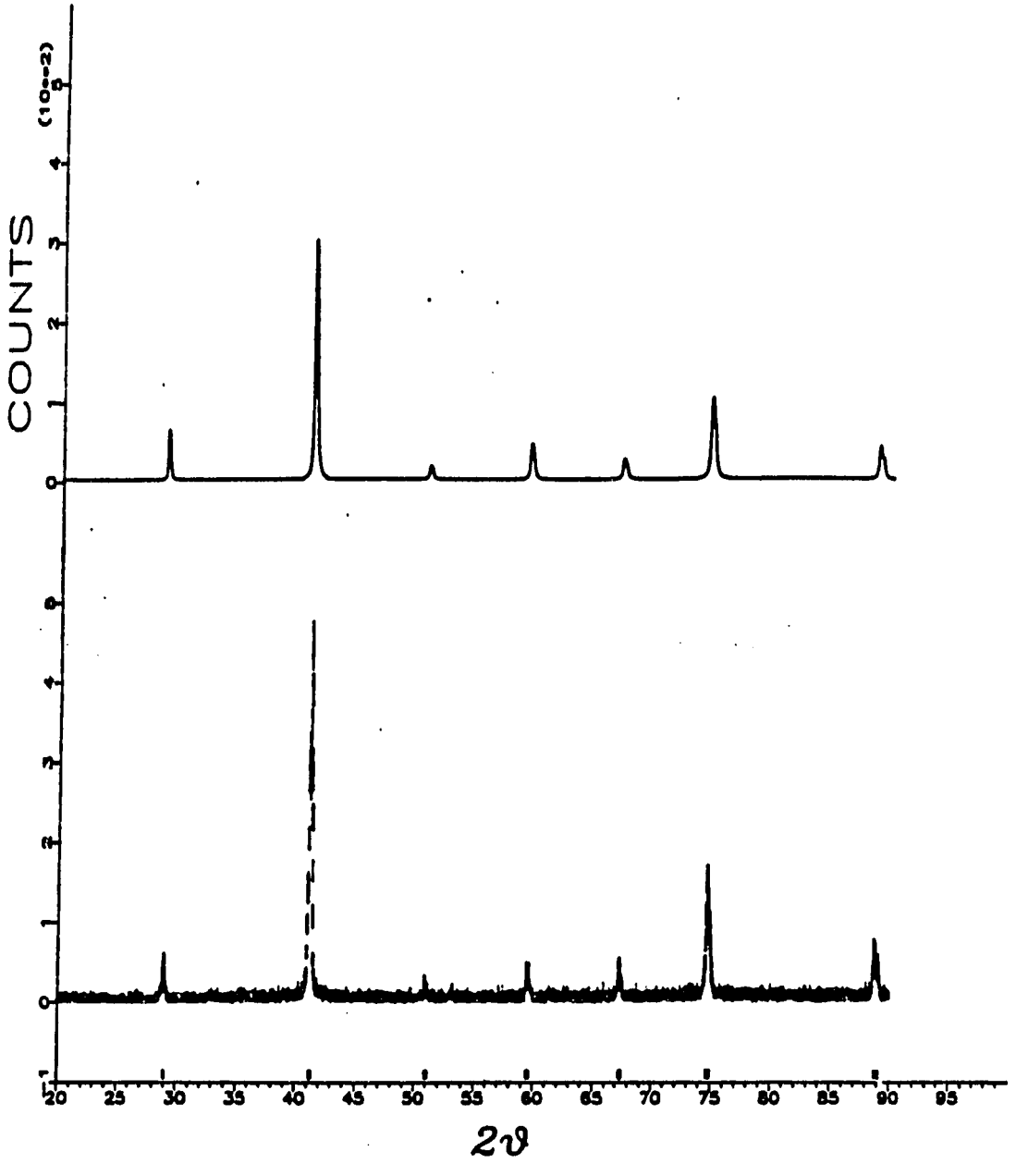

Figure II-3 Comparison of calculated and observed diffraction patterns for cubic RhTi at 1000°C

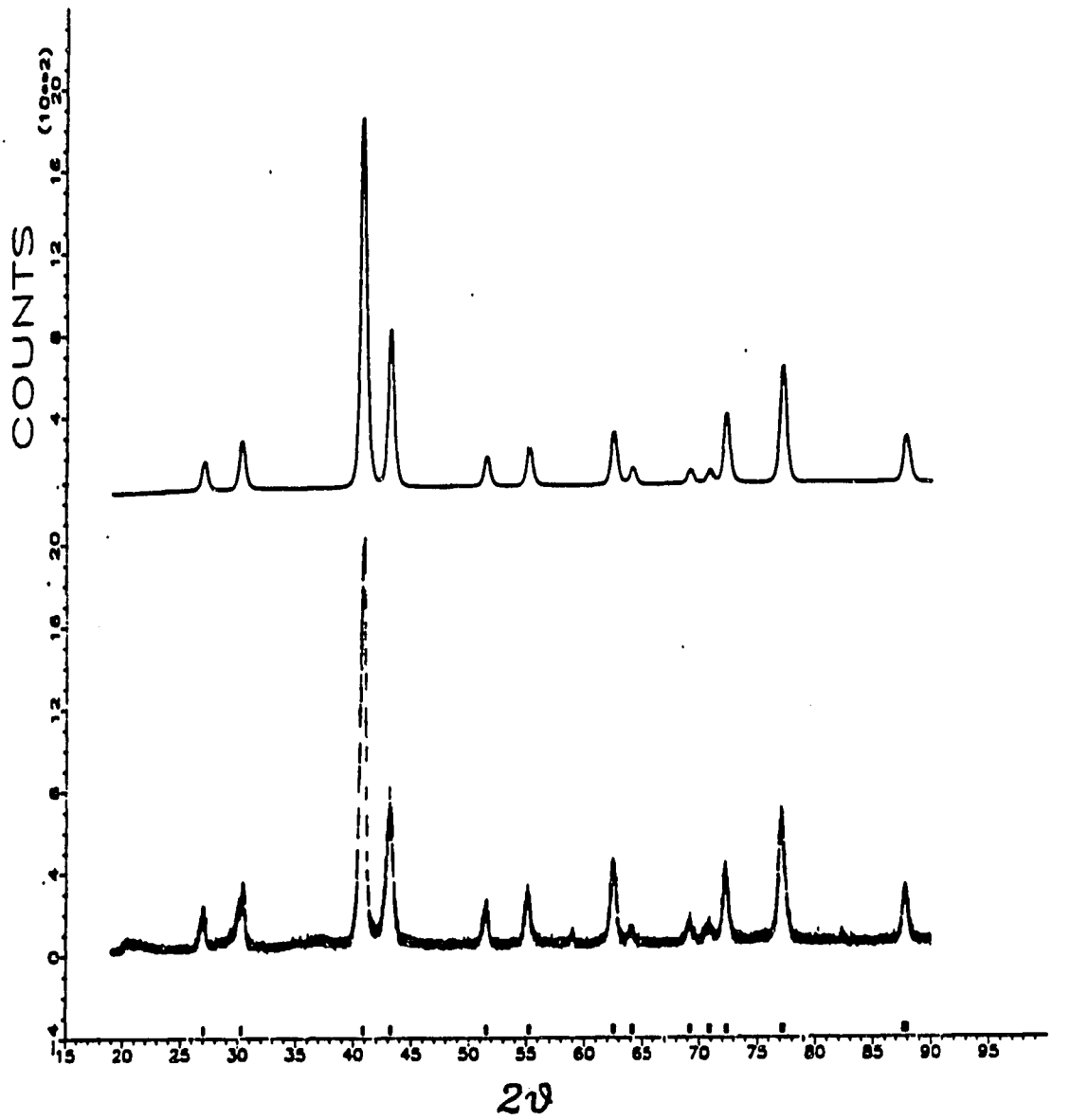

Figure II-4 Comparison of calculated and observed diffraction patterns for tetragonal RhTi at 83°C. The diffraction at 2θ ≈ 59° has its origin in the molybdenum sample holder

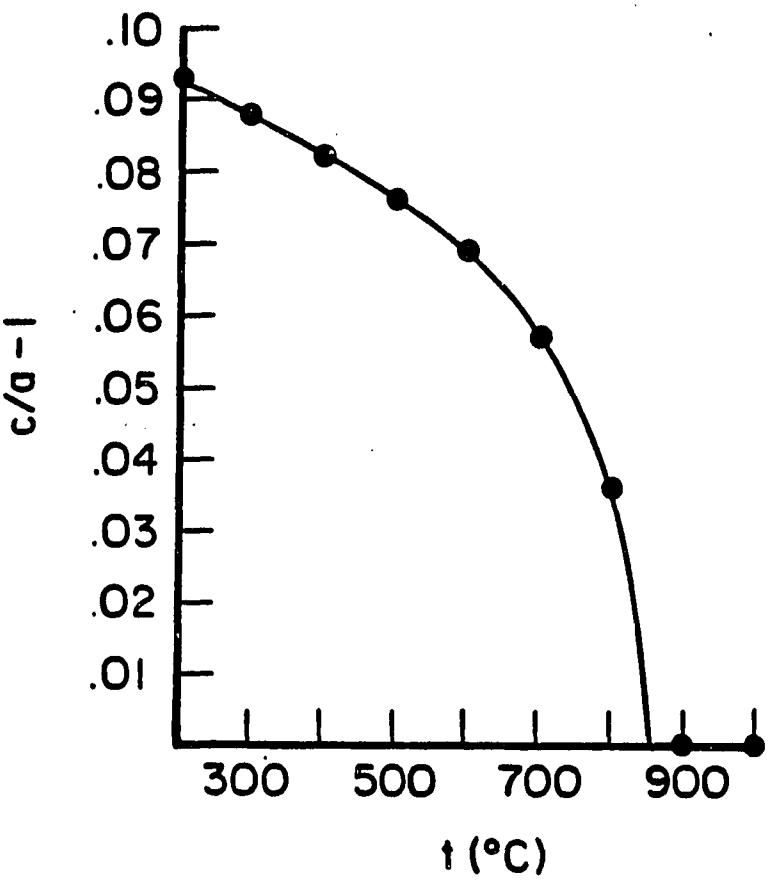

Figure II-5 Plot of c/a - 1 vs. temperature in the tetragonal RhTi

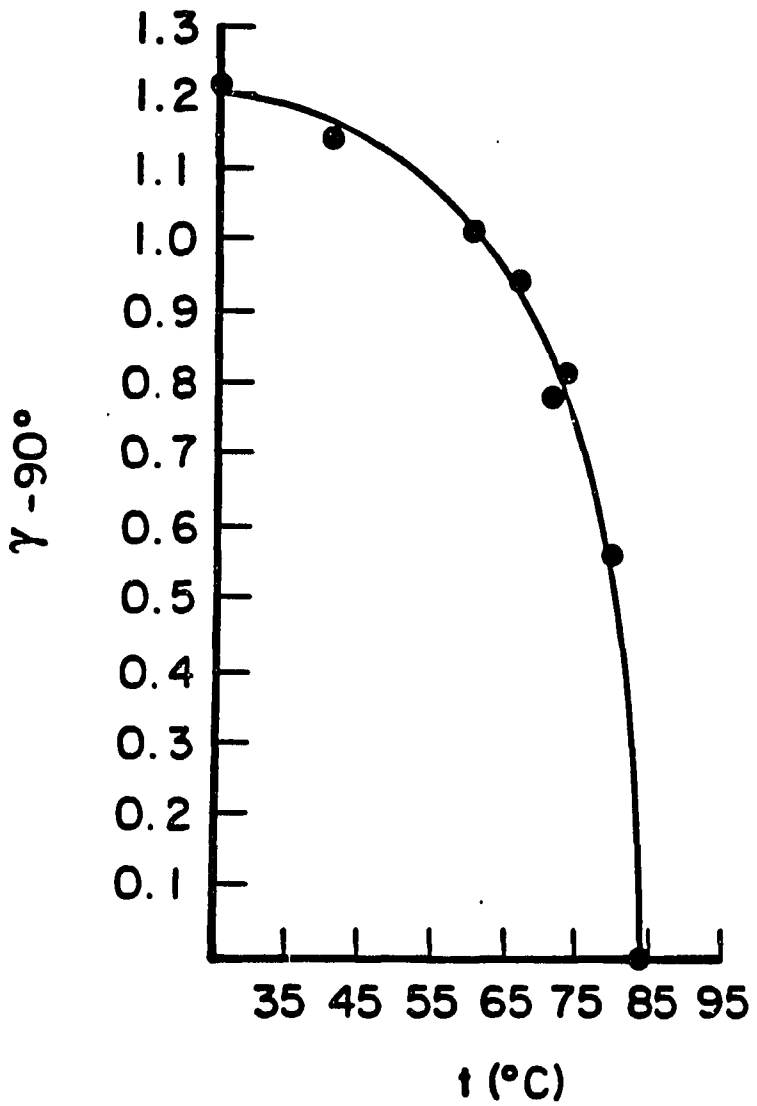

Figure II-6 Polt of $\gamma - 90°$ vs. temperature showing a second-order phase transition at 83°C

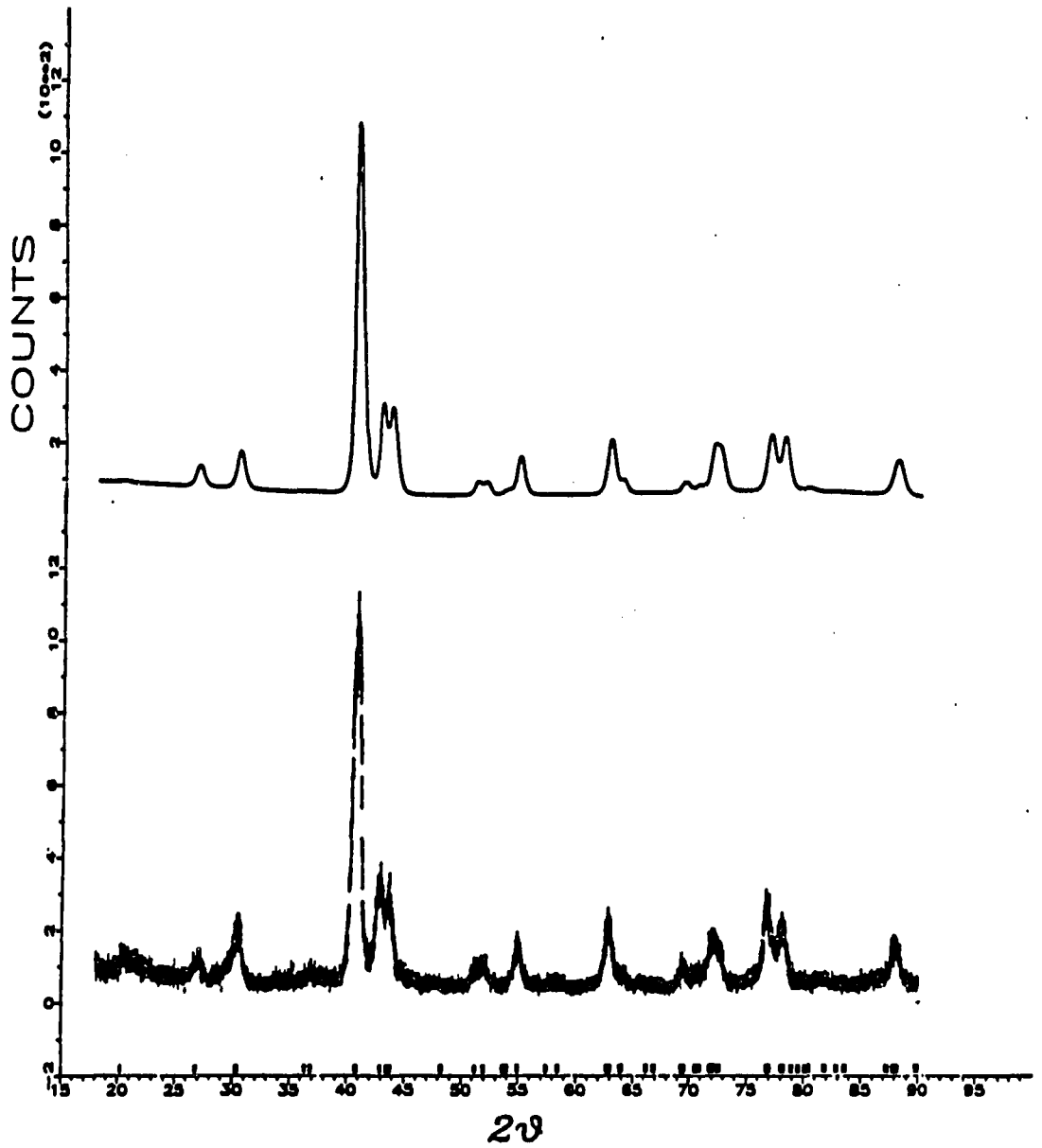

Figure II-7 Comparison of calculated and observed diffraction patterns for orthorhombic RhTi at room temperature

DISCUSSION

The sequence of a first-order distortion from cubic to tetragonal followed by a second-order distortion from tetragonal to orthorhombic observed for RhTi is in complete agreement with the predictions of Landau theory. The cubic → tetragonal distortion at k = 0 corresponds to e_g small representation of Pm3m to which there corresponds a third-order invariant requiring a first-order transition. Since this distortion corresponds to a single irreducible representation it is possible for the transition to follow a single order parameter and appear second-order at temperatures sufficiently removed from the transition temperature. Thus, the overall behavior observed, namely c/a tending towards unity with increasing temperature (Figure II-5), followed by the appearance of a cubic-tetragonal two-phase region, is in agreement with the Landau theory of the e_g representation (see Chapter I).

The 1-dimensional irreducible representation B_{1g} in P4/mmm is given in Table II-2. The basis function

Table II-2 The 1-D irreducible representation B_{1g} in D_{4h}

E	$2C_4$	C_2	$2C_2'$	$2C_2''$	i	$2S_4$	σ_h	$2\sigma_v$	$2\sigma_d$
1	-1	1	1	-1	1	-1	1	1	-1

transforms into itself under the symmetry operations E, C_2, $2C_2'$, i, σ_h and $2\sigma_v$ to yield space group Cmmm. The space group Cmmm contains half as many symmetry elements as the group Pm3m. According to the Landau theory[3], for every transition involving the halving of the number of symmetry operations of the crystal, a second-order phase transition is possible. Therefore, the Landau theory straightforwardly allows a second-order phase transition between P4/mmm and Cmmm at the k = 0 point, and this transition appears to occur in a second-order fashion.

The relation between the electronic structure of RhTi and the transition from the high-temperature cubic CsCl structure to the tetragonal structure has been studied by Folkerts and Haas,[9] using the augmented spherical wave (ASW) method. Based on ligand-field effect, they deduced that the first neighbors form a cubic coordination, with a ligand-field splitting with t_{2g} at higher energy than e_g; the second neighbors form an octahedral coordination, with inverted ligand-field effect.

The band of mainly Ti 3d e_g character is 25 % occupied and contains one electron. This is favourable situation for a Jahn-Teller instability. In the tetragonal case the 3d e_g band is split into two bands. The Fermi energy ε_F is lowered by 0.03 eV in comparison with the cubic phase. The density of the states at ε_F is lowered by 30 %. The total energy is lowered by 0.04 eV $(\text{unit cell})^{-1}$. Thus the band

structure calculation shows a greater stability for the tetragonal phase.

REFERENCES

1. Goldbeck, O. K.-V.; Rogl, P. in Komarrek (ed.), "Atomic Energy Review"; Special Issue No.9, International Atomic Energy Agency: Vienna, 1983.

2. Massalski, T. B.; Murray, J. L.; Benett, L. H.; Baker, H. "Binary Alloy Phase Diagrams"; American Society for Metals: Metals Park, OH, 1986.

3. Landau, L.; Lifshitz E. "Statistical Physics"; Pergamon Press: London, 1958.

4. Franzen, H. F. "Physical Chemistry of Inorganic Crystalline Solids"; Springer-Verlag: Heidelberg, 1986.

5. Tolédano, J. -C.; Tolédano, P. "The Laudau Theory of Phase Transition"; World Scientific Lecture Notes in Physics, Vol. 3, World Scientific Publishing: Singapore, 1987.

6. Silvestre, J.; Tremel, W.; Hoffman, R.; J. Less-Common Met. 1986, 116, 113.

7. Yi, S. S.; Chen, B. H.; Franzen, H. F. J. Less-Common Met. 1989, 153, L13.

8. Chen, B. H.; Franzen, H. F. J. Less-Common Met. 1989, 153, L13.

9. Folkerts, W.; Haas, C. J. Less-Common Met. 1989, 147, 181.

SECTION III PHASE TRANSITIONS AND HETEROGENEOUS EQUILIBRIA IN THE NbRu HOMOGENEITY RANGE

INTRODUCTION

Earlier work has shown the structures and the phase transitions in near-equiatomic Nb-Ru alloys as summarized below. Greenfield and Beck[1] found by X-ray diffraction and microscopic methods that Nb-Ru alloys between 48 and 49 atomic % Ru have a body-centered tetragonal structure and that an alloy containing 32 atomic % Ru has a body centered cubic structure when quenched from 1200°C to room temperature. Raub and Fritzsche[2] confirmed the presence of a body-centered tetragonal phase between 41 and 46.5 atomic % Ru and further reported alloys having a face-centered orthorhombic structure in the composition range between 47 and 58 atomic % Ru. Hurley and Brophy[3] showed that an alloy containing 35 atomic % Ru has a body-centered cubic structure. Das, Schmerling, and Lieberman[4] studied phase transitions in three near-equiatomic Nb-Ru alloys by electrical resistivity measurements, hot stage optical metallography, X-ray diffraction, and magnetic susceptibility measurements. Although the cubic phase could not be found by quenching in their investigation, a requirement for the presence of the cubic phase found in previous works[1,3] was alloys of lower Ru content. They deduced that the high temperature cubic phase transforms to a face-centered tetragonal structure on cooling and that the

latter transforms to a face-centered orthorhombic phase on further cooling.

A recent study by high-temperature X-ray diffraction of the phase transitions in RhTi (Chapter II) indicated similar behavior. Such systems are currently of theoretical interest because of the application of band-theory methods to the consideration of symmetry breaking transitions. Furthermore, in spite of the previous discoveries, none of the structures discussed above, nor any information below 1000°C, appear in the accepted phase diagram.[5] Thus it was necessary to fill in the gap in our understanding of this system. It was therefore decided to investigate the phase transition and the phase diagram for $NbRu_{1+x}$ by high-temperature (up to 1200°C) X-ray diffraction, using full-profile refinement of powder X-ray diffraction data from single-phase and two phase samples.[6]

RESULTS

The high-temperature form (above 1000 to 1100°C) of $NbRu_{1.00}$, $NbRu_{1.13}$, and $NbRu_{1.27}$ was found to be cubic (Figure III-1). The small difference in the Nb and Ru atomic scattering factors did not permit the distinction between the CsCl-type and bcc-type structures. However, a very weak {001} diffraction line of the orthorhombic $NbRu_{1.27}$ on Guiner X-ray pattern at room temperature was found in this study. Furthermore, previous works[7] have, by analogy with RuTa, assumed that the structure is CsCl-type, an assumption that is supported by the similarity of the phase behavior with RhTi, which also has the CsCl-type structure at high temperatures. It is observed that the phases with these compositions transformed into a tetragonal structure via a first-order transition (the cubic and tetragonal phases were observed coexisting in samples held at temperatures between 880 and 1000°C with the temperature range depending upon the Nb/Ru ratio). It is was furthermore observed that at temperatures in the range 720 to 920°C, depending upon the Nb/Ru ratio, the samples transformed between tetragonal and orthorhombic symmetry in what appeared to be a continuous (no two-phase coexistence observed) symmetry breaking transition. Diffraction patterns for the tetragonal and orthorhombic phases are shown in Figures III-2 and III-3. The orthorhombic-

hexagonal (Mg-type structure) coexistence as shown in the diffraction patterns of Figure III-4 was observed for $NbRu_{1.50}$.

The crystal data from the earlier work[4] for the Nb-Ru alloys in near equiatomic region are given in Table III-1 and the crystal data obtained from this work by Rietveld refinement for $NbRu_{1+x}$ are given in Table III-2. The tetragonal lattice of Table IV-1 is equivalent to a $\sqrt{2} \times \sqrt{2}$ superstructure of that in Table III-2. The room-temperature data are in fairly good agreement. The thermal behavior observed in this work, together with the results of the earlier work as described above, can be represented on a T-X phase diagram with composition in the region of 40 to 60 atomic % Ru as shown in Figure III-5.

Table III-1 The crystal data obtained from Reference 4 at room temperature

Ru(%)	Crystal Structure	Lattice Parameter (Å) a	b	c
45.8	Face-centered tetragonal	4.388		3.311
51.1	Face-centered orthorhombic	4.373	4.228	3.401
55.8	Face-centered orthorhombic	4.295	4.192	3.439

Table III-2 The crystal data obtained from this work*

Rh(%)	T(°C)	Phase Symmetry	Parameter (Å) a	b	c	Scale Factor(%)	R_B
50	25	Cmmm	4.363	4.232	3.400		
54	1115	Pm3m	3.184				4.14
	1000	P4/mmm	3.110		3.332		5.43
	25	Cmmm	4.332	4.232	3.416		6.88
56	25	Cmmm	4.300	4.217	3.430		
60	25	Cmmm	4.2888	4.198	3.453	1.55×10^{-4}	4.77
	25	$P6_3/mmc$	2.763		4.443	1.65×10^{-4}	8.82

*The lattice parameters for alloys containing 50 and 56 atomic % Ru were determined by LLR refinement program[7] and R_B is Bragg R-factor.

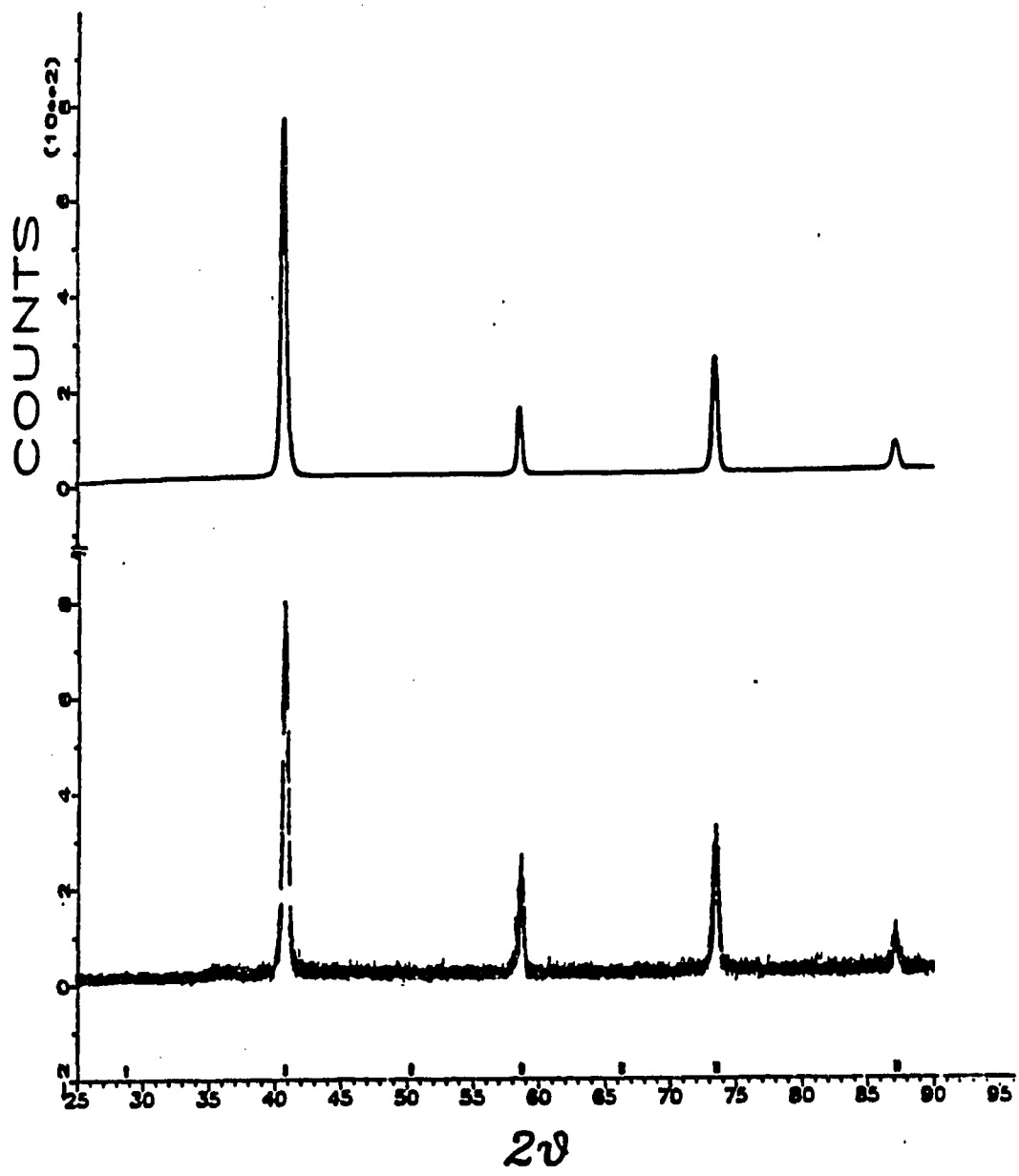

Figure III-1 The diffraction pattern observed for $NbRu_{1.13}$ at 1115°C and the pattern calculated assuming the CsCl-type structure

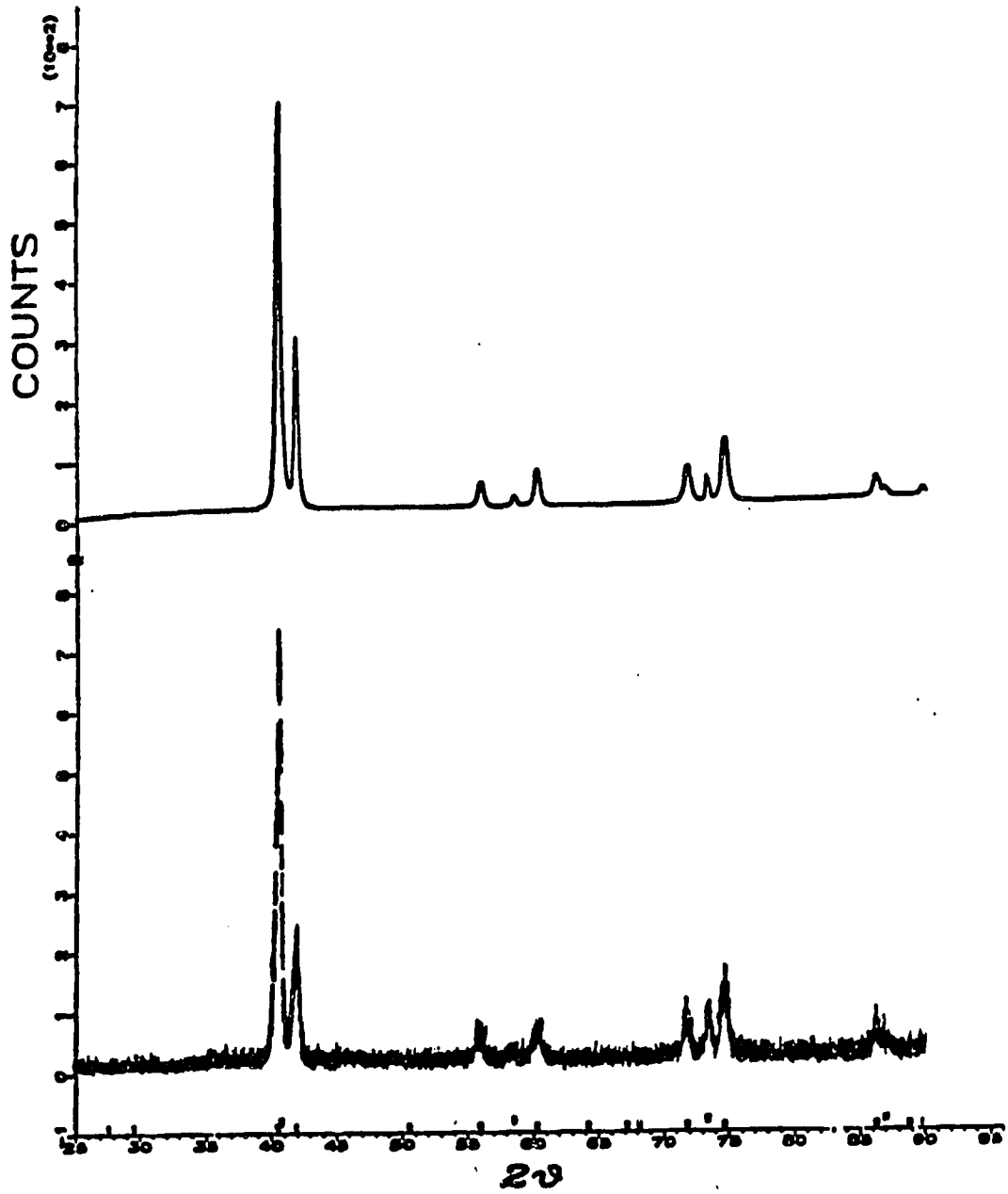

Figure III-2 The calculated and observed diffraction patterns for tetragonal $NbRu_{1.13}$ and Mo (the material of the sample holder) at 1000°C

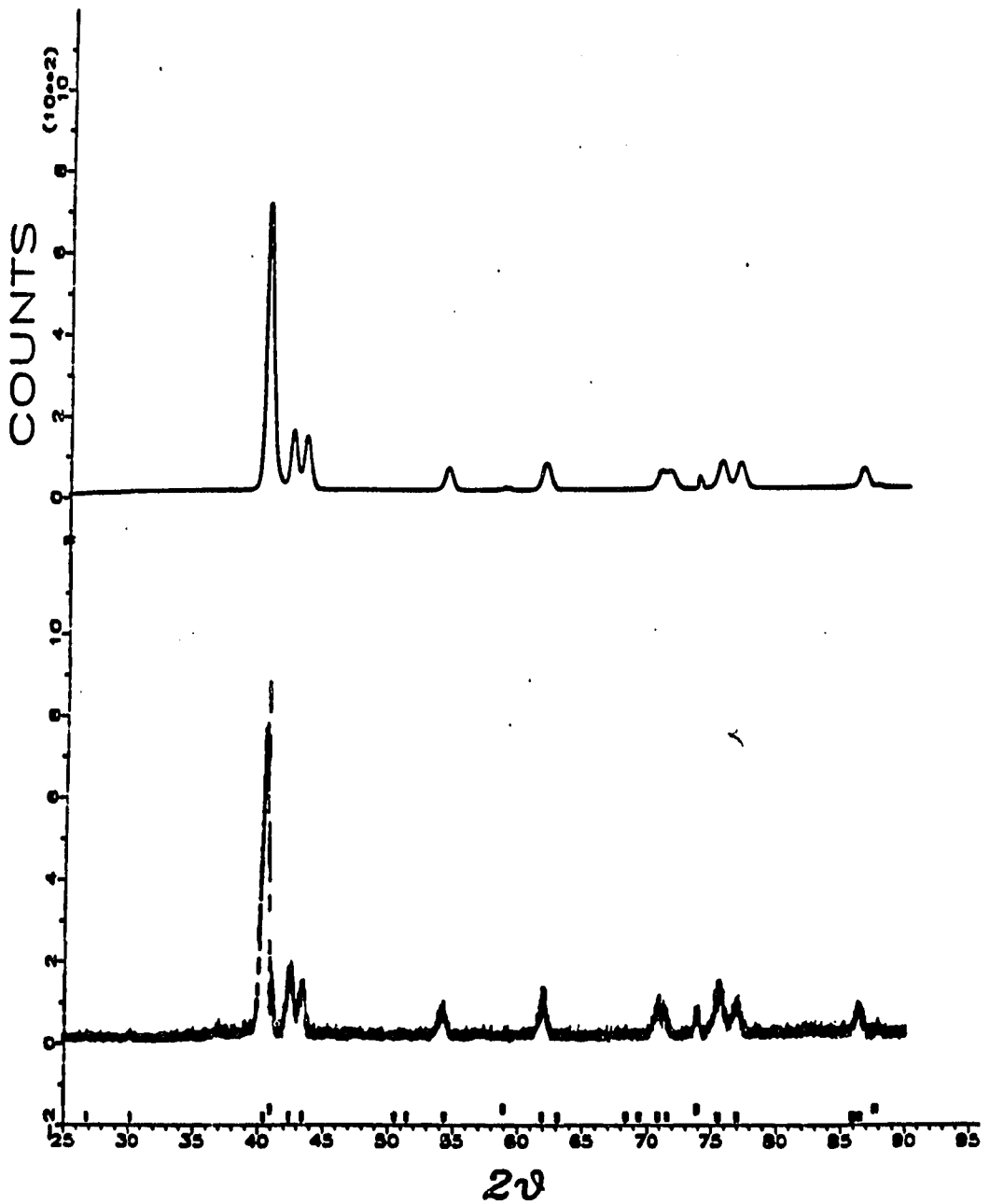

Figure III-3 The calculated and observed diffraction patterns for orthorhombic $NbRu_{1.13}$ at room temperature

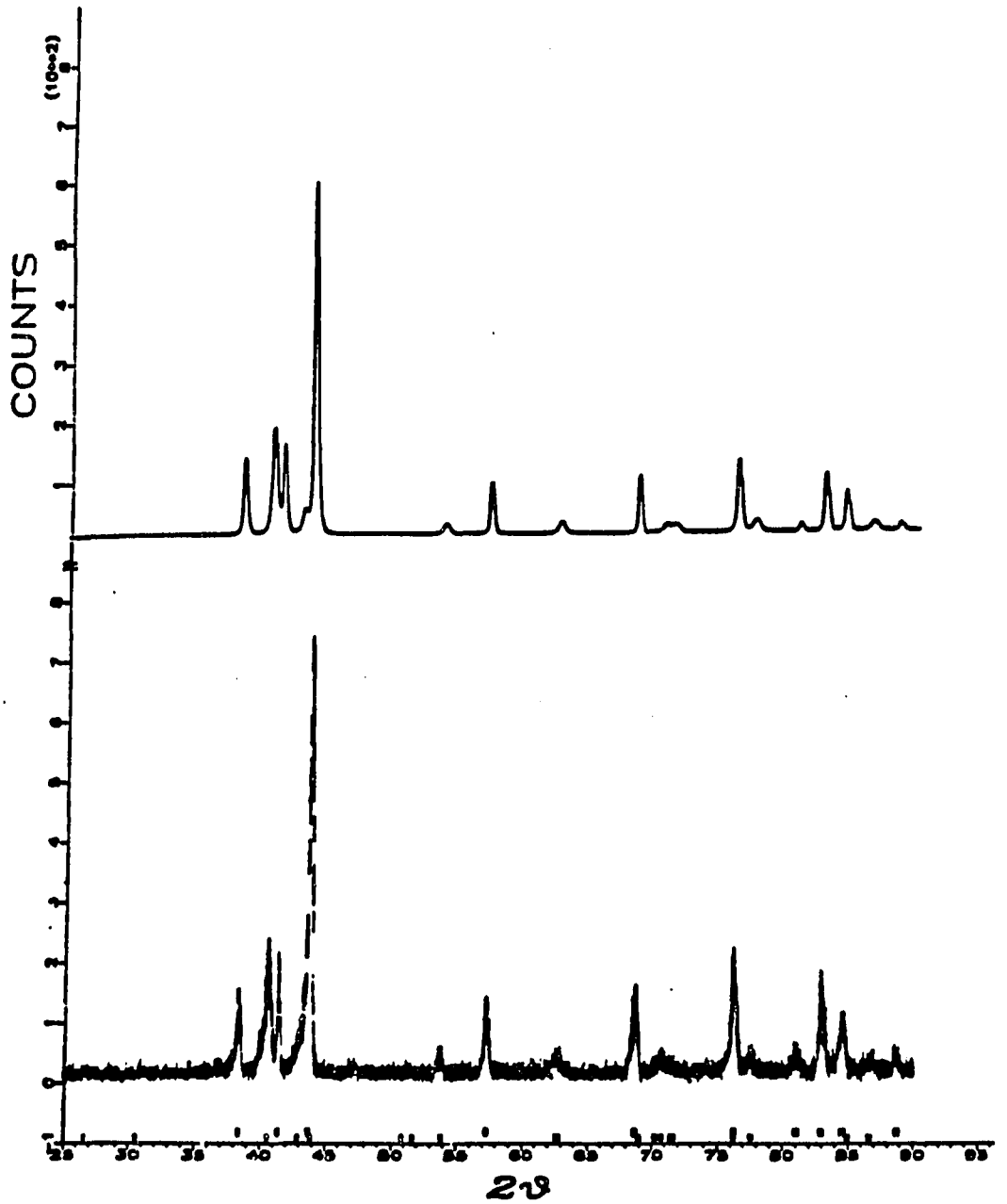

Figure III-4 The calculated and observed diffraction patterns for orthorhombic $NbRu_{1+x}$ and hexagonal $NbRu_{1+y}$ with Ru/Nb = 1.50 overall at room temperature

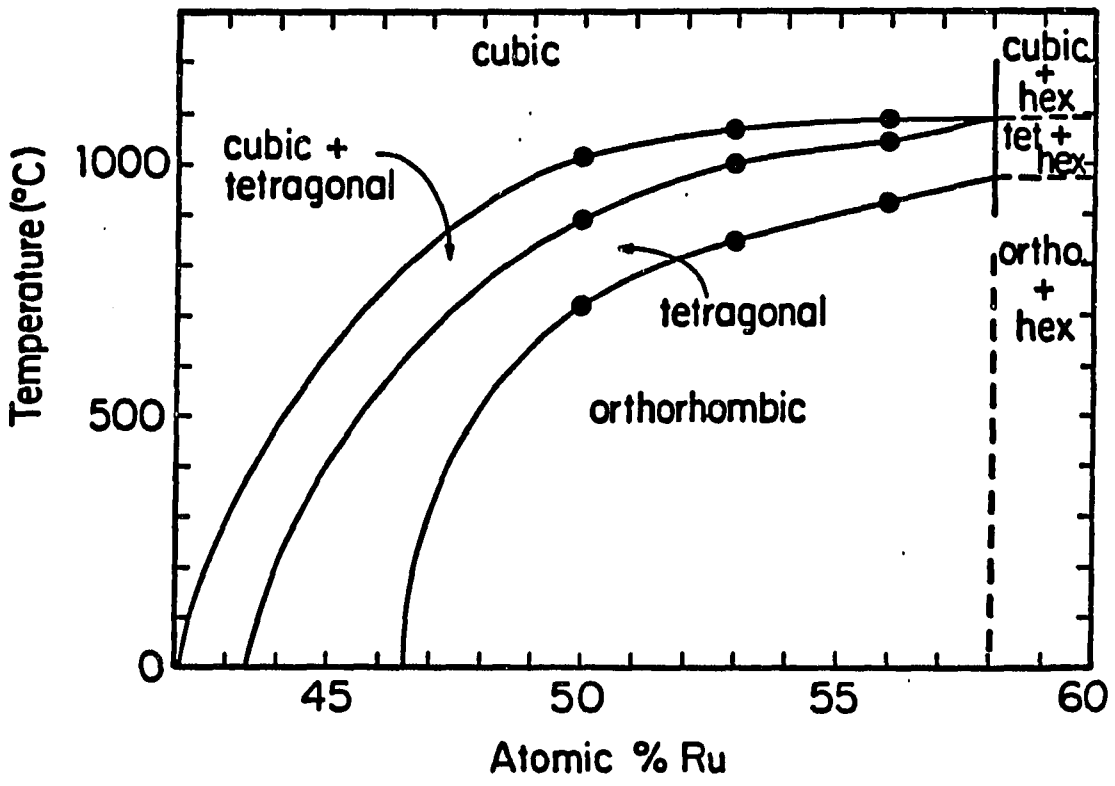

Figure III-5 The NbRu T-X phase diagram based upon data obtained in this study (black dots) and literature data at room temperature

DISCUSSION

As in the case of RhTi, investigations in the $NbRu_{1+x}$ system using powder X-ray diffraction between room-temperature and 1200°C show that the phase transition from cubic to tetragonal is first-order, and from tetragonal to orthorhombic is second-order. The Landau theory[8-10] can be applied to these two stage transitions as discussed in Section II.

Both NbRu and RhTi have 13 valence electrons and the atomic sizes of Nb and Ru are very close to Ti and Rh respectively. Therefore, the relation between the electronic structure of NbRu and the transition from the high-temperature cubic to the tetragonal structure may be similar to that for RhTi as discussed by Folkerts and Haas[11] using the augmented spherical wave (ASM) method. With the same argument, the band of mainly Nb 4d e_g character is 25 % occupied and contains one electron. This is a favorable situation for a Jahn-Teller instability. In the tetragonal structure the Nb 4d e_g band is split into two bands.

REFERENCES

1. Greenfield, P.; Beck, P. A. Trans. AIME 1965, 206, 265.

2. Raub, E.; Fritzsche, W. Z. Metallk. 1963, 54, 317.

3. Hurley, G. F.; Brophy, J. H. J. Less-Common Met. 1964, 7, 267.

4. Das, B. K.; Schmerling, M. A.; Lieberman, D. S. Mater. Sci. Eng. 1970, 6, 248.

5. Massalski, T. B.; Murray, J. L.; Benett, L. H.; Baker, H. "Binary Alloy Phase Diagrams"; American Society for Metals: Metals Park, OH, 1986.

6. Chen, B. H.; Franzen, H. F. J. Less-Common Met. 1989, 153, L13.

7. Chen, B. H.; Jacobson, R. A., to be published, Department of Chemistry, Iowa State University.

8. Landau, L.; Lifshitz E. "Statistical Physics"; Pergamon Press: London, 1958.

9. Franzen, H. F. "Physical Chemistry of Inorganic Crystalline Solids"; Springer-Verlag: Heidelberg, 1986.

10. Tolédano, J. -C.; Tolédano, P. "The Laudau Theory of Phase Transition"; World Scientific Lecture Notes in Physics, Vol. 3, World Scientific Publishing: Singapore, 1987.

11. Folkerts, W.; Haas, C. J. Less-Common Met. 1989, 147, 181.

SECTION IV PHASE TRANSITIONS AND HETEROGENEOUS EQUILIBRIA IN THE RuTa HOMOGENEITY RANGE

INTRODUCTION

Several papers dealing with the phase behavior in the RuTa homogeneity range have appeared in the literature since Beck and Greenfield[1] (1956) reported that the 38 atomic % Ru alloy has the CsCl-type structure, and that alloys with containing composition between 45 and 50 atomic % Ru apparently have a tetragonal structure when quenched from 1200°C to room temperature. Next, Hartley, Baun, Fisher, and Rapperport[2] found that the alloy at 30 atomic % Ru has the CsCl-type structure and that alloys between 40 and 45 atomic % Ru quenched from 1500°C have a tetragonal structure. They suggested that a tetragonally distorted CsCl-type structure may be formed from cubic CsCl-type on cooling. A reviewer stated,[3] "high-temperature X-ray work will be necessary to resolve these ambiguities." After that, Rudman[4] further confirmed the presence of CsCl-type and tetragonal phases. At the almost same time, Raub, Beeskow, and Fritzsche reported[5] that alloy at 50 atomic % Ru is a face-centered orthorhombic (fco) structure, and that alloy at 55 atomic % Ru is a face-centered tetragonal (fct) structure when quenched from 1600°C.

Although the investigation of the structures and the phase behavior in near equiatomic Ru-Ta alloys has been extensively studied, no information below 1300°C is presented in the accepted phase diagram.[6] Schmerling, Das,

and Lieberman[7] have investigated phase transitions in such systems with X-ray powder diffraction at room temperature and resistance, metallographic, and susceptibility measurements as a functions of temperature. The results suggested "two step" phase transitions cubic → tetragonal → orthorhombic. Again, they were unable to obtain the cubic phase in quenched alloys. A pseudophase diagram was constructed based on their study (see Figure IV-1). However, analysis of the phase boundaries in the phase diagram using the Gibbs-Konovalow equation[8] and the phase law indicated some unresolved problems. For example, the phase diagram at 50 atomic % Ta shows that $(\partial X/\partial T)_p = 0$ and $\Delta X \neq 0$. In fact, $(\partial X/\partial T)_p = 0$ requires that $\Delta X = 0$. Furthermore, the T-X line between ~47.5 (~650°C) and ~54 (~420°C) atomic % Ta, contrary to the phase law, shows the coexistence of three phases.

Among the nonstoichiometric compounds with the cubic CsCl-type structure at high temperatures a number (MnAu,[9] RhTi,[10,11] and NbRu[11]) are known to undergo thermal symmetry breaking transitions upon cooling. The transitions in RhTi and NbRu are first to tetragonal in a first-order transition, then to end-centered orthorhombic in a second-order transition. Such behavior is of interest in connection with electron-phonon interactions and martensitic transitions. Because of the similarity of the behavior of RuTa, as described above, to that of NbRu, and the

uncertainty in the nature of the phase behavior of RuTa,[7] a high-temperature (up to 1650°C) X-ray diffraction investigation was undertaken using full-profile refinement of powder X-ray diffraction data from single-phase and two-phase samples in the range $0.49 < Ru/Ta < 1.60$.[12]

RESULTS

The known lattice symmetries and parameters at room temperature for various samples in the RuTa homogeneity range are summarized in Table IV-1. These lattices, although unconventionally described as face-centred in some cases (the conventional tetragonal cell is primitive, the conventional orthorhombic cell is end-centered) suffice to describe the phase behavior of samples in the neighborhood of RuTa. Samples richer than 57.2 atomic % Ru were found to contain hexagonal close-packed solid solution phase at all temperatures up to 1500°C. The results of 13 refinements for seven compositions at various temperatures are given in Table IV-2. Nine of the resultant data sets were analyzed by Rietveld refinement. The patterns, together with the calculated profiles, are shown in Figures IV-2 to IV-10. The lattice parameters for the rest were determined by the LLR program.[13]

In Table IV-2, the first column gives the synthetic composition (estimated uncertainty < ±1.1 %), second column gives the temperature as determined by W-Re thermocouples (estimated uncertainty < ±20°C), the third column lists the mass lost during synthesis, the fifth column gives, where appropriate, the reference to Figures V-1 to V-10, the sixth column gives the space group symmetries (Pm3m for the CsCl-type structure, P4/mmm for the tetragonal distortion without

loss of translational symmetry, and Cmmm for the orthorhombic distortion without loss of translational symmetry), the seventh-ninth column gives the lattice parameters (estimated uncertainty = $\pm 5 \times 10^{-3}$ Å) and the last column gives the defined Bragg R values from the results of Rietveld refinement.

Table IV-1 The lattice parameters from the previous work

Ru(%)	Phase	a (Å)	b (Å)	c (Å)	Reference
37.5	C	3.181			3
40	T	3.155		3.206	3
40	T	3.114		3.277	4
45	T	3.096		3.297	3
45	FCT	4.387*		3.320	6
47.7	FCT	4.385	4.277	3.376	6
50	O	4.351	4.199	3.388	4
50	FCO	4.368	4.241	3.387	6
55	T	4.271*		3.395	4
55	FCT	4.288*		3.385	6

*The lattice containing four atoms is equivalent to a $\sqrt{2} \times \sqrt{2}$ superstructure of that containing two atoms.

CONCLUSIONS

The investigation of the phase transitions by high-temperature X-ray diffraction in alloys of Ru-Ta within the composition range from 33 to 62 atomic % Ru yields the phase diagram shown in Figure IV-10. The room temperature data obtained from this work are in good agreement with those obtained from the earlier work as listed in Table IV-1. The transitions from cubic-to-tetragonal and from tetragonal-to-orthorhombic are both first-order transitions. The former is required by Laudau theory to be first-order, the latter may be second-order but is not. For both RhTi[10,11] and NbRu[11] it is was concluded that the tetragonal-to-orthorhombic transition is second-order. The difference between a first-order and second-order when the Landau and Lifshitz[14] conditions are met, as they are for this distortion at the Γ point, results from a difference in the sign of the fourth-order term in the Gibbs free-energy expansion, i.e., if it is positive a second-order phase transition will occur when the second-order term changes sign, if it is negative only a first-order transition can occur.

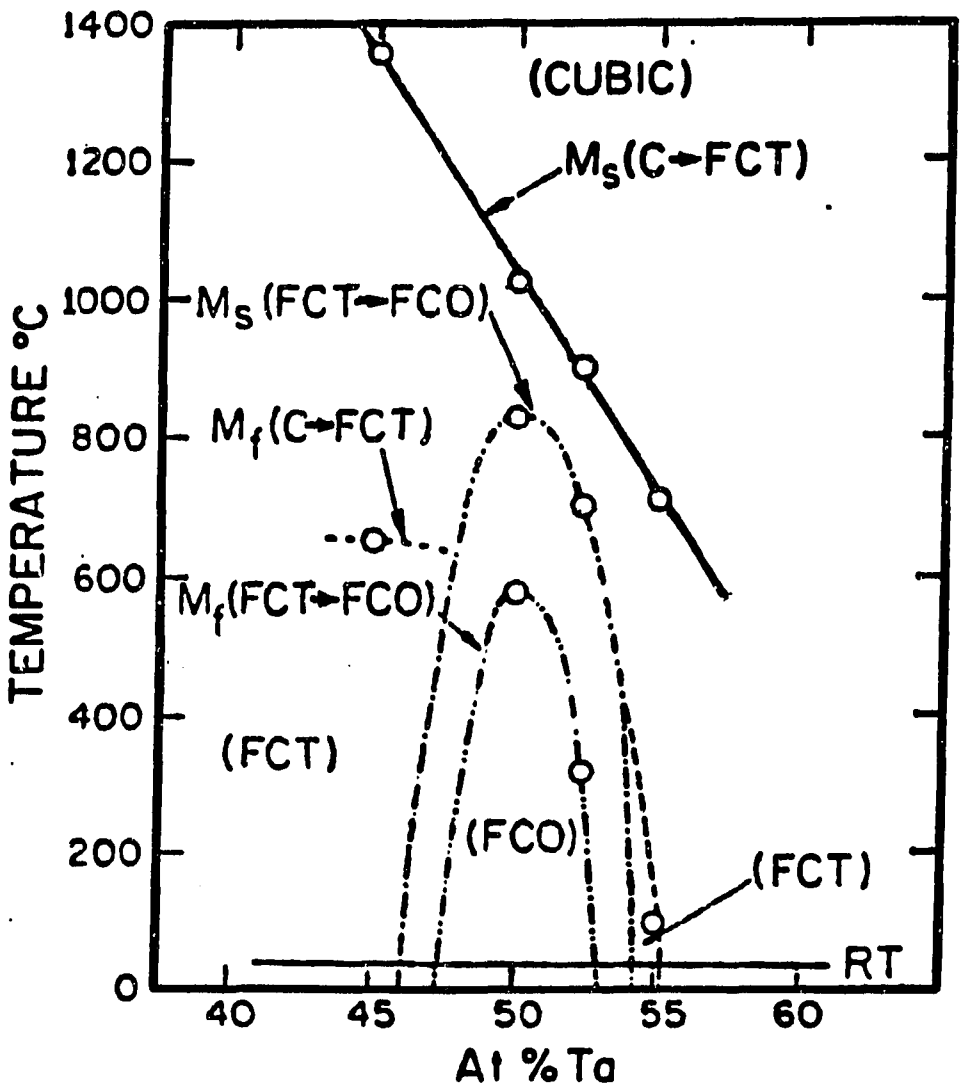

Figure IV-1 Pseudophase diagram for near equiatomic Ru-Ta alloys[7]

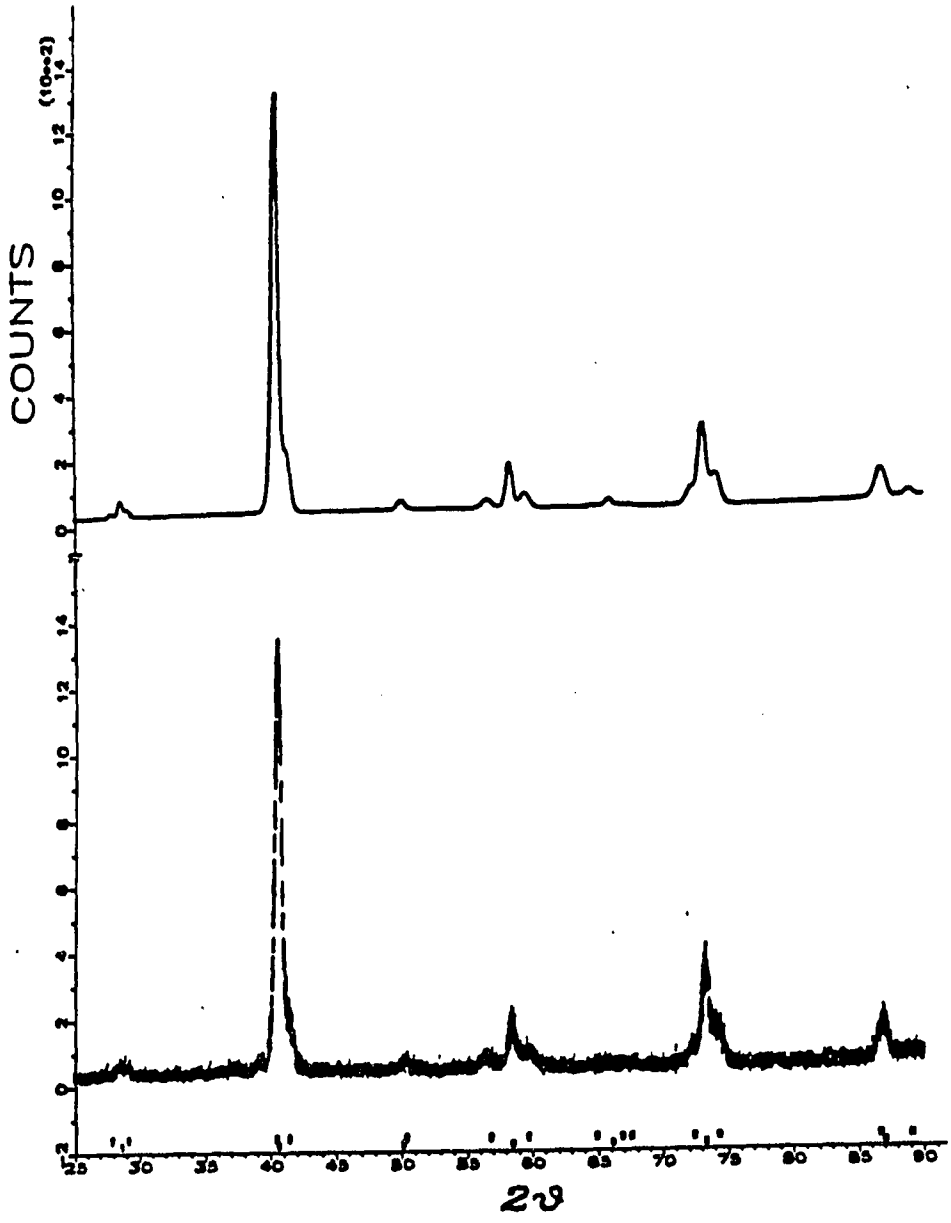

Figure IV-2 The calculated and observed diffraction patterns for Ru/Ta = 0.664 at room temperature. Cubic and tetragonal phases present

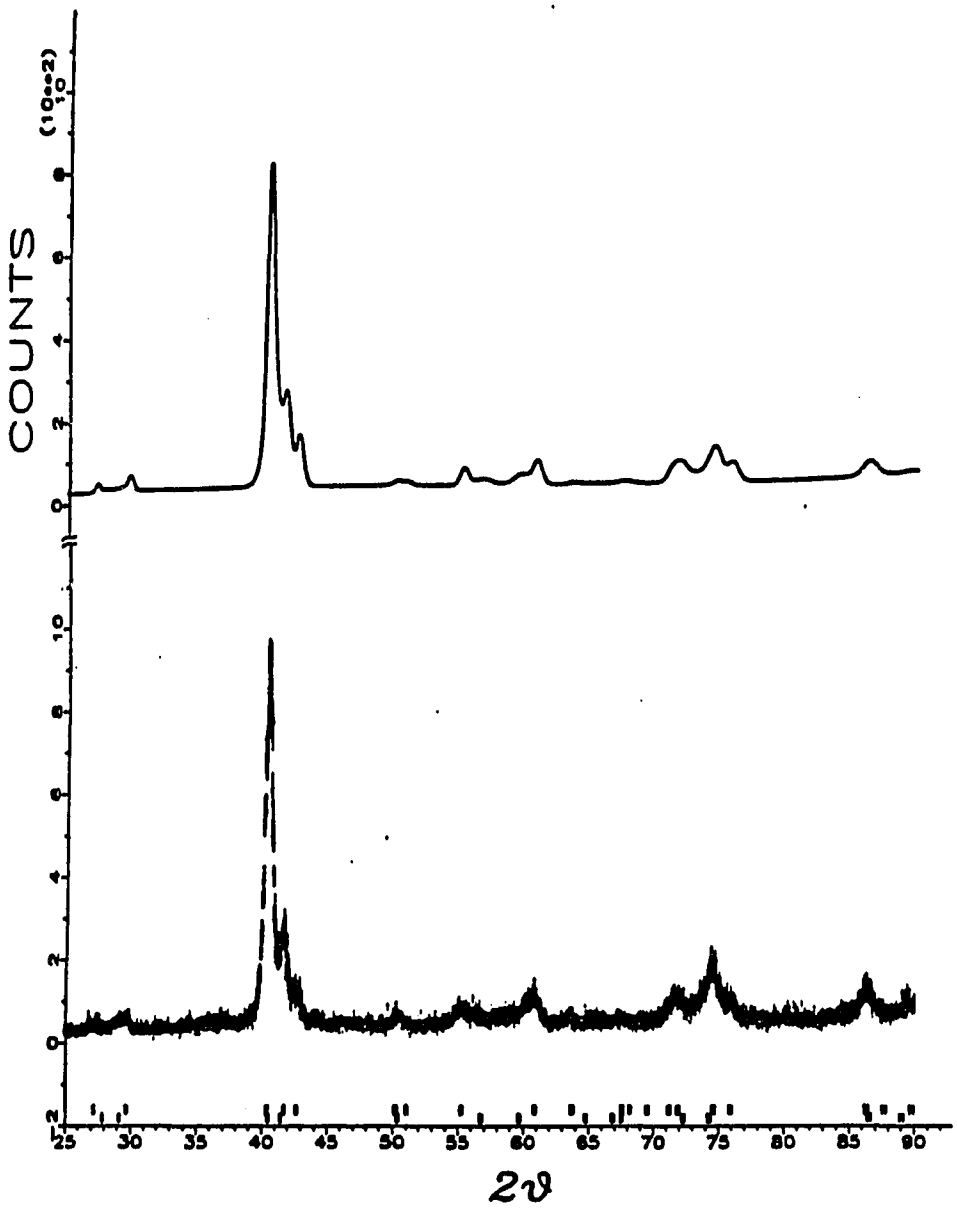

Figure IV-3 The calculated and observed diffraction patterns for Ru/Ta = 0.869 at room temperature. Tetragonal and orthorhombic phases present

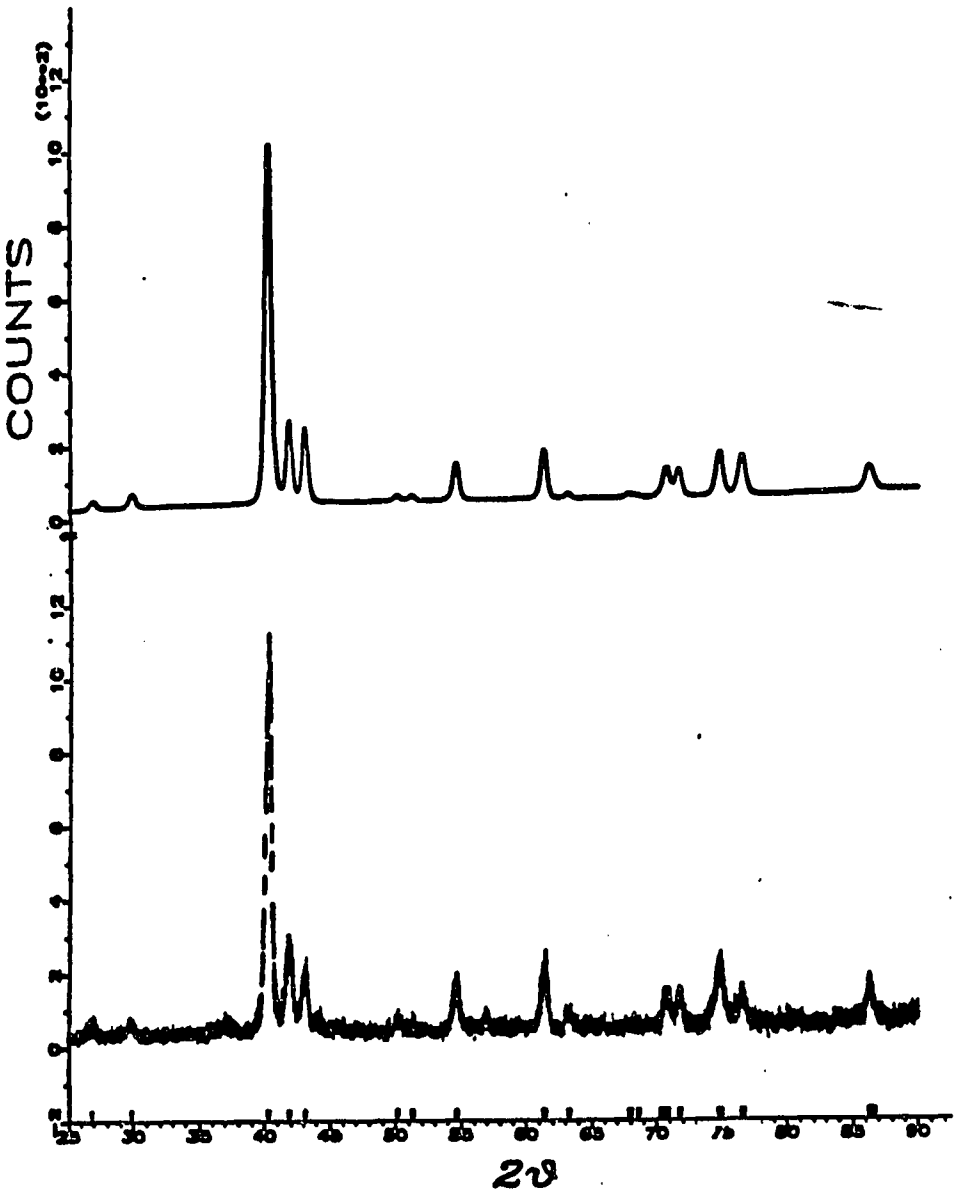

Figure IV-4 The calculated and observed diffraction patterns for Ru/Ta = 1.00 room temperature. Orthorhombic phase present

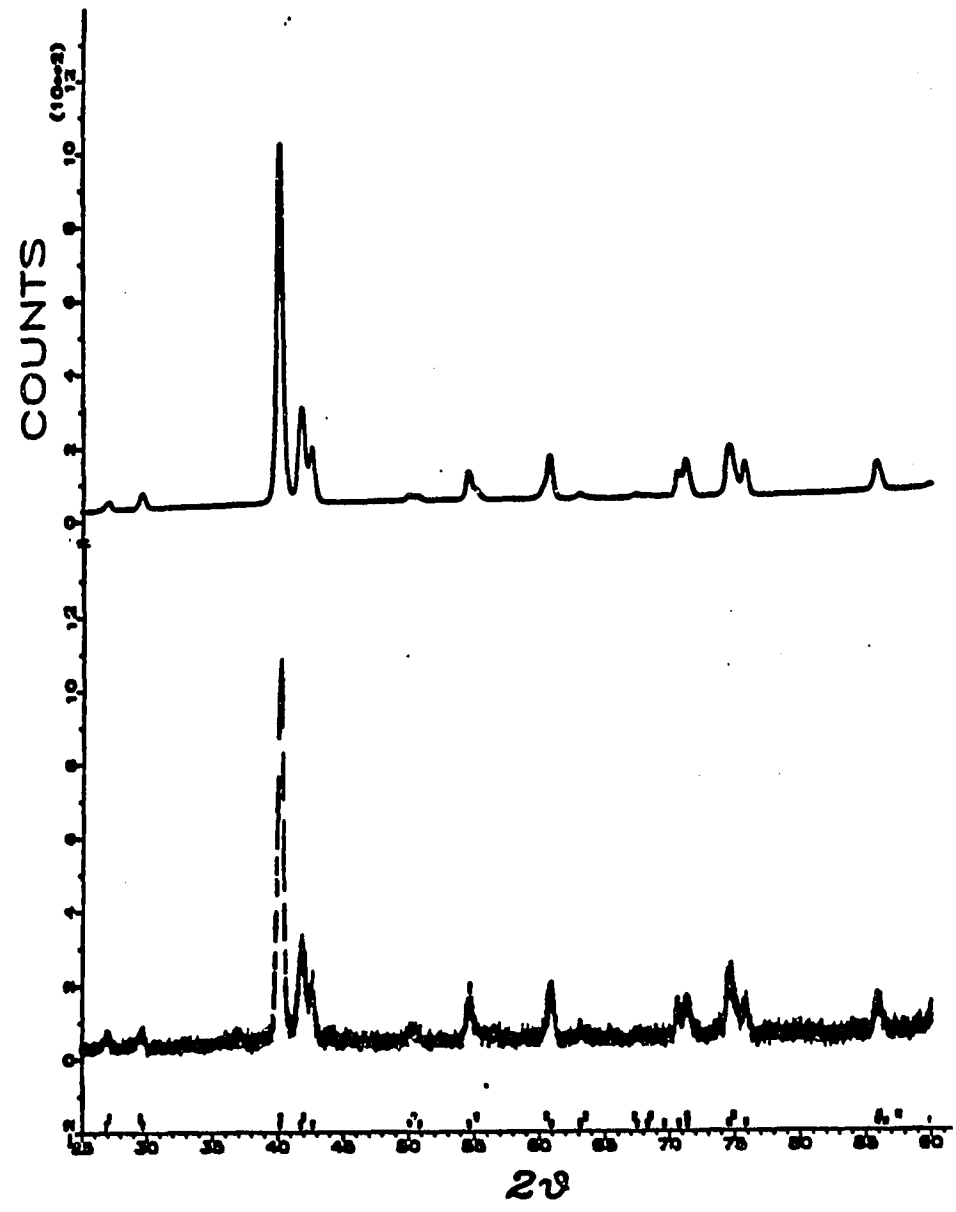

Figure IV-5 The calculated and observed diffraction patterns for Ru/Ta = 1.00 at 730°C. Tetragonal and orthorhombic phases present

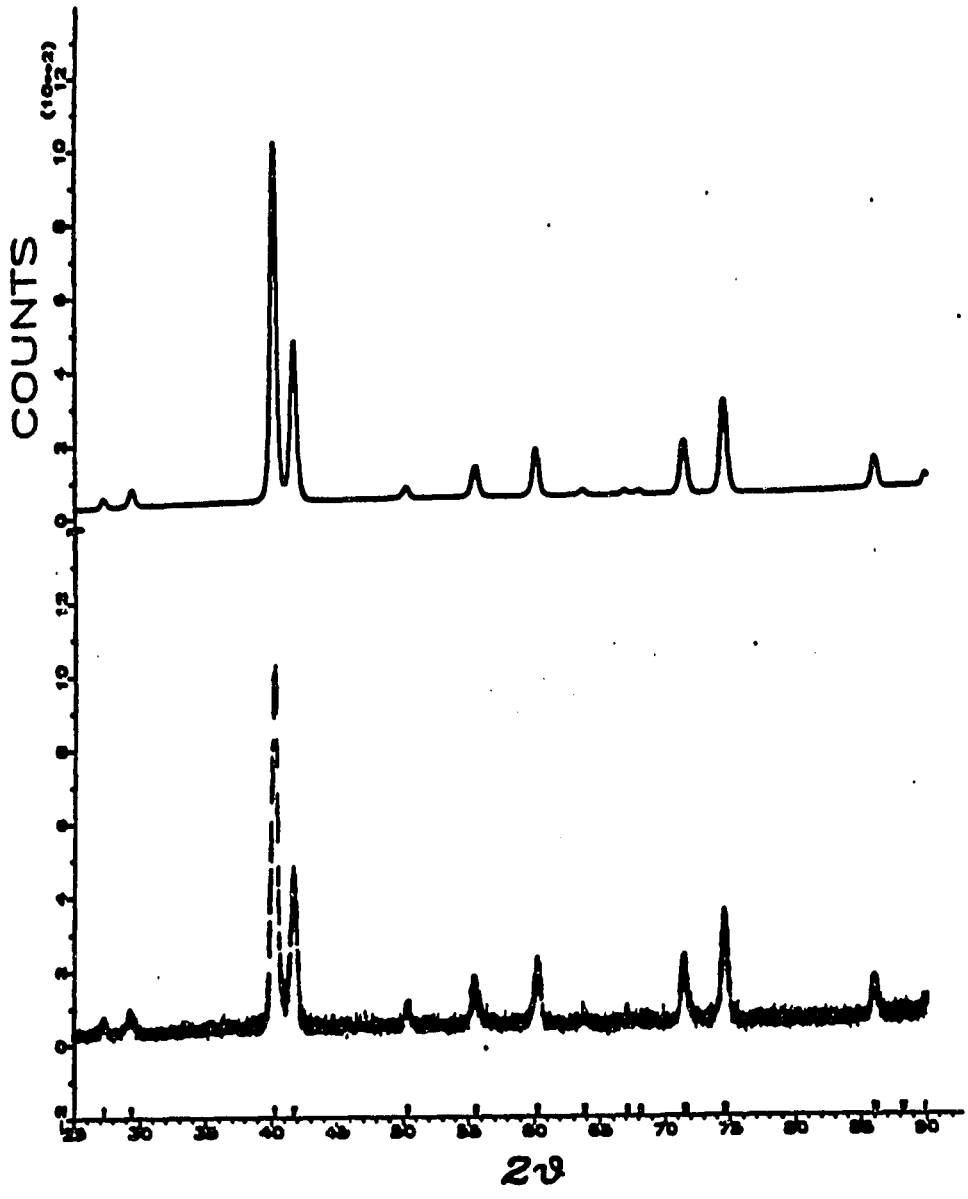

Figure IV-6 The calculated and observed diffraction patterns for Ru/Ta = 1.00 at 900°C. Tetragonal phase presently

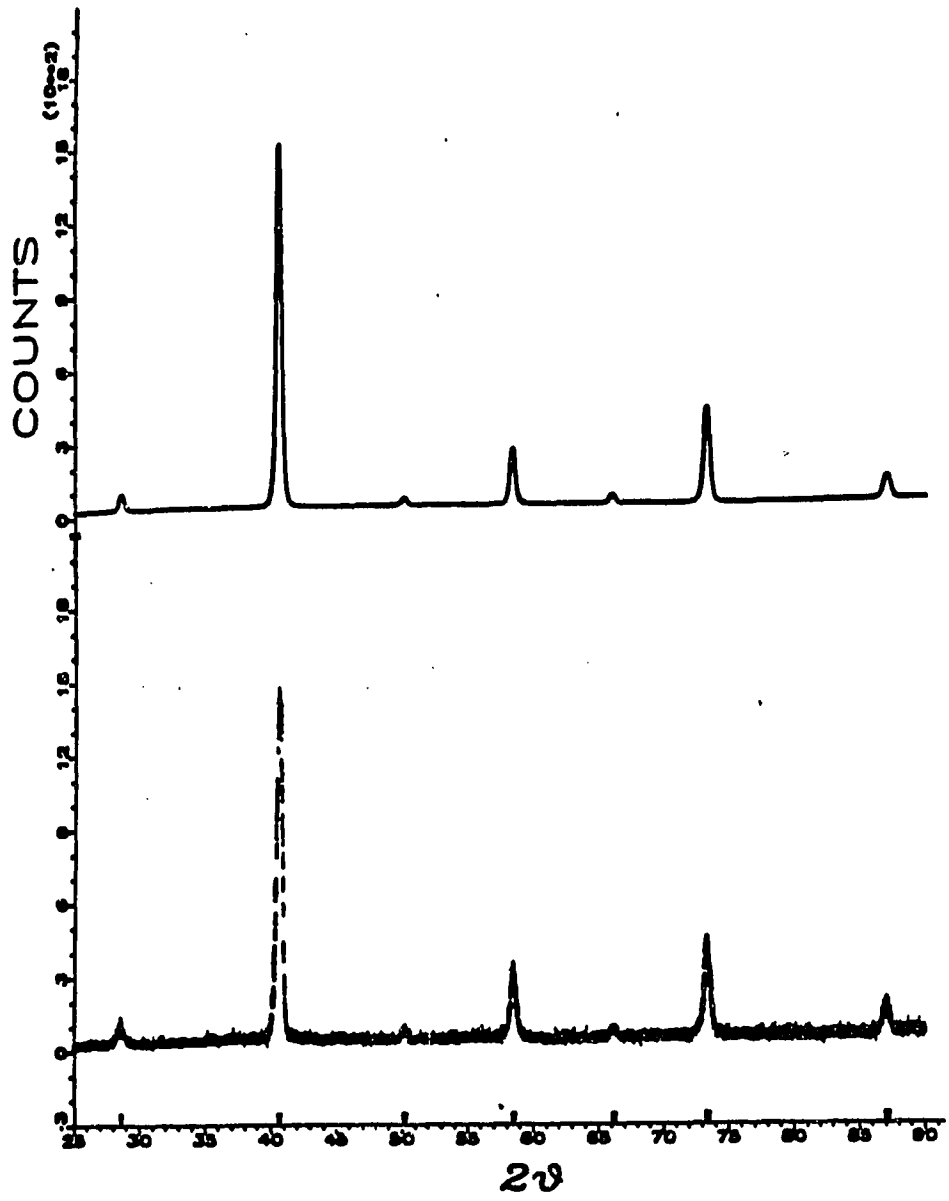

Figure IV-7 The calculated and observed diffraction patterns for Ru/Ta = 1.00 at 1160°C. Cubic phase present

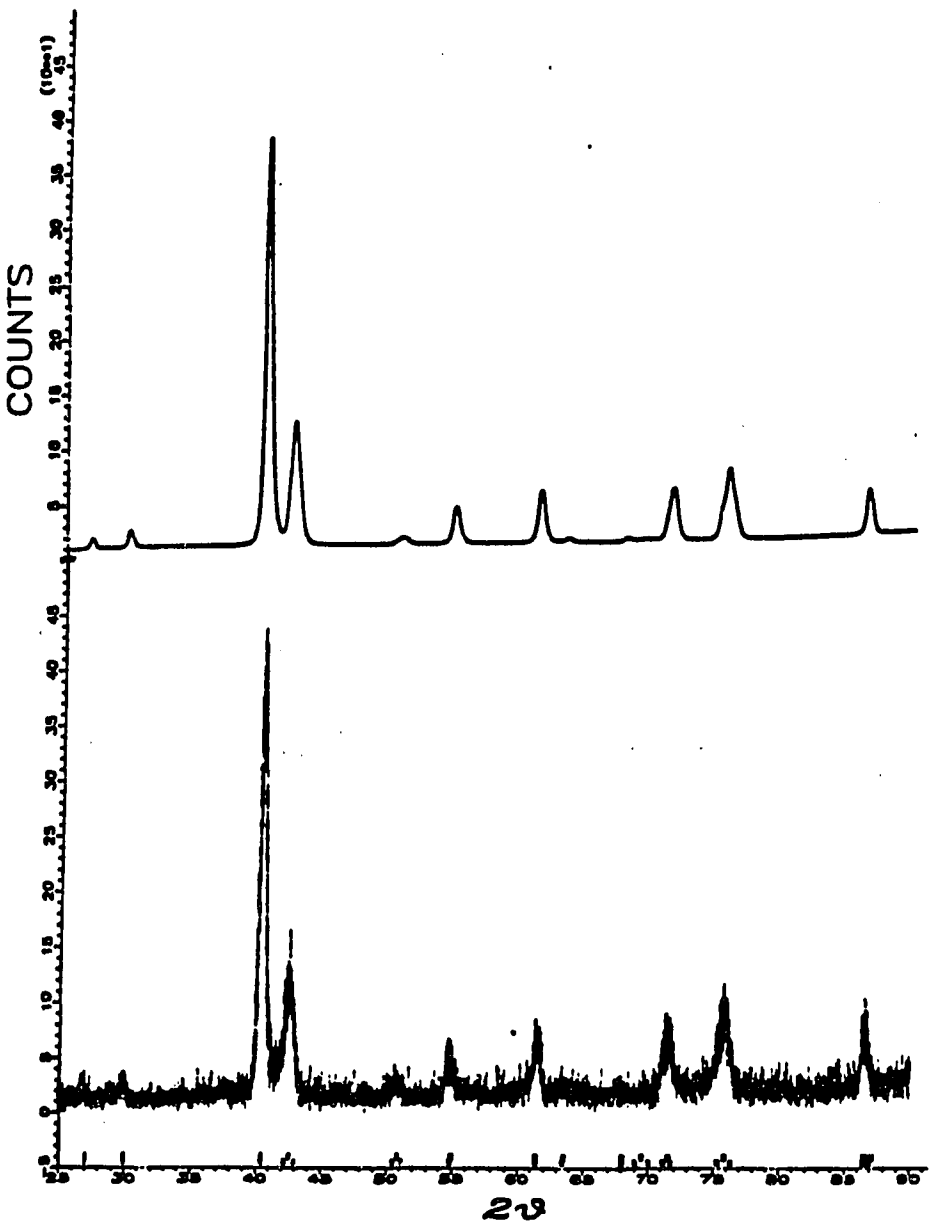

Figure IV-8 The calculated and observed diffraction patterns for Ru/Ta = 1.07 at room temperature. Tetragonal and orthorhombic phases present

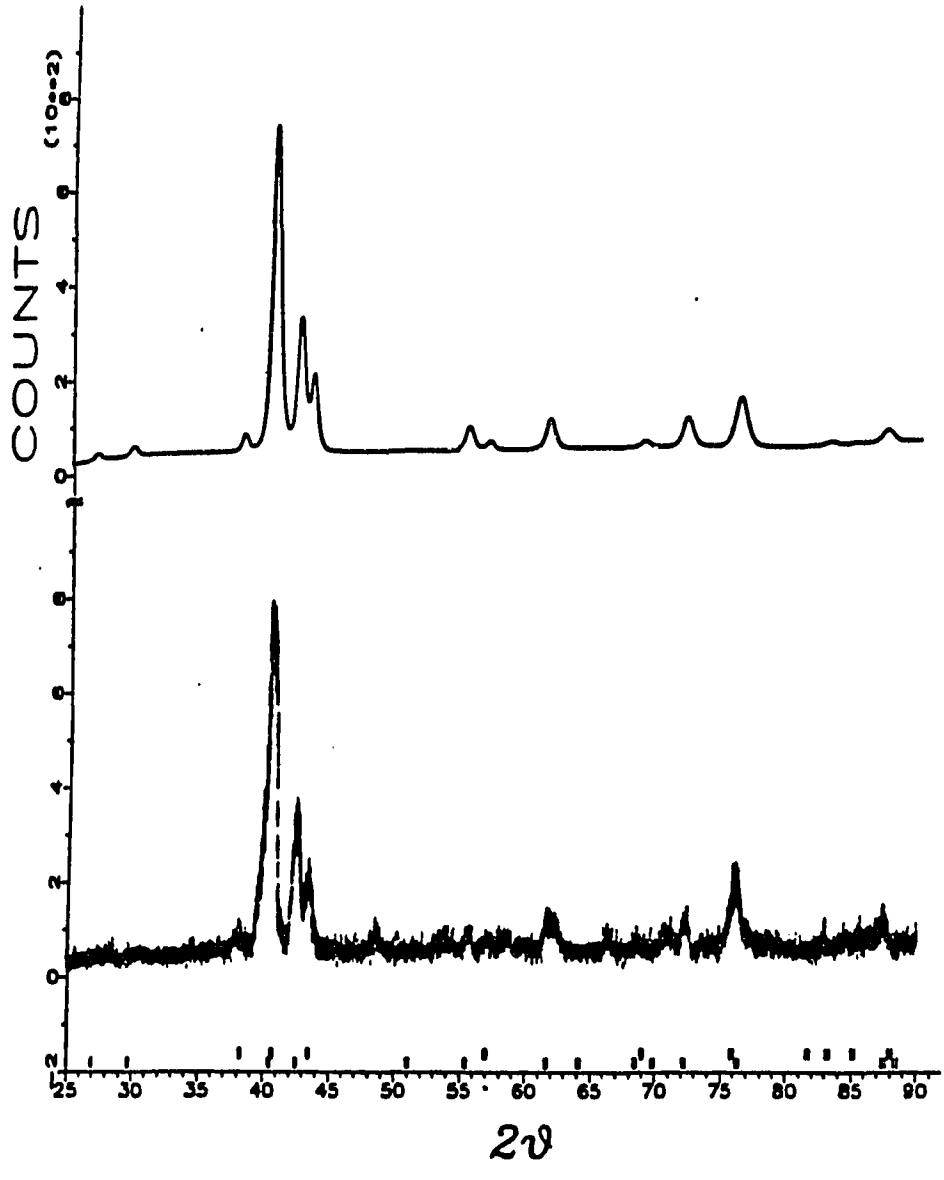

Figure IV-9 The calculated and observed diffraction patterns for Ru/Ta = 1.60 at room temperature. Tetragonal and hexagonal phases present

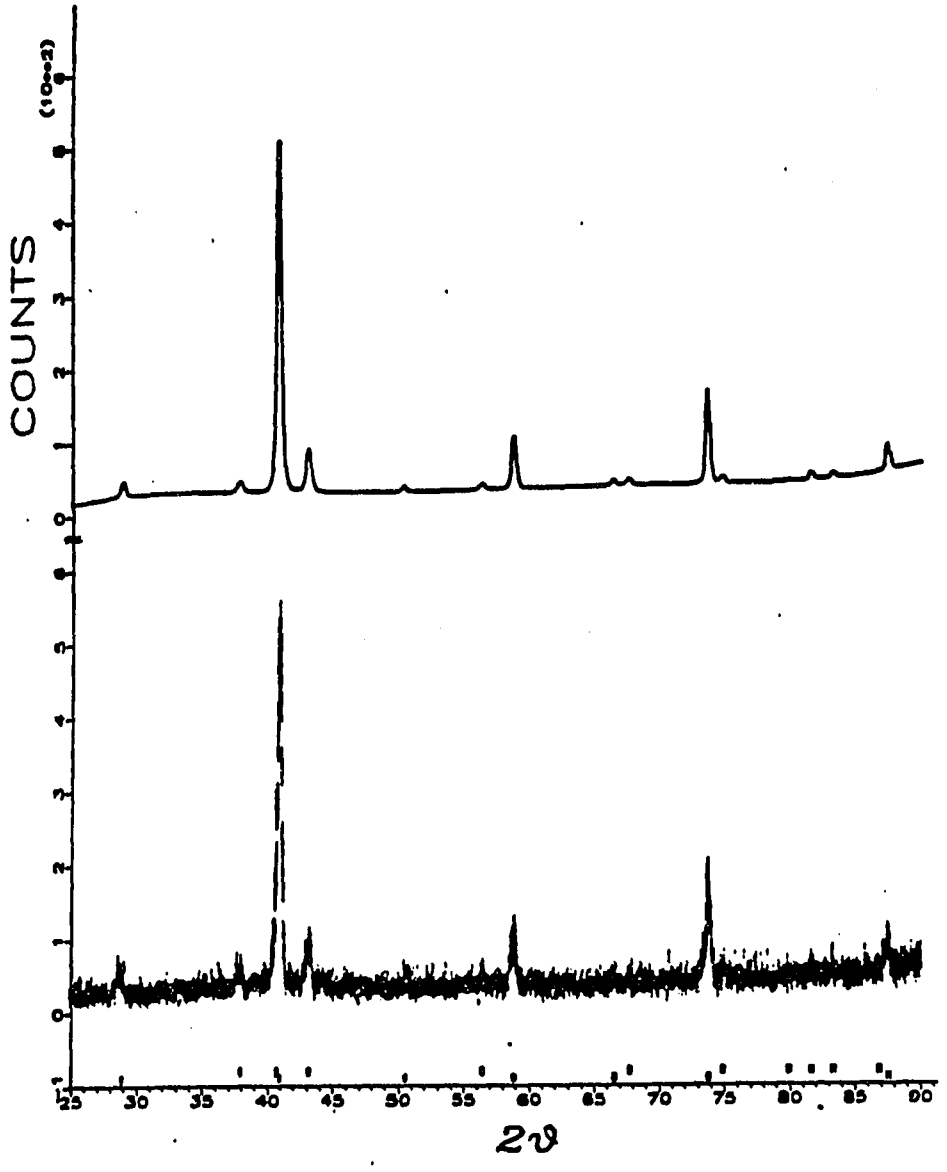

Figure IV-10 The calculated and observed diffraction patterns for Ru/Ta = 1.60 at 1640°C. Cubic and hexagonal phases present

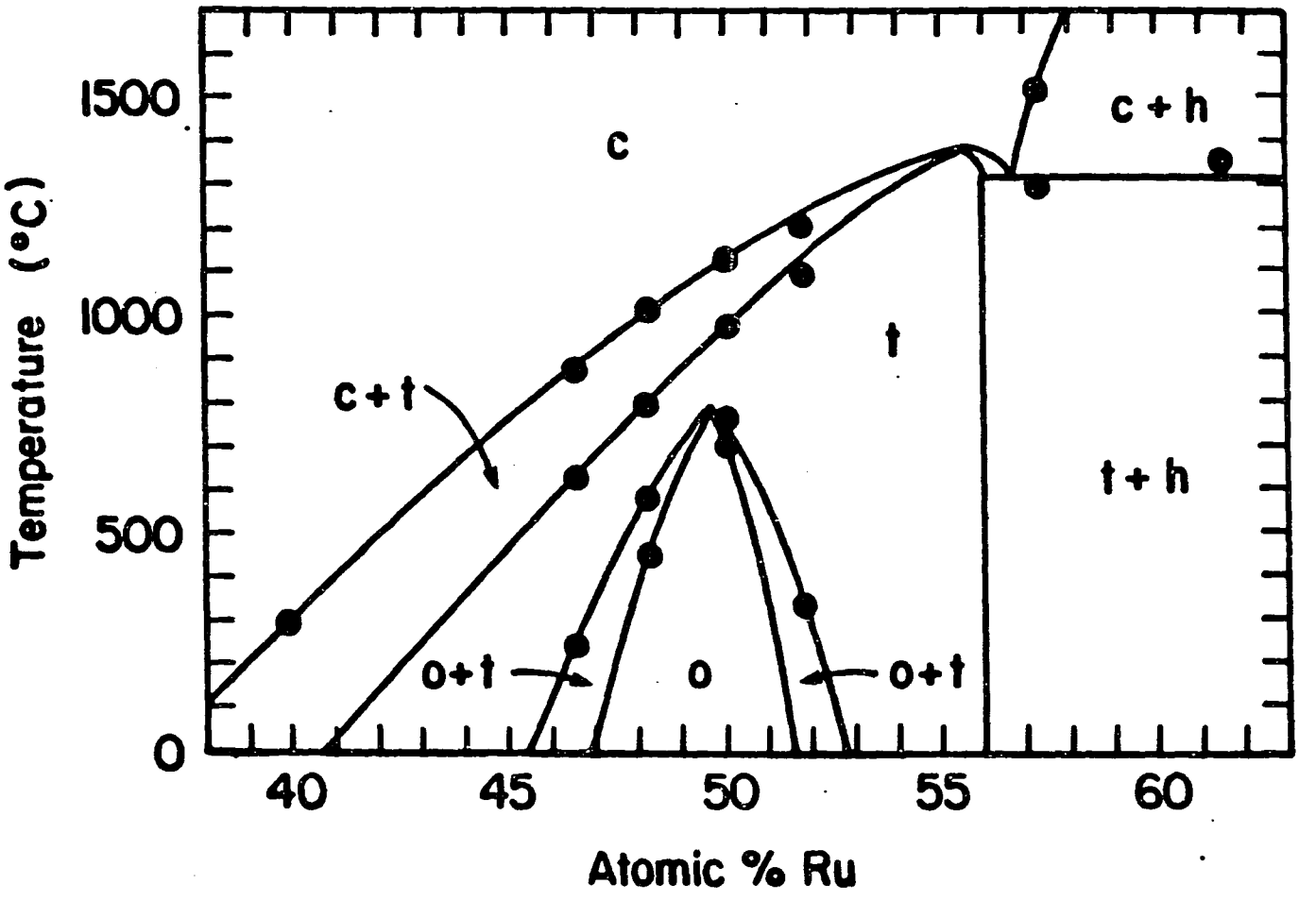

Figure IV-11 The temperature-composition diagram for Ta-Ru in the neighborhood of TaRu

REFERENCES

1. Beck, P. A.; Greenfield, P. AIME Trans. 1956, 206, 265.

2. Hartley, C. S.; Baun, W. L.; Fisher, D. W.; Rapperport, E. J. WADD Tech. Note 60-288, 1961, 18.

3. Elliott, R. P.; "Constitution of Binary Alloys"; First Supplement, McGraw-Hill: New York, 1965.

4. Rudman, P. S. Quarterly Progress Reports 6 and 7 on Contract Nonr-2547(00), NR-039-067 (AD 429068), 1963, 9.

5. Raub, E.; Beeskow, H.; Fritzsche, W. Z. Metallk. 1963, 54, 451.

6. Massalski, T. B.; Murray, J. L.; Benett, L. H.; Baker, H. "Binary Alloy Phase Diagrams"; American Society for Metals: Metals Parks, OH, 1986.

7. Schmerling, M. A.; Das, B. K.; Lieberman, D. S. Metallurgical Transactions 1970, 1, 3273.

8. Franzen, H. F. "Physical Chemistry of Inorganic Crystalline Solids"; Springer-Verlag: Heidelberg, 1986.

9. Chen, B. H.; Franzen, H. F. J. Less-Common Met. 1988, 143, 331.

10. Yi, S. S.; Chen, B. H.; Franzen, H. F. J. Less-Common Met. 1988, 143, 243.

11. Chen, B. H.; Franzen, H. F. J. Less-Common Met. 1989, 153, L13.

12. Chen, B. H.; Franzen, H. F. J. Less-Common Met. in press.

13. Chen, B. H.; Jacobson, R. A., to be published. Department of Chemistry, Iowa State University.

14. Tolédano, J. -C.; Tolédano, P. "The Laudau Theory of Phase Transition"; World Scientific Lecture Notes in Physics, Vol. 3, World Scientific Publishing: Singapore, 1987.

SECTION V PHASE TRANSITIONS IN $IrTi_{1+x}$

INTRODUCTION

The currently accepted phase diagram[1] for the Ir-Ti system given in Figure V-1 shows that IrTi alloys in a wide homogeneity range of 39 to 55 atomic % Ir have a CsCl-type structure at high temperature and distort to a monoclinic structure (a = 2.990 Å, b = 2.883 Å, c = 3.525 Å , and β = 90°52′ for Ir/Ti = 1) with decreasing temperature as a second-order phase transition. The phase diagram is based on the investigation by Eremenko and Shtepa[2] using thermal analysis, X-ray diffraction, and metallographic measurement. In disagreement with this phase diagram, Raman and Schubert[3] reported that IrTi (annealed at 820°C) has a face-centered orthorhombic structure (a = 4.174 Å, b = 4.107 Å, and c = 3.460 Å), that $Ir_{55}Ti_{45}$ has a AuCu-type structure (a = 4.409 Å and b = 3.51 Å), and that $Ir_{35}Ti_{65}$ possibly has a CsCl-type superstructure (a = 9.375 Å).

Because of the similarity of the behavior of IrTi to that of RhTi[4,5], NbRu[5], and RuTa[6] the phase transitions c → t → o in IrTi could be expected. The high-temperature X-ray investigation described here was undertaken in order to better understand the phase behavior of this system.

RESULTS

Alloys, IrTi, $Ir_{45}Ti_{55}$, and $Ir_{35}Ti_{65}$, were examined by powder X-ray diffraction from room temperature to the melting point. The X-ray data for IrTi and $Ir_{35}Ti_{65}$ were analyzed by Rietveld refinement and that for $Ir_{45}Ti_{55}$ was analyzed by the LLR refinement.[7] The results are as follows. Contrary to the accepted phase diagram, the high-temperature form of IrTi and $Ir_{45}Ti_{55}$ is the AuCu-type structure rather than the cubic structure,[1] and the low-temperature form of both is the NbRu-type structure rather than the monoclinic structure.[1] The phase transition appears to occur continuously, i.e., as a second-order transition. The powder diffraction patterns for IrTi at 1020°C (a = 2.9484 Å and b = 3.4986 Å) and at room temperature (a = 4.1628 Å, b = 4.1017 Å, and c = 3.4172 Å) are given in Figures V-2 and V-3 respectively. The lattice parameters a = 4.1866 Å, b = 4.1087 Å, and c = 3.4567 Å were found for $Ir_{45}Ti_{55}$ at room temperature. The $Ir_{35}Ti_{65}$ alloy has the CsCl-type structure, and no second phase was found for this composition. The powder diffraction patterns at room temperature (a = 3.1149 Å) are given in Figure V-4. These results indicate that a cubic, CsCl-type, homogeneity range is separated from a tetragonal, AuCu-type, range by a two phase gap, whereas an orthorhombic, NbRu-type, region is separated from the tetragonal region by a second-order

transition line passing through Ir/Ti = 1, T ≈ 1000°C and Ir/Ti = 0.82, T ≈ 400°C.

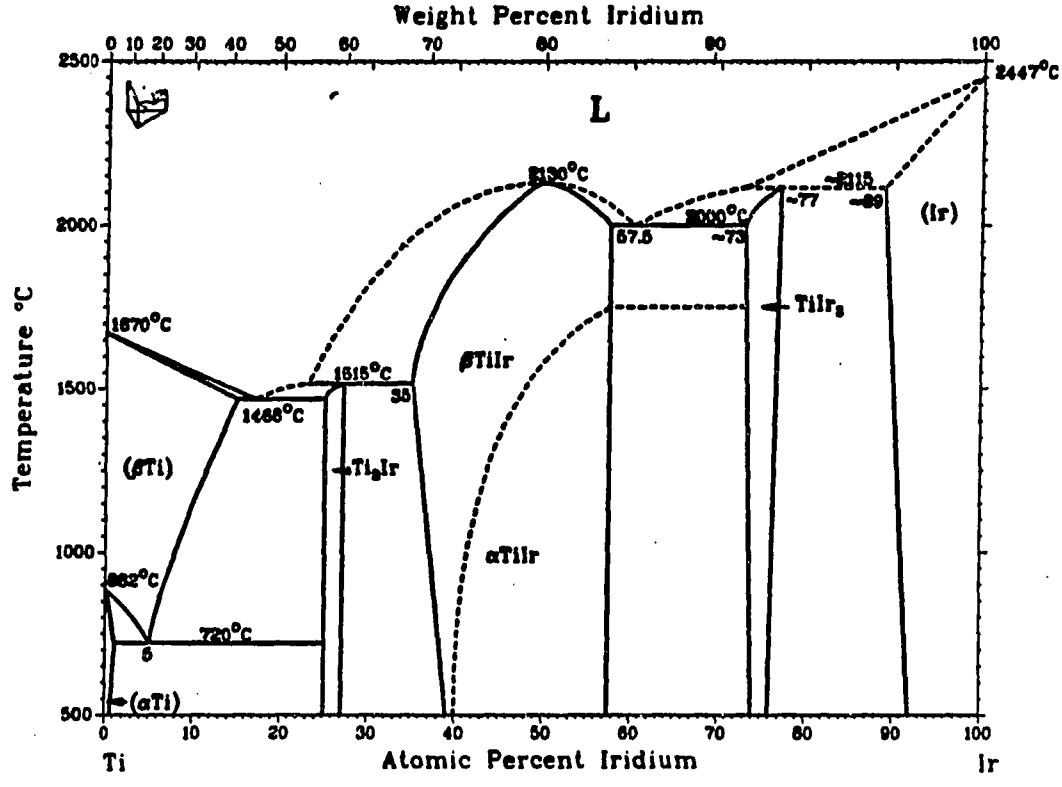

Figure V-1 The accepted phase diagram for Ir-Ti[1]

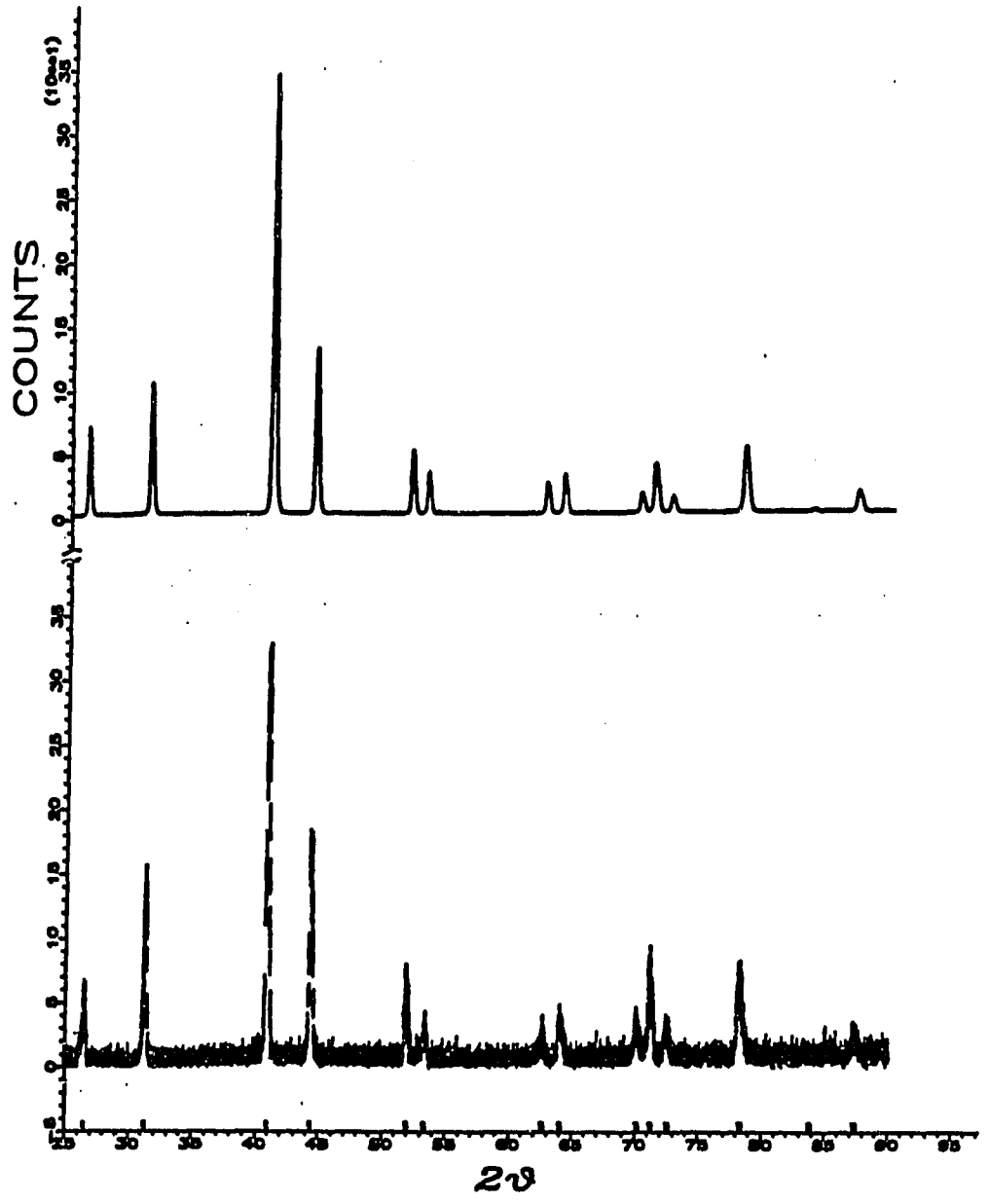

Figure V-2 The calculated and observed diffraction patterns for tetragonal IrTi at 1020°C

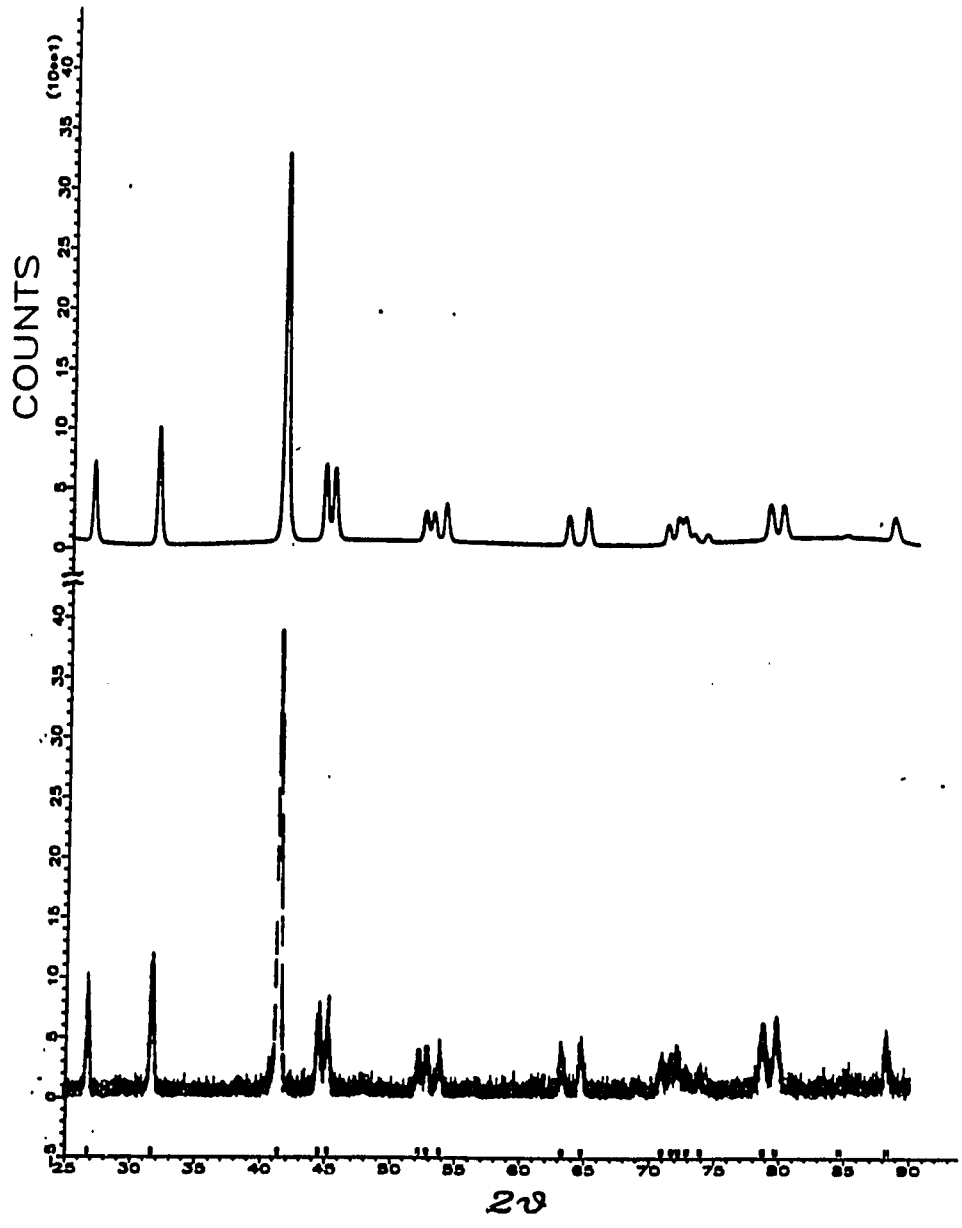

Figure V-3 The calculated and observed diffraction patterns for orthorhombic IrTi at room temperature

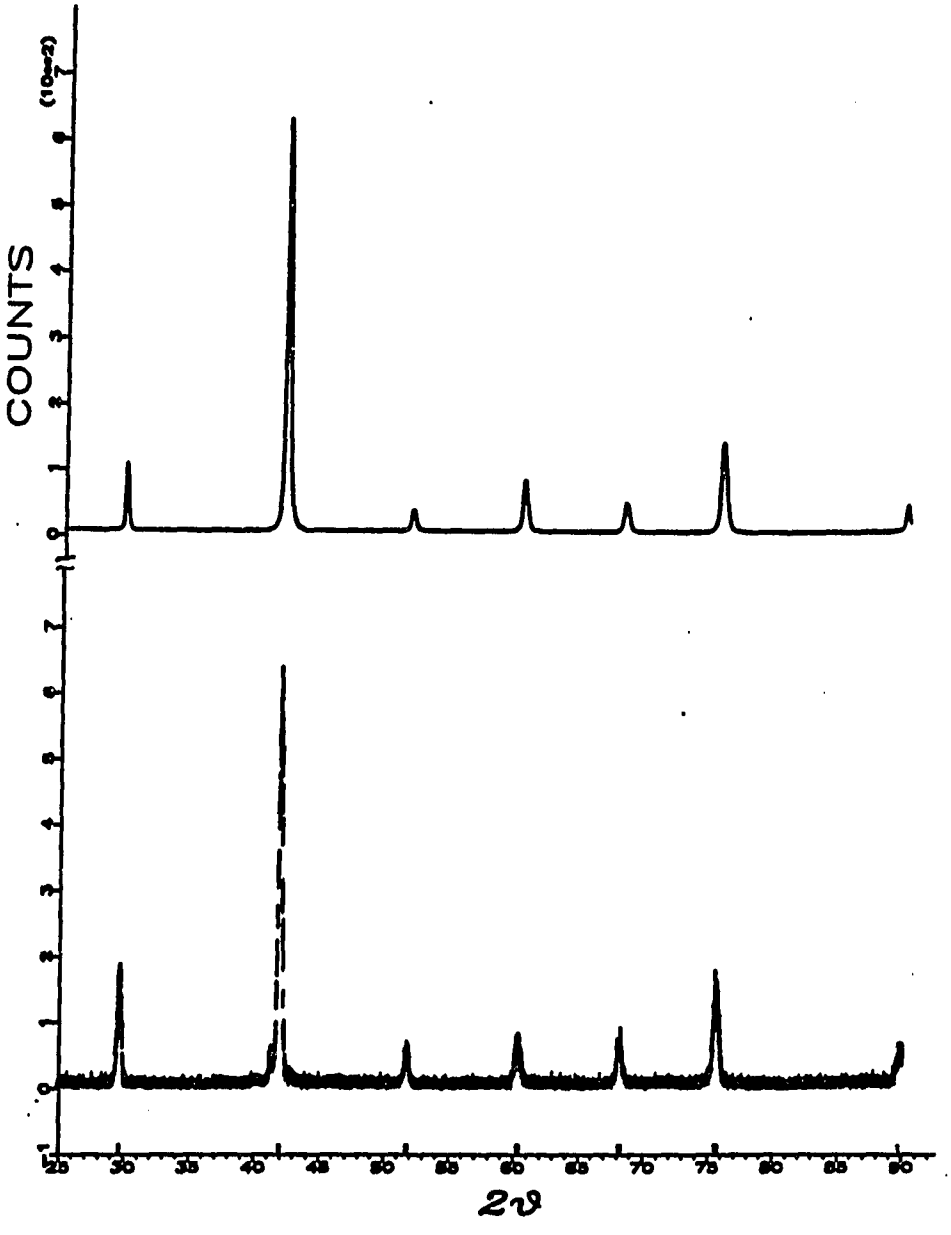

Figure V-4 The calculated and observed diffraction patterns for cubic $Ir_{35}Ti_{65}$ at room temperature

DISCUSSION

The crystal data are in good agreement with those reported by Raman and Schubert[3] except the conventional orthorhombic cell should be end-centered rather than face-centered. The previous report of a monoclinic cell was not confirmed. In fact, the monoclinic cell, if a = b, is equivalent to an end-centered orthorhombic cell. No CsCl-type superstructure was found.

As in the case of RhTi[4,5] and NbRu[5], a second-order phase transition from tetragonal to orthorhombic in IrTi within the homogeneity range is in agreement with the predictions of Landau theory[8,9] as described previously.[4,5]

REFERENCES

1. Massalski, T. B.; Murray, J. L.; Benett, L. H.; Baker, H. "Binary Alloy Phase Diagrams"; American Society for Metals: Metals Park, OH, 1986.

2. Eremenko, V. N.; Shtepa, T. D. Russ. Metall. 1970, 6, 127.

3. Raman, A.; Schubert, k. Z. Metallkd. 1964, 55, 704.

4. Yi, S. S.; Chen, B. H.; Franzen, H. F. J. Less-Common Met. 1988, 143, 243.

5. Chen, B. H.; Franzen, H. F. J. Less-Common Met. 1989, 153, L13.

6. Chen, B. H.; Franzen, H. F. J. Less-Common Met. in press.

7. Chen, B. H.; Jacobson, R. A., to be published. Department of Chemistry, Iowa State University.

8. Tolédano, J. -C.; Tolédano, P. "The Laudau Theory of Phase Transition"; World Scientific Lecture Notes in Physics, Vol. 3, World Scientific Publishing: Singapore, 1987.

9. Landau, L.; Lifshitz E. "Statistical Physics"; Pergamon Press: London, 1958.

SECTION VI A SECOND-ORDER PHASE TRANSITION IN $V_{54}Ir_{46}$

INTRODUCTION

The binary system V-Ir has been studied previously by Giessen, Dangel, and Grant.[1] All samples were annealed at 1800°C before X-ray measurement. It was found that two structures exist for nominally 1:1 V-Ir intermetallic phases, one with P4/mmm symmetry and $c/a \simeq \sqrt{2}$ and a AuCu-like structure between 52±1 to 59±1 atomic % Ir, the other with Cmmm symmetry between 50±0.5 to 51±0.5 atomic % Ir. Although they recognized that the orthorhombic structure can be regarded as a distorted AuCu-type superstructure by axial reorientation, the heterogeneous relationship between these phases was not determined. They suggested that the two structures occur in different composition ranges with a first-order transition between them, as indicated in the previous phase diagram.[1]

In the study[2] reported here, a single composition, namely $V_{54}Ir_{46}$, was studied by high-temperature powder X-ray diffraction using Rietveld full-profile refinement. An apparent second-order transition at about 506°C was observed. The Landau theory[3-5] was found to allow a second-order transition to a tetragonal symmetry with doubling of both lattice parameters a and c yielding in a body-centered cell.

RESULTS

At temperatures above 506°C the powder diffraction pattern of the V-Ir sample was consistent with the tetragonal structure with, to a first approximation, Ir at the origin and V at the body center. The diffraction pattern from the sample at 556°C is given in Figure VI-1. At temperatures below 506°C the tetragonal symmetry was broken to yield an orthorhombic distortion, the extent of distortion was observed to vary continuously with temperature. The diffraction pattern from the sample at room temperature is given in Figure VI-2. The structural Results given in Table VI-1 yielded by Rietveld refinement for both patterns show that the orthorhombic structure has the lattice parameters $a_o \simeq 2a_{tet}$, $b_o \simeq 2c_{tet}$, and $c_o \simeq a_{tet}$.

Table VI-1 The structural results for $V_{54}Ir_{46}$

T(°C)	Symmetry	Lattice Parameters(Å)	Atomic Positions (x, y, z)
556	P4/mmm	a = 2.770 c = 3.651	Ir: 0, 0, 0 V: 0.5 0.5 0.5
25	Cmmm	a = 5.797 b = 6.762 c = 2.805	Ir: 0, 0.2178, 0.5 V: 0.2871, 0, 0

DISCUSSION

The second-order phase transition from tetragonal to orthorhomblic observed for $V_{54}Ir_{46}$ is in complete agreement with the predictions of Landau theory.[2-4] The group Cmmm is a subgroup of P4/mmm. The transition from P4/mmm to Cmmm doubles the periods along a° and c° (or, equivalently, along b° and c°) and thus corresponds to $k = (a^* + c^*)/2$ (or $(b^* + c^*)/2$). The groups of these wave vectors contain the essential symmetry operations of Cmmm because the translations by 2a°, 2c°, and a° + c° remain, while by a° and c° are lost. Thus the distortion corresponds to the totally symmetric small representation at one of these two k points. The two k vectors form a star, and basis functions for the corresponding two-dimensional representation are $\phi_1 = \cos\pi z \cos\pi x$ and $\phi_2 = \cos\pi z \cos\pi y$. There are no third-order combinations that are not antisymmetric under transition by a° (or b°) of the tetragonal lattice, thus the transition meets the first three conditions of Landau theory. The fourth condition is also met since inversion is in the group of the wave-vector.

There are two independent fourth-order invariants, namely $\phi_1^4 + \phi_2^4$ and $\phi_1^2\phi_2^2$, and thus two fourth-order terms, $\gamma_1^4 + \gamma_2^4$ and $\gamma_1^2\gamma_2^2$, in the expansion of the Gibbs free-energy. However, $\gamma_1^2\gamma_2^2$ can be eliminated by using $(\gamma_1^2 + \gamma_2^2)^2 = 1$. Thus G to terms of fourth-order is:

$$G = G^\circ + A\eta^2 + [C_1 + C_2 (\gamma_1^4 + \gamma_2^4)]\eta^4$$

There are two possible minima under the constraint $\gamma_1^2 + \gamma_2^2 = 1$ for this G. On one hand, if $C_2 < 0$, $\gamma_1 = 1$ and $\gamma_2 = 0$ (or vice versa). The stable structure is given by $\rho = \rho^\circ + \phi_1\eta$. On the other hand, if $C_2 > 0$, $\gamma_1 = \gamma_2 = 1/\sqrt{2}$. The stable structure is given by $\rho = \rho^\circ + (\phi_1 + \phi_2)\eta/\sqrt{2}$. The first yields the distortion observed in $V_{54}Ir_{46}$ showing that this transition can, by Landau theory, occur as a second-order process. The second solution has I4/mmm symmetry with $a = 2a^\circ$ and $c = 2c^\circ$ and atoms in the positions: 0, 0, 1/4 + δ; 0, 1/2, 1/4; 1/4 - ε, 1/4 - ε, 0. The structure of $AgInLa_2$ has been reported to be of this type.[6]

At high-temperatures the Ir-V intermetallic studied here has a tetragonal structure that is best described as a superstructure of the disordered, cubic close-packed structure, with tetragonal symmetry arising from alteration of layers of (predominantly) Ir and V along one of the cubic axial directions. Upon cooling this tetragonal symmetry undergoes a symmetry breaking which can be viewed as the alternate lengthening and shortening of trans M-M distances in chains of M_2M_4' octahedra (M and M′ alternate between Ir and V (Figure VI-3)). The continuous character of the transition suggests that it occurs as the result of a Fermi level instability at $(a_J + c_J)/4$.

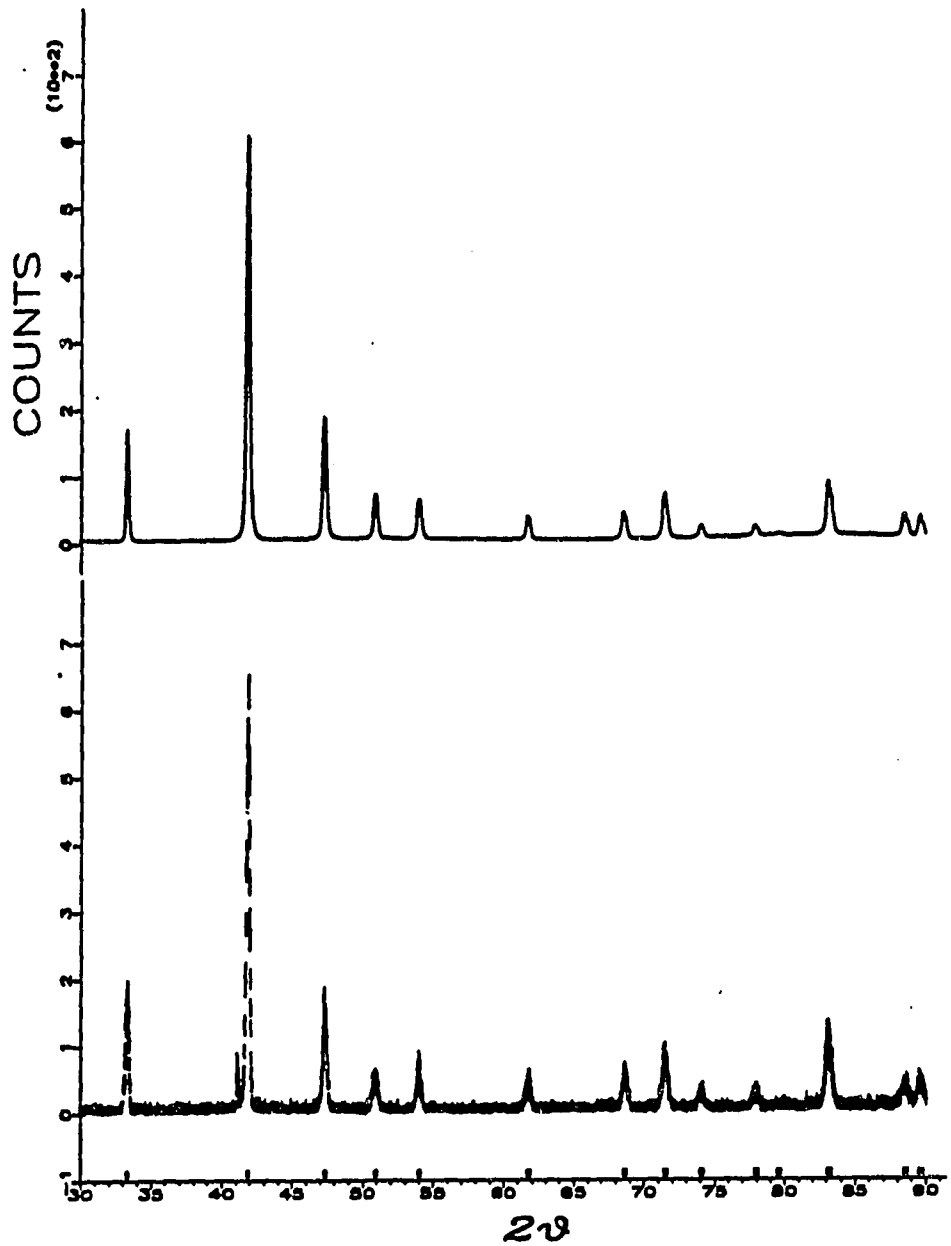

Figure VI-1 The calculated and observed diffraction patterns for tetragonal Ir-V at 556°. The extra line at 2θ = 41° arises from the sample holder

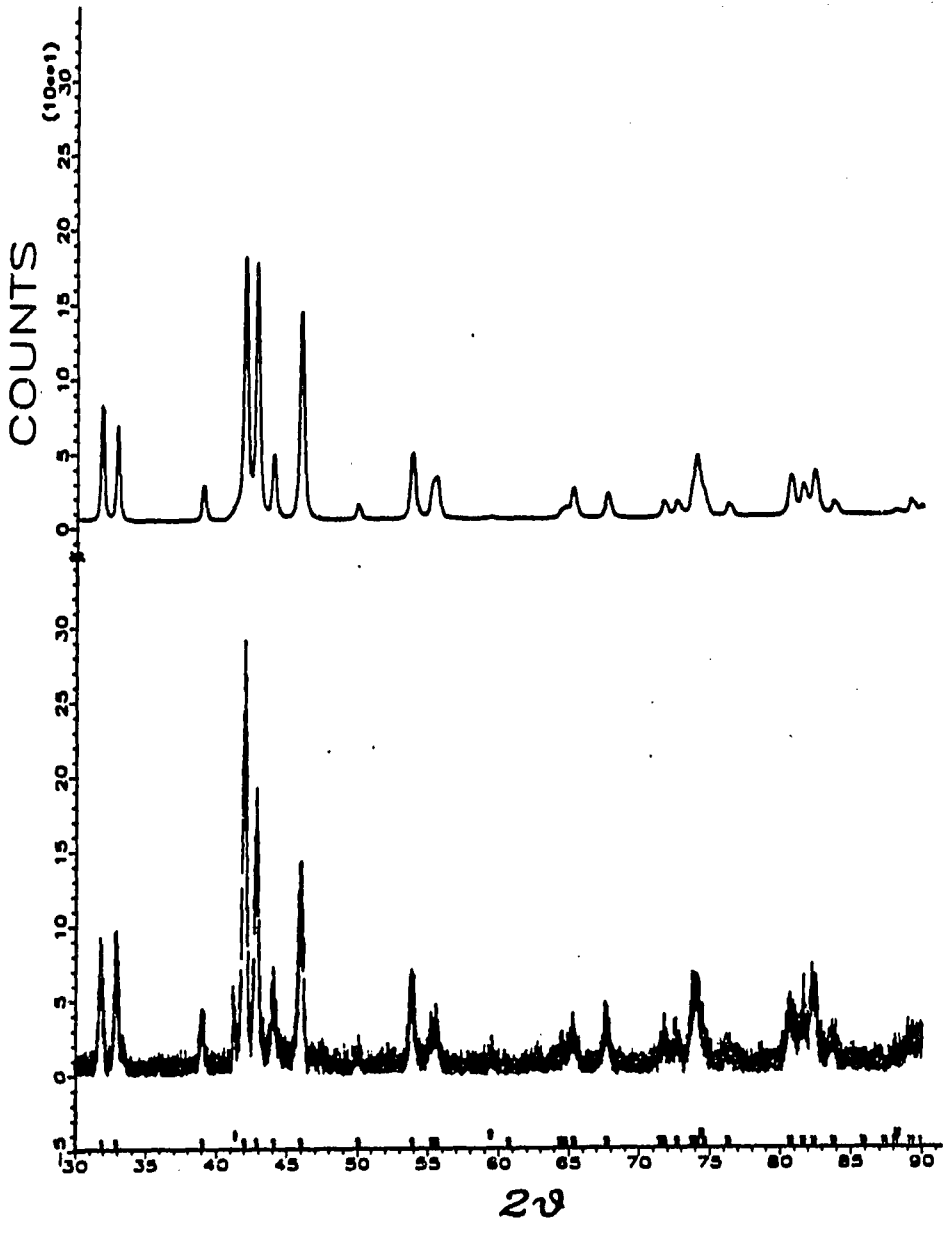

Figure VI-2 The calculated and observed diffraction patterns for orthorhombic Ir-V at room temperature. The locations of the diffraction maxima arising from the sample holder are indicated by the upper set of vertical marks just above the horizontal axis

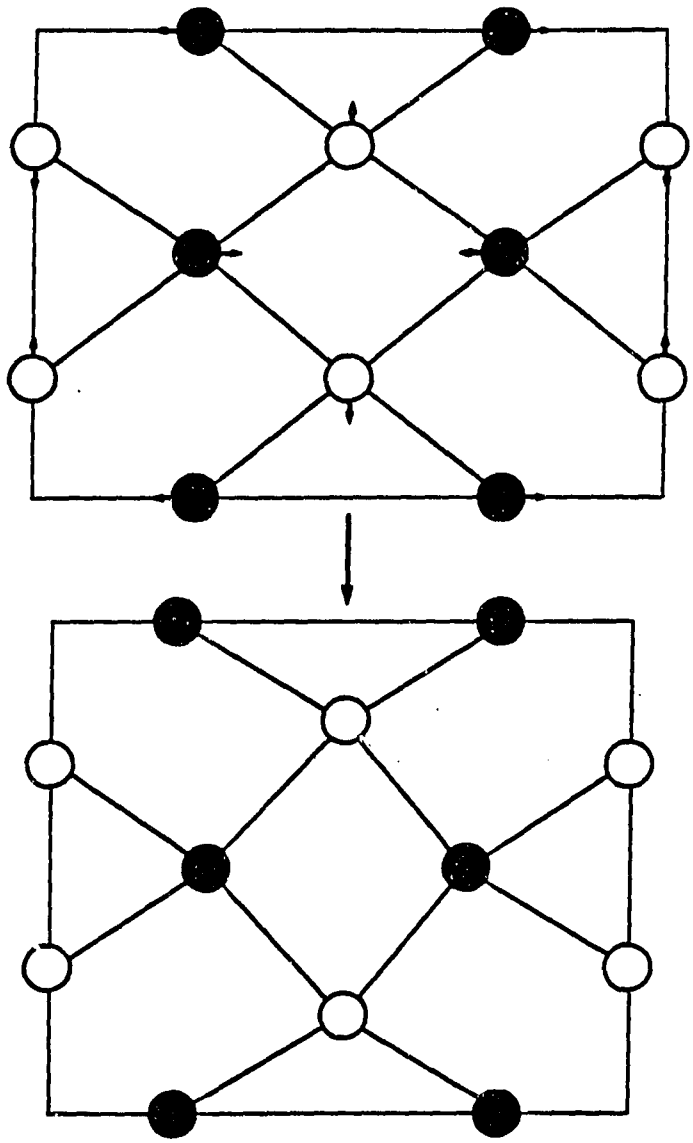

Figure VI-3 The Ir-V structure viewed along the short (c) axis of the orthorhombic form. The relative scales are calculated from the structures reported here (P4/mmm symmetry (on the left) at 556°C, Cmmm symmetry (on the right) at room temperature)

REFERENCES

1. Giessen, B. C.; Dangel, P. M.; Grant N. J. J. Less-Common Met. 1967, 13, 62.

2. Chen, B. H.; Franzen, H. F. J. Less-Common Met., in press.

3. Tolédano, J. -C.; Tolédano, P. "The Landau Theory of Phase Transition"; World Scientific Lecture Notes in Physics, Vol. 3, World Scientific Publishing, Singapore, 1987.

4. Landau, L.; Lifshitz E. "Statistical Physics"; Pergamon Press: London, 1958.

5. Franzen, H. F. "Physical Chemistry of Inorganic Crystalline Solids", Springer-Verlag: Heidelberg, 1986.

6. Maetz, J.; Mullner, M.; Jex, H; Assmus, W.; Takke, R. Zeitschrift fur Physik B. 1980, 37, 39.

APPENDIX A: THE PROGRAM FOR LATTICE PARAMETER REFINEMENT IN CRYSTAL SYSTEMS WITH ORTHORHOMBIC SYMMETRY OR HIGHER

```
CCCCCCCCCCCCCCCCCCCCCCCCCCCCCCCCCCCCCCCCCCCCCCCCCCCCCCCCCCCCCCCCCC
C                                                                   C
C   LINEAR LEAST-SQUARES LATTICE PARAMETER REFINEMENT               C
C                          (LLR)                                    C
C                                                                   C
C   PURPOSE:                                                        C
C       Use a linear least-squares method to refine                 C
C   lattice parameters for crystal with symmetry                    C
C   orthorhombic or higher.                                         C
C                                                                   C
CCCCCCCCCCCCCCCCCCCCCCCCCCCCCCCCCCCCCCCCCCCCCCCCCCCCCCCCCCCCCCCCCC

        REAL TT(500),W(500),E(4,4),D(4),KA1,KA2
        COMMON N,M,ER,HH,A,B,C,LI
        KA1=1.540562
        KA2=1.544390
        READ(8,*)N,CTH,(TT(I),I=1,N)
        TYPE 30
30      FORMAT(1X,'$ INPUT 0-2TH')
        ACCEPT*,T0
        TYPE 40
40      FORMAT(1X,'$MAX INDEX')
        ACCEPT*,M
        TYPE 50
50      FORMAT(1X,'$ REFINE 0-TH ?(N=0,Y=1)')
        ACCEPT*,LI
        DO 90 I=1,N
        TT(I)=TT(I)+T0
        TW=TAND(TT(I)/2.)/TAND(CTH/2.)
        W(I)=(2.*KA1+(1.-TW)*KA2)/(3.-TW)
90      IF(TW.GE.1) W(I)=KA1
        TYPE 95
95      FORMAT(1X,'$LIMITED ERR IN 2THETA')
        ACCEPT*,ER
100     TYPE 110
110     FORMAT(1X,'$INDEX: 1.CUBIC 2.HEXA 3.TETRA 4.ORTH(TY:1.2...)')
```

```
      ACCEPT*,HH
      TYPE 120
120   FORMAT(1X,'$DO YOU WISH TO GIVE A,B,C ? N=0, Y=1')
      ACCEPT*, LP
      IF(LP.EQ.0) GO TO 140
      TYPE 125
125   FORMAT(1X,'TYPE A,B, AND C')
      ACCEPT*, A,B,C
      IF(HH.EQ.1) KK=1+LI
      IF(HH.EQ.2.OR.HH.EQ.3) KK=2+LI
      IF(HH.EQ.4) KK=3+LI
      CALL MATCH(TT,W,KK,E,D)
      GO TO 150
140   IF(HH.EQ.1)  CALL CUBIC(TT,W)
      IF(HH.EQ.2.OR.HH.EQ.3)   CALL HANDT(TT,W)
      IF(HH.EQ.4)  CALL ORTH(TT,W)
150                                        STOP
      END
C     ****************  CUBIC  ******************

      SUBROUTINE CUBIC(TT,W)
      DIMENSION TT(N),R(8,500),W(N),E(4,4),D(4)
      INTEGER H1,K1,L1,MM,MMM,N1
      COMMON N,M,ER,HH,A,B,C,LI
      TYPE 200
200   FORMAT(1X,'$INPUT H1,K1,L1,#PEAK')
      ACCEPT*,H1,K1,L1,N1
      A=0.5*W(N1)*SQRT(FLOAT(H1*H1+K1*K1+L1*L1))/SIND(TT(N1)/2.)
      WRITE(6,210)
210   FORMAT('1',15X,'!!!!!!!!!!!!  CUBIC  !!!!!!!!!!!!'/)
      WRITE(6,220)H1,K1,L1,TT(N1)
220   FORMAT(10X,'HKL  ',3I1,5X,'2-THETA',F7.2)
      B=A
      C=A
      KK=3+LI
      CALL MATCH(TT,W,KK,E,D)
                                        RETURN
      END
```

```
C       *******  HEXAGONAL AND TETRAGONAL   *******

        SUBROUTINE HANDT(TT,W)
        REAL TT(N),R(8,500),X,W(N),E(3,3),D(3)
        INTEGER H1,K1,L1,H2,K2,L2,MM,MMM,N1,N2
        COMMON N,M,ER,HH,A,B,C,LI
        F(X)=SIND(X)**2
        TYPE 310
310     FORMAT(1X,'$INPUT H1,K1,L1,#PEAK')
        ACCEPT*,H1,K1,L1,N1
        TYPE 320
320     FORMAT(1X,'$INPUT H2,K2,L2,#PEAK')
        ACCEPT*,H2,K2,L2,N2
        IF(HH.EQ.2) THEN
          WRITE(6,325)
325       FORMAT('1',15X,'!!!!!!!!!!  HEXAGONAL  !!!!!!!!!!'/)
          TYPE 330
330       FORMAT(1X,'!:((H1*H1+K1*K1+H1*K1)(L2*L2)'/
     1    1X,'-(H2*H2+K2*K2+H2*K2)*(L1*L1)).NE.ZERO')
          D1=W(N1)**2*FLOAT(H1*H1+K1*K1+H1*K1)/3.
          D2=W(N2)**2*FLOAT(H2*H2+K2*K2+H2*K2)/3.
        ELSE
          WRITE(6,355)
355       FORMAT('1',15X,'!!!!!!!!!!  TETRAGONAL  !!!!!!!!!!'/)
          TYPE 365
365       FORMAT(1X,'!:((H2*H2+K2*K2)L1*L1-(H1*H1+K1*K1)L2*L2).NE.0'/)
          D1=W(N1)**2*FLOAT(H1**2+K1**2)/4.
          D2=W(N2)**2*FLOAT(H2**2+K2**2)/4.
        ENDIF
        WRITE(6,370)H1,K1,L1,H2,K2,L2,TT(N1),TT(N2)
370     FORMAT(10X,'HKL  ',3I1,2X,3I1,5X,'2-THETA',2F7.2)
        C1=(W(N1)*FLOAT(L1))**2
        C2=(W(N2)*FLOAT(L2))**2
        AA=(F(TT(N2)/2.)*C1-F(TT(N1)/2.)*C2)/(D2*C1-D1*C2)
        CC=(F(TT(N1)/2.)*D2-F(TT(N2)/2.)*D1)/(D2*C1-D1*C2)
        A=1./SQRT(AA)
```

```
      B=A
      C=0.5/SQRT(CC)
      KK=2+LI
      CALL MATCH(TT,W,KK,E,D)
                                  RETURN
      END
C*********************  ORTHORHOMBIC  ********************************
      SUBROUTINE ORTH(TT,W)
      REAL TT(N),R(8,500),O(3,3),BB(3),W(N),T(3),E(4,4),D(4)
      INTEGER ID(3,3),IN(3)
      COMMON N,M,ER,HH,A,B,C,LI
      WRITE(6,400)
400   FORMAT(15X,'!!!!!!!!!!  ORTHORHOMIC  !!!!!!!!!!'/
     1   4X,'H K L',10X,'2-THETA')
      TYPE 405
405   FORMAT(1X'$INPUT HKL(1),#P1,HKL(2),#P2,HKL(3),#P3'/)
      ACCEPT*,((ID(I,J),J=1,3),IN(I),I=1,3)
      DO 410 I=1,3
          T(I)=TT(IN(I))
          V=W(IN(I))
          BB(I)=SIND(T(I)/2.)**2
      DO 410 J=1,3
410       O(I,J)=(FLOAT(ID(I,J))*V)**2
      WRITE(6,420) ((ID(I,J),J=1,3),T(I),I=1,3)
420   FORMAT(12X,3I2,10X,F6.2)
      KKK=3
      KS=0
      CALL SIMQ(O,BB,KKK,KS)
      A=0.5/SQRT(BB(1))
      B=0.5/SQRT(BB(2))
      C=0.5/SQRT(BB(3))
      KK=3+LI
      CALL MATCH(TT,W,KK,E,D)
                                  RETURN
      END
```

```
C************************  SUB MATCH  ******************************

      SUBROUTINE MATCH(TT,W,KK,E,D)
      REAL TT(N),R(8,500),E(KK,KK),D(KK),TR(8,500),W(N),G(4)
      INTEGER NNN,NN,LL,II,JJ,H,K,L,KK1
      COMMON N,M,ER,HH,A,B,C,LI
      WRITE(6,800)A,B,C
800   FORMAT(10X,'INITIAL:',1X,'A =',F8.5,3X,'B =',F8.5,3X,'C =',F8.5)
      DD=0.
      MM=0
      TYPE 805
805   FORMAT(3X,'# OF CYCLES ?')
      ACCEPT *, III
810   NN=0
      MM=MM+1
      DO 850 L=0,M
      DO 850 K=0,M
      DO 850 H=0,M
      IF(HH.EQ.2) THEN
        CT=SQRT(FLOAT(H*H+K*K+H*K)/(3.*A*A)+(FLOAT(L)/(2.*C))**2)
      ELSE IF(HH.EQ.3) THEN
        CT=0.5*SQRT(FLOAT(H*H+K*K)/(A*A)+(FLOAT(L)/C)**2)
      ELSE
        CT=0.5*SQRT((H/A)**2+(K/B)**2+(L/C)**2)
      ENDIF
      LL=0
      DO 820 I=1,N
        TTM=CT*W(I)
        IF(TTM.GE.1.) GO TO 850
        CTT=2.*ASIND(TTM)
        EM=TT(I)-CTT
        IF(ABS(EM).GE.ER) GO TO 820
        LL=LL+1
        TR(1,LL)=TT(I)
        TR(2,LL)=CTT
        TR(3,LL)=ABS(EM)
```

```
          TR(4,LL)=0.02/TAND(TT(I)/2.)
          TR(5,LL)=FLOAT(I)
          TR(6,LL)=FLOAT(H)
          TR(7,LL)=FLOAT(K)
          TR(8,LL)=FLOAT(L)
820     CONTINUE
        IF(LL.EQ.0) GO TO 850
        IF(LL.EQ.1) GO TO 830
        NNN=3
        CALL BUBB(TR,LL,NNN)
830     NN=NN+1
        DO 840 I=1,8
840       R(I,NN)=TR(I,1)
850     CONTINUE
        ER=0.9*ER
        IF(MM.EQ.III) GO TO 980
        DO 870 I=1,KK
        DO 870 J=1,KK
          E(I,J)=0.
870     D(J)=0.
        DO 950 I=1,NN
          JJ=IFIX(R(5,I))
            P=SIND(R(1,I)/2.)**2
            IF(HH.EQ.2) THEN
              G(1)=4.*(R(6,I)**2+R(6,I)*R(7,I)+R(7,I)**2)*(W(JJ)**2)/3.
            ELSE IF(HH.EQ.3) THEN
              G(1)=(R(6,I)**2+R(7,I)**2)*(W(JJ)**2)
            ELSE
              G(1)=(R(6,I)*W(JJ))**2
              G(2)=(R(7,I)*W(JJ))**2
            ENDIF
              G(KK-LI)=(R(8,I)*W(JJ))**2
            IF(LI.EQ.0) GO TO 935
              G(KK)=-SIND(R(1,I))/2.
935         DO 940 J=1,KK
              D(J)=D(J)+P*G(J)
```

```
            DO 940 K=1,KK
940           E(K,J)=E(K,J)+G(K)*G(J)
950       CONTINUE
          KS=0
          CALL SIMQ(E,D,KK,KS)
          A=0.5/SQRT(D(1))
          B=A
          IF(HH.EQ.1.OR.HH.EQ.4) B=0.5/SQRT(D(2))
          C=0.5/SQRT(D(KK-LI))
          IF(LI.EQ.0) GO TO 810
          TD=2.*D(KK)*45./ATAN(1.)
          DD=DD+TD
          DO 970 I=1,N
970       TT(I)=TT(I)+TD
          GO TO 810
980       WRITE(6,985)A,B,C,DD
985       FORMAT(10X,'FINAL:',3X,'A =',F8.5,3X,'B =',F8.5,3X,'C =',F8.5,
       1    3X,'0-THE =',F7.3)
          MMM=1
          CALL BUBB(R,NN,MMM)
          CALL PRINT(R,NN)
                                                        RETURN
          END
C************************  SUB BUBB  **********************

          SUBROUTINE BUBB(R,NN,H)
          REAL R(8,NN)
          INTEGER NN,NI,NJ,H
          NI=NN-1
          DO 1020 K=1,NI
            NJ=NN-K
              DO 1020 L=1,NJ
                IF(R(H,L).LE.R(H,L+1)) GO TO 1020
                  DO 1010 I=1,8
                    TEMP=R(I,L)
                    R(I,L)=R(I,L+1)
1010                R(I,L+1)=TEMP
```

```
1020        CONTINUE
                                                    RETURN
        END
C
C******************  PRINTING RESULTS  ********************
C
        SUBROUTINE PRINT(R,NN)
        REAL R(8,500),RR(4,500),SS(2,500),ST
        INTEGER II(4,500),NN
        ST=0.
        DO 1030 I=1,NN
          SS(1,I)=SIND(R(1,I)/2.)**2
          SS(2,I)=SIND(R(2,I)/2.)**2
          ST=ST+R(3,I)**2
        DO 1030 J=1,4
          II(J,I)=IFIX(R(J+4,I))
1030      RR(J,I)=R(J,I)
        ST=SQRT(ST/FLOAT(NN-1))
        WRITE(6,1035)ST
1035    FORMAT(10X,'STANDARD DEVIATION',F16.6/)
        WRITE(6,1040)
1040    FORMAT(10X,'#P',2X,'  H   K   L  ',2X,'O2T',5X,'C2T',
     1    5X,'DIFF',5X,'DE',5X,'OSIN',6X,'CSIN'/)
        DO 1055 J=1,NN
          WRITE(6,1050) (II(I,J),I=1,4),(RR(I,J),I=1,4),(SS(I,J),I=1,2)
1050      FORMAT(9X,I3,1X,3I4,1X,2F8.3,2F8.3,2F9.5)
1055    CONTINUE
        WRITE(6,1060)
1060    FORMAT(/10X,'* DE--0.02/TAN(THETA)'/)
                                                      RETURN
        END
C     ..................................................................
C
      SUBROUTINE SIMQ(A,B,N,KS)
      DIMENSION A(1),B(1)
```

```
C         FORWARD SOLUTION
C
      TOL=0.0
      KS=0
      JJ=-N
      DO 65 J=1,N
      JY=J+1
      JJ=JJ+N+1
      BIGA=0
      IT=JJ-J
      DO 30 I=J,N
C
C         SEARCH FOR MAXIMUM COEFFICIENT IN COLUMN
C
      IJ=IT+I
      IF(ABS(BIGA)-ABS(A(IJ))) 20,30,30
   20 BIGA=A(IJ)
      IMAX=I
   30 CONTINUE
C
C         TEST FOR PIVOT LESS THAN TOLERANCE (SINGULAR MATRIX)
C
      IF(ABS(BIGA)-TOL) 35,35,40
   35 KS=1
      RETURN
C
C         INTERCHANGE ROWS IF NECESSARY
C
   40 I1=J+N*(J-2)
      IT=IMAX-J
      DO 50 K=J,N
      I1=I1+N
      I2=I1+IT
      SAVE=A(I1)
      A(I1)=A(I2)
      A(I2)=SAVE
```

```
C        DIVIDE EQUATION BY LEADING COEFFICIENT
C
   50 A(I1)=A(I1)/BIGA
      SAVE=B(IMAX)
      B(IMAX)=B(J)
      B(J)=SAVE/BIGA
C
C        ELIMINATE NEXT VARIABLE
C
      IF(J-N) 55,70,55
   55 IQS=N*(J-1)
      DO 65 IX=JY,N
      IXJ=IQS+IX
      IT=J-IX
      DO 60 JX=JY,N
      IXJX=N*(JX-1)+IX
      JJX=IXJX+IT
   60 A(IXJX)=A(IXJX)-(A(IXJ)*A(JJX))
   65 B(IX)=B(IX)-(B(J)*A(IXJ))
C
C        BACK SOLUTION
C
   70 NY=N-1
      IT=N*N
      DO 80 J=1,NY
      IA=IT-J
      IB=N-J
      IC=N
      DO 80 K=1,J
      B(IB)=B(IB)-A(IA)*B(IC)
      IA=IA-N
   80 IC=IC-1
      RETURN
      END
```

APPENDIX B: THE PROGRAM FOR LATTICE PARAMETER REFINEMENT IN CRYSTAL SYSTEMS WITH MONOCLINIC SYMMETRY

```
CCCCCCCCCCCCCCCCCCCCCCCCCCCCCCCCCCCCCCCCCCCCCCCCCCCCCCCCCCCCCCCC
C                                                                 C
C     LATTICE REFINEMENT PROGRAM FOR MONOCLINIC CELL              C
C                          (MONO)                                 C
C                                                                 C
C     PURPOSE:                                                    C
C         Use a Gridls least-squares method to refine             C
C     lattice parameters for monoclinic symmetry.                 C
C                                                                 C
CCCCCCCCCCCCCCCCCCCCCCCCCCCCCCCCCCCCCCCCCCCCCCCCCCCCCCCCCCCCCCCC

      REAL TT(100),W(500),KA1,KA2
      COMMON N,M,ER,A,B,C,SB,CB,BETA
      KA1=1.540562
      KA2=1.544390
      READ(8,*)N,CTH,(TT(I),I=1,N)
      TYPE 30
30    FORMAT(1X,'$ INPUT 0-2TH')
      ACCEPT*,T0
      TYPE 40
40    FORMAT(1X,'$MAX INDEX')
      ACCEPT*,M
      DO 90 I=1,N
      TT(I)=TT(I)+T0
      TW=TAND(TT(I)/2.)/TAND(CTH/2.)
      W(I)=(2.*KA1+(1.-TW)*KA2)/(3.-TW)
90    IF(TW.GE.1) W(I)=KA1
      TYPE 95
95    FORMAT(1X,'$LIMITED ERR IN 2THETA')
      ACCEPT*,ER
      CALL MONO(TT,W)
                                              STOP
      END
```

```
C********************   MONOCLINIC   ****************************
      SUBROUTINE MONO(TT,W)
      REAL TT(N),O(4,5),BB(4),W(N),T(4)
      INTEGER ID(4,3),IN(4),MI,MJ
      COMMON N,M,ER,A,B,C,SB,CB,BETA
      TYPE 100
100   FORMAT(1X,'$INPUT BETA')
      ACCEPT*, BETA
      SB=SIND(BETA)
      CB=COSD(BETA)
      WRITE(6,400)
400   FORMAT(17X,'!!!!!!!!!!  MONOCLINIC  !!!!!!!!!!'//
     1   4X,'H K L',4X,'2-THETA',4X,'BETA')
      TYPE 402
402   FORMAT(1X,'$DO YOU WISH TO GIVE A,B,C? N=0,Y=1')
      ACCEPT*, AP
      IF(AP.EQ.0) GO TO 404
      TYPE 403
403   FORMAT(1X,'$TYPE A,B,C')
      ACCEPT*, A,B,C
      GO TO 425
404   TYPE 405
405   FORMAT(1X,'$INPUT HKL(1),#P(1)...,HKL(4),#P(4)'/)
      ACCEPT*,((ID(I,J),J=1,3),IN(I),I=1,4)
      DO 410 I=1,4
          T(I)=TT(IN(I))
          V=W(IN(I))
          O(I,4)=FLOAT(ID(I,1)*ID(I,3))
          O(I,5)=(SIND(T(I)/2.)/V)**2*4.
      DO 410 J=1,3
410       O(I,J)=FLOAT(ID(I,J))**2
      WRITE(6,420) ((ID(I,J),J=1,3),T(I), BETA,I=1,4)
420   FORMAT(13X,3I2,4X,F6.2,F9.2)
```

```
      KN=4
      KL=5
      CALL LE(O,KN,KL,BB)
      A=1./(SQRT(BB(1))*SB)
      B=1./SQRT(BB(2))
      C=1./(SQRT(BB(3))*SB)
      KK=4
425   CALL MATCH(TT,W,KK,E,D)
                              RETURN
      END
C************************  SUB MATCH  ******************************
      SUBROUTINE MATCH(TT,W,KK,E,D)
      DIMENSION TT(N),R(8,500),D(4),TR(8,500),W(N),
     1   X(3,500),Y(500),DELTAA(4),SIGMAA(4),YFIT(500)
      INTEGER NNN,NN,LL,II,JJ,H,K,L
      COMMON N,M,ER,A,B,C,SB,CB,BETA
      WRITE(6,800)A,B,C
800   FORMAT(11X,'INITIAL:',3X,'A',F8.4,3X,'B',F8.4,3X,'C',F8.4)
      II=0
      ED=1.
      TYPE  880
880   FORMAT(1X,'$  # OF INTERACTIONS')
      ACCEPT *,INTER
810   NN=0
      II=II+1
      ER=ER*0.9
      ED=ED*0.9
      DO 850 L=-M,M
      DO 850 K=0,M
      DO 850 H=0,M
        CCTT=((H/A)**2-2.*CB*FLOAT(H*L)/(A*C)+(L/C)**2)/SB**2
        CT=SQRT(CCTT+(K/B)**2)
```

```
      LL=0
      DO 820 I=1,N
        TTM=0.5*CT*W(I)
        IF(TTM.GE.1.) GO TO 850
        CTT=2.*ASIND(TTM)
        EM=ABS(CTT-TT(I))
        IF(EM.GE.ER) GO TO 820
        LL=LL+1
        TR(1,LL)=FLOAT(I)
        TR(2,LL)=FLOAT(H)
        TR(3,LL)=FLOAT(K)
        TR(4,LL)=FLOAT(L)
        TR(5,LL)=TT(I)
        TR(6,LL)=CTT
        TR(7,LL)=EM
        TR(8,LL)=0.02/TAND(TT(I)/2.)
820   CONTINUE
      IF(LL.EQ.0) GO TO 850
      IF(LL.EQ.1) GO TO 830
      NNN=7
      CALL BUBB(TR,LL,NNN)
830   NN=NN+1
      DO 840 I=1,8
840     R(I,NN)=TR(I,1)
850   CONTINUE
      IF (II.EQ.INTER) GO TO 900
C************  DATA FOR LEAST SQUARE  ****************
      NTERMS=4
      D(1)=1./(A*SB)
      D(2)=1./B
      D(3)=1./(C*SB)
      D(4)=CB
      DO 870 I=1,NN
      JJ=IFIX(R(1,I))
```

```
        Y(I)=4.*(SIND(R(5,I)/2.)/W(JJ))**2
        X(1,I)=R(2,I)
        X(2,I)=R(3,I)
870     X(3,I)=R(4,I)
        DO 860 I=1,3
860     DELTAA(I)=D(I)*0.02*ED
        DELTAA(4)=D(4)*0.05*ED
        CALL GRIDLS(X,Y,NN,NTERMS,D,DELTAA,
     1      SIGMAA,YFIT,CHISQR)
        BETA=ACOSD(D(4))
        SB=SQRT(1.-D(4)**2)
        CB=D(4)
        A=1./(D(1)*SB)
        B=1./D(2)
        C=1./(D(3)*SB)
        TYPE 884,CHISQR,A,B,C,BETA
884     FORMAT(1X,'CHISQR',E12.4,5X,'A',F8.5,5X,'B',F8.5,5X,'C',F8.5,
     1          5X,'BETA',F7.3)
        DO 970 I=1,NN
970     TT(I)=TT(I)+TD
        GO TO 810
900     WRITE(6,985)A,B,C,DD,BETA
985     FORMAT(11X,'FINAL:',5X,'A',F8.4,3X,'B',F8.4,3X,'C',F8.4/
     1    12X,'0-THE',F6.3,5X,'BETA',F10.3)
        MMM=1
        CALL BUBB(R,NN,MMM)
        CALL PRINT(R,NN,CHISQR)
                                                    RETURN
        END
C************************  SUB BUBB  **********************
        SUBROUTINE BUBB(R,NN,H)
        REAL R(8,NN)
        INTEGER NN,NI,NJ,H
        NI=NN-1
```

```
      DO 1020 K=1,NI
        NJ=NN-K
          DO 1020 L=1,NJ
            IF(R(H,L).LE.R(H,L+1)) GO TO 1020
              DO 1010 I=1,8
                TEMP=R(I,L)
                R(I,L)=R(I,L+1)
1010            R(I,L+1)=TEMP
1020        CONTINUE
                                          RETURN
      END
C******************  PRINTING RESULTS  ***************************
      SUBROUTINE PRINT(R,NN,CHISQR)

      REAL R(8,200),SS(2,200),ST
      ST=0.
      DO 1030 I=1,NN
       SS(1,I)=SIND(R(5,I)/2.)**2
       SS(2,I)=SIND(R(6,I)/2.)**2
1030    ST=ST+R(7,I)**2
      ST=SQRT(ST/FLOAT(NN-1))
      WRITE(6,1035)ST,CHISQR
1035  FORMAT(11X,'STAN. DEV.(2-THE)',F8.4,8X,'CHISQR',E12.4/)
      WRITE(6,1040)
1040  FORMAT(12X,'#P',4X,'H',4X,'K',4X,'L',4X,'O2T',
     1   5X,'C2T',4X,'DIFF',5X,'DE',4X,'OSIN',4X,'CSIN')
      DO 1055 J=1,NN
        WRITE(6,1050)  (R(I,J),I=1,8), (SS(I,J),I=1,2)
1050    FORMAT(10X,4F5.0,2F7.2,2F8.4,2F8.5)
1055  CONTINUE
      WRITE(6,1060)
1060  FORMAT(/11X,'* DE--0.02/TAN(THETA)'/)
```

```
                                                        RETURN
      END
C***********   SOLVE LINEAR EQUATIONS (L=N+1)  **************
      SUBROUTINE LE(A,N,L,X)
      DIMENSION A(N,L), X(N)

      DO 60 K=1,N-1
        J=K
        DO 10 I=K+1,N
10        IF(ABS(A(J,K)).LT.ABS(A(I,K))) J=I
        IF(J.EQ.K) GO TO 40
        DO 30 I=K,L
           T=A(K,I)
           A(K,I)=A(J,I)
30      A(J,I)=T
40      DO 50 M=K+1,N
          D=-A(M,K)/A(K,K)
            DO 50 I=K,L
50      A(M,I)=A(M,I)+D*A(K,I)
60    CONTINUE
      X(N)=A(N,L)/A(N,N)
      DO 100 J=1,N-1
        K=N-J
        SUM=0.
          DO 80 I=1,N-K
            M=K+I
80          SUM=SUM+A(K,M)*X(M)
100   X(K)=(A(K,L)-SUM)/A(K,K)
                                RETURN
      END
```

```
C******************    INPUT FUNCTION     ************************

      FUNCTION FUNCTN(X,I,A)
      DIMENSION X(3,1),A(1)
      FUNCTN=(A(1)*X(1,I))**2+(A(2)*X(2,I))**2+(A(3)*X(3,I))**2
     1          -2.*A(1)*A(3)*A(4)*X(1,I)*X(3,I)
                                RETURN
      END
C*********************************************************************
      SUBROUTINE GRIDLS(X,Y,NPTS,NTERMS,A,DELTAA,SIGMAA,YFIT,CHISQR)

      DIMENSION X(3,1),Y(1),A(1),DELTAA(1),SIGMAA(1),YFIT(1)
      DOUBLE PRECISION CHISQ1,CHISQ2,CHISQ3
      FREE=FLOAT(NPTS-NTERMS)
      DO 90 J=1,NTERMS
      DO 22 I=1,NPTS
22    YFIT(I)=FUNCTN(X,I,A)
      CHISQ1=FCHISQ(Y,NPTS,YFIT)
      FN=0.
      DELTA=DELTAA(J)
41    A(J)=DELTA+A(J)
      DO 43 I=1,NPTS
43    YFIT(I)=FUNCTN(X,I,A)
      CHISQ2=FCHISQ(Y,NPTS,YFIT)
      IF(CHISQ1-CHISQ2)51,41,61
51    DELTA=-DELTA
      A(J)=A(J)+DELTA
      DO 54 I=1,NPTS
54    YFIT(I)=FUNCTN(X,I,A)
      SAVE=CHISQ1
      CHISQ1=CHISQ2
      CHISQ2=SAVE
61    FN=FN+1.
      A(J)=A(J)+DELTA
      DO 64 I=1,NPTS
64    YFIT(I)=FUNCTN(X,I,A)
```

```
      CHISQ3=FCHISQ(Y,NPTS,YFIT)
66    IF(CHISQ3-CHISQ2) 71,81,81
71    CHISQ1=CHISQ2
      CHISQ2=CHISQ3
      GO TO 61
81    DELTA=DELTA*(1./(1.+(CHISQ1-CHISQ2)/(CHISQ3-CHISQ2))+0.5)
      A(J)=A(J)-DELTA
      SIGMAA(J)=DELTAA(J)*SQRT(2./(FREE*(CHISQ3-2.*CHISQ2+CHISQ1)))
      DELTAA(J)=DELTAA(J)*FN/3.
90    CONTINUE
      DO 92 I=1,NPTS
92    YFIT(I)=FUNCTN(X,I,A)
      CHISQR=FCHISQ(Y,NPTS,YFIT)
                                          RETURN
      END
C*************************************************************************
      FUNCTION FCHISQ(Y,NPTS,YFIT)
      DIMENSION Y(1),YFIT(1)
      DOUBLE PRECISION FCHISQ
      FCHISQ=0.
      DO 100 I=1,NPTS
101   FORMAT(1X,3F8.5)
100   FCHISQ=FCHISQ+(Y(I)-YFIT(I))**2/Y(I)
                                          RETURN
      END
```

GENERAL SUMMARY

Phase transitions in binary intermetallic compounds with the CsCl-type structure have been studied by a novel combination of high-temperature powder X-ray diffraction and Rietveld full-profile refinement. The Landau theory of symmetry and phase transitions and the Gibbs-Knonvalow equation have been applied to understand the phase behavior of some systems with the CsCl-type structure.

Alloys in near equiatomic MnAu have the CsCl-type structure with Pm3m symmetry at high temperature. With decreasing temperature the cubic phase distorts to the AuCu-type tetragonal phase with P4/mmm symmetry with $c/a < 1$ and then further distorts to another AuCu-type tetragonal phase with $c/a > 1$.

The nonstoichiometric compounds RhTi, NbRu, and RuTa with the CsCl-type structure at high temperature undergo thermal symmetry breaking transitions upon cooling. The transitions are first to the AuCu-type tetragonal, and then to the orthorhombic NbRu-type with Cmmm symmetry. Alloys Ir-Ti which are titanium rich have the CsCl-type structure. This cubic structure transforms to the AuCu-type tetragonal structure and then to the NbRu-type structure with increasing atomic percent iridium.

The high-temperature form of nonstoichiometric VIr has the AuCu-type structure, and the low-temperature form is the

VIr-type orthorhombic structure with Cmmm symmetry. The lattice parameters for the orthorhombic structure are a = $2a_{tet}$, b = $2b_{tet}$, and c = a_{tet}. The phase transition appears to occur continuously.

New partial phase diagrams for the composition ranges in near equiatomic MnAu, NbRu, and RuTa are also presented.

ACKNOWLEDGEMENTS

First, I would particularly like to express my sincere thanks to my thesis advisor, Professor Hugo F. Franzen, for his valuable advice and guidance throughout this research. I am also grateful to the other members of my thesis committee, Professors Klaus Ruedenberg, Cheuk-Yiu Ng, Walter S. Trahanovsky, and Ronald Fuchs, who reviewed and improved the writing of my thesis. It is my pleasure to acknowledge to Jim Anderegg and Shirley Standley as well as our group members for their assistance and friendship.

I specially wish to thank my wife and my son for their understanding and support in so many ways. They always share the joys and hardships with me. Most of all, I would like to thank my parents for their hundreds of letters brimming over with infinite love, encouragement, and support.

This research was supported by the Office of Basic Energy Sciences, Materials Sciences Division under contract No. W-7405-Eng-82.